Metabolic Alterations in a Murine Model of Barth Syndrome

Nicola Laprano, MSc

This Thesis is submitted to the University of Glasgow in accordance with the requirements for the degree of Doctor of Philosophy

The Beatson Institute for Cancer research
Garscube Estate, Switchback Road
Bearsden, Glasgow

Institute of Cancer Science
College of Medical, Veterinary and Life Sciences
University of Glasgow

September 2017

Abstract

Barth syndrome (BTHS) is a rare monogenic disease characterized by cardiomyopathy, skeletal myopathy and neutropenia, caused by mutations in the Xq28 locus. Mutations in the locus result in the loss of function of the Tafazzin protein (Taz), a transacylase responsible for the final step in the production of mature cardiolipin (CL). CL is a fundamental component of the inner mitochondrial membrane, where it cooperates in the maintenance of membrane stability and in various cellular processes such as mitochondrial respiration, autophagy and reactive oxygen species sensing.

Using a novel murine model of BTHS, we investigated the mitochondrial phenotype, the metabolic signature and the gene expression profile in the heart of Taz knockout (KO) mice.

We identified extensive heart-specific changes in the structure and composition of the mitochondria accompanied by alterations of the metabolome and gene expression. The alterations are specific to the adult, so probably derive from a developmental process happening after birth. The alteration of the gene expression seems to indicate activation of the unfolded protein response, suggesting an effect of stress response pathways in the cellular processes which underlie Barth syndrome.

Table of Contents

List of Figures

List of Tables

List of Abbreviations

AcCoA	Acetyl-CoA
ALCAT1	Acyl-CoA:lysocardiolipin acyltransferase-1
Asn	Asparagine
Asns	Asparagine synthase
Asp	Aspartate
BTHS	Barth syndrome
CL	Cardiolipin
CM	Cardiomyopathy
CoA	Coenzyme A
DCM	Dilated Cardiomyopathy
D-loop	displacement loop
Dox	Doxycycline
ECAR	extracellular acidification rate
eIF	eukaryotic translation initiation factor complex
EM	electron microscopy
ER	endoplasmic reticulum
ERAD	endoplasmic reticulum-associated protein degradation
ESCs	embryonic stem cells
ETC	electron transport chain
FAD/FADH	Flavin adenine dinucleotide (oxydised/reduced form)
G3P	Glyceraldehyde 3-Phosphate
G6P	glucose 6-Phosphate
G-CSF	granulocyte colony-stimulating factor
Gln	Glutamine
Glu	Glutamate
Gly	Glycine
GSH	Glutathione
GSSG	Glutathione disulphide

HCM	Hypertrophic Cardiomyopathy
HSR	heat shock response
IMM	inner mitochondrial membrane
iPSCs	induced pluripotent stem cells
ISR	integrated stress response
KD	Knockdown
KO	Knockout
4L-CL	Tetralinoleoylcardiolipin
LPC	Lyso-Phosphatidylcholines
LPE	Lyso-Phosphatidylethanolamines
LVNC	Left ventricular non compaction
MS	Mass spectrometry
Met	Methionine
MLCAT1	Monolysocardiolipin acyltransferase-1
MLCL	Monolysocardiolipin
MSF	murine skin fibroblasts
mtRNA	Mitochondrial RNA
NAD^+/NADH	Nicotinamide adenine dinucleotide (oxydised/reduced form)
Neo	Neomycin
OCR	oxygen consumption rate
ORF	open reading frame
P1	postnatal day 1
PEP	Phosphoenolpyruvate
piRNA	Piwi-interacting RNA
Pyr	Pyruvate
RMCE	recombinase-mediated cassette exchange
ROS	reactive oxygen species
ROSA26	Gt(ROSA)26Sor
Ser	Serine
shRNA	short hairpin RNA

Taz	tafazzin
TCA	tricarboxylic acid cycle
Tert	telomerase reverse transcriptase
UPR	unfolded protein response
UPR^{ER}	ER unfolded protein response
UPR^{MT}	Mitochondrial unfolded protein response
αKG	αKetoglutarate

Acknowledgements

First and foremost I would like to express my gratitude to CRUK and the Beatson institute for funding my research and granting me the opportunity to learn, grow and develop skills invaluable for a scientist and a human being.

To my supervisor Douglas Strathdee and my advisor Kevin Ryan, for helping me through challenging times by providing priceless insight and feedback to my ideas. To Doug my special thanks for giving me the opportunity to work under his supervision, for endless support and inspiration to outgrow my potential. Though we have not always seen eye to eye, I will always be grateful for the experience I gained with you. I have really enjoyed being a member of the lab. A big thank you goes to Saverio Tardito, good friend and priceless collaborator, who has been instrumental to the metabolomics work and provided great pieces of advice, both scientific and personal.

To the Y30 lab, past and present, my special thanks. Thanks to Farah, Eve and Sheila for all the technical and scientific support, but most of all for all laughter and good natured teasing. Special thanks to David, who supported me and introduced me to the joys and pains of Scottish football. Thanks to Laurance who started the project and to Fiona and Seren who helped along the way. Thanks to all of Y30 for putting up with me for four long years.

Special Thanks to the other Beatson staff and researchers. Special mentions to Gillian Mackay and David Sumpton from the metabolomics core facility for the help in running all my samples. Thanks to the people of the BSU, of the BAIR and the histology facility for making my work an awful lot easier in my PhD. Thanks to the people from M06, especially Evangelos Giampazolias and Joel Riley, for providing me with expert opinions on mitochondria and for supplying some of the reagents I used in my experiments. Thanks to Elaine Marshall and Jiska Van der Reest from R12 for supplying some of the reagents for Seahorse assays and for the expert advice.

My thanks to the lab of Frederic Vaz, at the Academic Medical Centre of the university of Amsterdam for running the lipid content analysis on Taz mice

samples. Also thanks to Kevin Mackenzie and Gillian Milne at the microscopy and histology core facility at the university of Aberdeen for cutting and imaging the electron microscopy samples.

Thanks to my friends Alvaro Roman, Arantxa Perez, Evangelos Giampazolias, Matthew Davidson, Florian Beaumatin and Sergi Marco for all the good times we had in these four years together. A special thank you goes to my fellow PhD students Pablo Sierra and Elodie Kuntz for being awesome friends and being my second family in Scotland. I will never forget all your support and all the laughter we've had together.

Finally, to my family, for all the support, the help and the skype calls. Thank you for always being there for me, in the good times and the bad.

My greatest thank you goes to Brunella, for the endless support, for the joy the laughter and for putting up with me for almost ten years. A big piece of this work should be credited to her, because without her support and understanding I would not have been able to pull this thing off.

1. Introduction

1.1 Barth Syndrome

Barth syndrome (BTHS) was first identified and described by Dr. Peter Barth in 1983 as a systemic disease consisting of cardiomyopathy, skeletal myopathy and neutropenia (Barth et al., 1983).

Barth identified the disease by analysing data obtained from an affected family presenting several cases of perinatal death from heart decompensation and bacterial infections in male offspring. Autopsy reports from deceased patients revealed mitochondria ultrastructural defects in cardiac muscle cells, neutrophils from the bone marrow and in a minority of cases in skeletal muscle cells.

The analysis also discovered respiratory chain abnormalities, both at a molecular and at a functional level, with reduction of the concentration of components of the respiratory chain and reduction in oxidation ratio (Barth et al., 1983).

1.1.1 Aetiology and prevalence of Barth syndrome

Barth syndrome is a monogenic X-linked recessive disorder, caused by mutation in the *Tafazzin* gene (*TAZ*), located in Xq28 (Bolhuis et al., 1991). The Human Tafazzin Gene Mutation and Variation Database identifies at least 120 types of mutations in the gene, most of them small insertions and deletions, all resulting in the loss of function of Taz with no genotype/phenotype correlation (Barth Syndrome Foundation, 2018). *TAZ* encodes an acyltransferase responsible for the maturation of cardiolipin (CL), an essential phospholipid of the mitochondrial membrane (Houtkooper and Vaz, 2008).

The official BTHS data state the syndrome affects the male population with a prevalence of 1/300000-400000 live births (Barth syndrome foundation, 2006) and it is deemed to be widely underdiagnosed, mainly due to a great variability in the symptomatology of the disease. Diagnosis was in fact based on the identification of the three main pathologic components of BTHS. These, however are not always present in the affected population, with ~30% of BTHS patients not exhibiting any

neutropenia in the initial stages of the disease and a portion of these never developing neutropenia in their life (Bowron et al., 2015).

The introduction of advancements in diagnostic protocols, such as genetic testing for mutations in Taz and cardiolipin profiling, are contributing to a more efficient identification of BTHS, adjusting for a prevalence as high as 1/140000 live births in the UK (Clarke et al., 2013).

Location of Taz gene restricts the pathology to the male population, with the mother acting as an asymptomatic carrier for the disease. While, as a result of X-inactivation, it is still possible for women to display symptoms of BTHS, however the only known cases of female BTHS patients presented other underlying chromosomal defects of the X chromosome (Cosson et al., 2012). The vast majority of the other carrier females analysed presented clearly skewed X-inactivation, with various degrees of preference for the expression of the wildtype Taz allele over the mutated one (Orstavik et al., 1998). The mechanism behind the skewed X-inactivation is still poorly understood. Orstavik et al. proposed the phenomenon may be due to the presence of a post-inactivation selection process, triggered by defects in the respiratory chain caused by *TAZ* mutation, leading to negative selection of the cells expressing mutant *TAZ* (Orstavik et al., 1998).

1.1.2 Physiologic function of Tafazzin

Cardiolipin is a negatively charged glycerophospholipid formed by two phospatidate moieties sharing the same glycerol head. CL presents four esterified fatty acyl chains forming a conical structure (Ikon and Ryan, 2017). Mammalian CL is highly enriched in the mitochondrion and it is almost entirely restricted to the inner mitochondrial membrane (IMM).

In the heart the most common (~80% of total) form of cardiolipin in the membrane is tetralinoleoylcardiolipin (4L-CL) (Houtkooper and Vaz, 2008), with all four fatty acyl side chains formed by linoleic acid. *In vitro* analysis of Tafazzin activity shows that Taz catalyses the final step in the formation of the mature molecule: the transfer of an acyl group from the sn-2 position of phosphatidylcholine to the

corresponding hydroxyl group of the immature precursor monolysocardiolipin (MLCL) (Houtkooper and Vaz, 2008) to obtain 4L-CL (Figure 1.1).

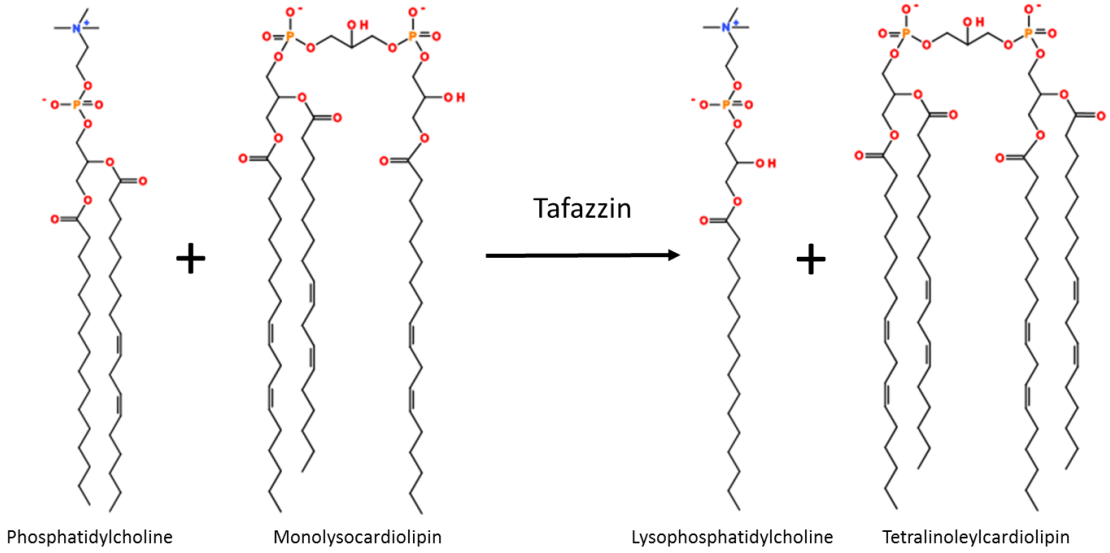

Figure 1.1: schematic representation of the transacylation catalysed by Tafazzin, central to correct maturation of cardiolipin and production of Tetralinoleoylcardiolipin

Mature CL can also be produced via two alternative metabolic routes: in the endoplasmic reticulum, via transacylation of the side chain of fatty acyl CoA to MLCL, catalysed by ALCAT1; in mitochondria where the enzyme MLCAT1 catalyses the transfer of an acyl side chain from Linoleoyl CoA to MLCL (Cao et al., 2004, Taylor and Hatch, 2009). However, it has been shown that, in the absence of Taz, the turnover of CL is increased, with faster degradation of CL caused by disassociation of the phospholipid from the membrane supercomplexes (Xu et al., 2016).

Thus, disruption of the principal pathway for CL synthesis catalysed by Taz causes a shift in the CL/MLCL concentration ratio, which is insufficiently compensated by ALCAT1 and MLCAT1, resulting in reduced presence of 4L-CL, leading to inner mitochondrial membrane disruption (Gonzalvez et al., 2013, Xu et al., 2005).

Cardiolipin is in fact associated with a number of membrane proteins, working to stabilize the organisation of the respiratory chain reaction supercomplex. Due to this function as an anchoring molecule CL is fundamental to maintain mitochondrial membrane structure (Koshkin and Greenberg, 2002). Therefore Taz loss of function and shift of the MLCL/CL balance causes structural abnormalities in the mitochondria structure in BTHS patients.

1.1.3 Clinical presentation of Barth syndrome

Due to the rarity of the disease, the vast majority of clinical data on Barth syndrome derives from case reports and small case series (Rigaud et al., 2013, Roberts et al., 2012). However, in recent years, bigger cohorts have been analysed, allowing for a better characterization of symptomatology. As stated before, the prominent clinical signs of BTHS are cardiomyopathy, skeletal muscle myopathy and neutropenia, accompanied by growth delay, increased concentration of 3-methylglutaconic acid in the urine and, in some cases, mild learning disabilities (Kelley et al., 1991). The global phenotype is however broader and includes a number of multisystem defects painting a much more complex situation than the one that was identified in 1983 (Table 1.1)

Cardiovascular	Dilated Cardiomyopathy Left ventricular non-compaction Extended QT interval Endocardial fibroelastosis Arrhythmia/sudden cardiac death Undulating cardiomyopathy Hypertrophic cardiomyopathy (rare)
Neuromuscular/ neurological	Delayed motor milestones Proximal myopathy Abnormal fatigue levels Exercise intolerance Mild learning impairment ADD Stroke
Haematological/ Infectious	Neutropenia Recurrent mouth infections Perianal dermatitis Recurrent bacterial infections Septicaemia
Endocrine/metabolic	3-Methylglutaconic aciduria Delayed bone growth Delayed puberty Low cholesterol Low blood sugar Lactic acidosis Osteopenia
Gastrointestinal	Oromotor feeding problems Chronic/episodic diarrhoea
Dismorphic features	Deep set eyes Full cheeks Prominent ears
Foetal	Cardiomyopathy Foetal hydrops Male miscarriage and stillbirth

Table 1.1: the principal clinical features of Barth syndrome adapted from (Clarke et al., 2013).

1.1.3.1 Cardiomyopathy

Cardiomyopathy (CM) is the most prominent symptom of BTHS, with 70% of patients developing a form of CM within the first year of age (Roberts et al., 2012).

In BTHS patients CM often presents itself as a dilated cardiomyopathy (DCM), and in rare cases there have been reports of hypertrophic cardiomyopathy (HCM). Cardiac phenotypes are highly variable, with reports of patients with DCM and patients with HCM in the same family (Spencer et al., 2006). Reports also show the presence of phenotypes transitioning from DCM to HCM in the same patient, in what is indicated as an undulating cardiomyopathy (Pignatelli et al., 2003). These occurrences are however very rare, with most patients presenting symptoms coherent with DCM. 50% of the patients also present the formation of trabecular cavities in the wall of the left ventricle, coincident with left ventricular non compaction (LVNC) (Ades et al., 1993).

The cardiac phenotype leads to an increased risk of ventricular arrhythmia in around 15% of BTHS patients. Severe arrhythmia seems to be present only in older children, but there have been reports of cases of life endangering arrhythmia in young children as well (Spencer et al., 2005). Patients with documented arrhythmia have also been reported to suffer sudden cardiac death (Roberts et al., 2012).

A large percentage of BTHS patients (43%), display prolonged QT interval of the action potential (Spencer et al., 2006). QT interval is the measure of the interval of time passing between de-polarization and re-polarization in the heart's electrical cycle. Longer QT interval has been linked to ventricular arrhythmia and sudden cardiac death. However, in BTHS, QT interval doesn't appear to correlate with the documented cases of arrhythmia (Spencer et al., 2006). Defects of the polarization/de-polarization cycle have been linked to defects in myofibril organization and in the calcium homeostasis machinery of the cardiac muscle (Acehan et al., 2011); both of these features are present in BTHS patients.

The main therapeutic agents used for treatment of BTHS are drugs administered to reduce the risk of cardiac failure. BTHS patients respond generally well to treatment with standard DCM medication. These however, must be maintained throughout childhood and into adulthood (Spencer et al., 2006).

Some patients show a deterioration of the cardiac phenotype before five years of life. This deterioration is due to a reduction in the effectiveness of

pharmacological therapy and therefore, these patients require heart transplantation (Roberts et al., 2012).

1.1.3.2 Muscular defects

Most BTHS patients present a certain degree of disruption to neuromuscular development. It is common for affected children to display some delay in the achievement of motor development milestones (Spencer et al., 2006, Barth et al., 1999).

Children affected by BTHS present proximal non-progressive muscle weakness and reduced grip strength; the phenotype tends to improve during adolescence (Spencer et al., 2006). The muscle phenotype clearly manifests itself as a general exercise intolerance in BTHS patients, characterized by heightened fatigue and reduced resistance to prolonged physical activity (Spencer et al., 2011).

Patients exhibit an exaggerated heart rate response when in a graded physical activity regime, showing increased heart rate at peak activity compared to healthy sedentary controls. Near-infrared spectroscopy data show that this exercise intolerance is linked to an impairment of the extraction and metabolism of O2 in the skeletal muscle, which leads to an increased reliance of BTHS patients on glycolytic metabolism. The heightened activity of glycolysis causes a severe lactic academia in BTHS patients, compared to patients with other mitochondrial myopathies (Spencer et al., 2011, Bashir et al., 2017).

Recent studies also reported an impairment in post-exercise recovery in BTHS patients, measured using phosphocreatine recovery as a marker for the activity of the oxidative metabolism (Bashir et al., 2017).

Exercise intolerance can be mildly improved (~5%) by endurance exercise training. Cade et al. reported mild improvements in exercise tolerance and general quality of life in 4 BTHS patients treated by endurance exercise training for 12 weeks (Cade et al., 2017). Even though this improvement is not at the same level as the improvement shown by other mitochondrial myopathy patients, it still represents

a promising starting point for randomized clinical trials for exercise therapy for BTHS patients (Cade et al., 2017).

In at least one case, a BTHS patient has developed a disabling myopathy between 40 and 50 years of age (Ronvelia et al., 2012).

BTHS patients are also reported to be at high risk of stroke. Strokes normally occur in BTHS patients following severe cardiac failure. It has been proposed that the left ventricular non compaction contributes to the formation of clots which is facilitated in the trabecular cavities in the left ventricle wall (Ances et al., 2006).

1.1.3.3 Neutropenia

Neutrophils are the most common type of white blood cell in mammals and are an essential part of the innate immunity machinery. They are the first immune cells to be recruited at the site of an inflammation and play a role in both acute and chronic inflammatory events (Soehnlein et al., 2017).

Neutropenia is a less penetrant symptom of BTHS: about 30% of patients do not show any sign of white blood cell count alteration at initial presentation of the disease, however it has been shown that neutropenia is a persistent or intermittent phenotype in almost 90% of BTHS patients (Bowron et al., 2015).

Neutropenia in BTHS patients is well characterized but its primary cause has not yet been identified. Neutrophil function appears to be normal in BTHS patients (Barth et al., 1983), so it has been postulated that neutropenia could be linked to increased neutrophil apoptosis or increased targeting of the neutrophils by the macrophages (Kuijpers et al., 2004, van Raam and Kuijpers, 2009, Makaryan et al., 2012). Patients show fluctuating neutrophil counts with low general levels which reach normality a few days after the development of an infection (Kelley et al., 1991).

The impaired ability to react to acute infection caused by neutropenia is a heightened risk factor for BTHS patients. Patients in fact present an increased susceptibility to bacterial infections with a range of different possible outcomes. Clinical records show that patients are prone to develop mild infections, mouth

ulcers and dermatitis due to an inefficient first response mechanism to bacterial infection. In the most severe cases neutropenia can lead to patient death due to multi organ failure (Kelley et al., 1991).

Typical treatment for symptomatic neutropenia is a combination therapy of prophylactic antibiotics and granulocyte colony-stimulating factor (G-CSF) (Bolyard et al., 2013). The aim of the therapy is to raise average neutrophil levels rather than normalise it to avoid neutrophilia. The treatment seems to have beneficial effects on the patients, contributing to lowering the risk of serious infection (Bolyard et al., 2013).

1.1.4 Cardiolipin depletion affects the energy production machinery

CL makes up 15% of the lipid fraction of the mitochondrial membrane and it has structural functions within the inner mitochondrial membrane (IMM) architecture (Acehan et al., 2009).

Mitochondria are the main hub for energy production in cells: the IMM houses the components of the electron transport chain and the matrix is the site of the tricarboxylic acid cycle (TCA), so it is not surprising that a defect in CL maturation and an accumulation of the immature form has measurable effects on the energy production balance.

1.1.4.1 Alterations in CL composition inhibit the optimal function of the electron transport chain

Data obtained in yeast suggest that CL plays a key structural role in the integrity of the IMM: its distinctive conical shape makes it fundamental for the proper formation of mitochondrial cristae (Renner and Weibel, 2011). CL is in fact enriched in the negative curvature zone of the membrane, so a depletion of this lipid affects correct cristae folding, causing a disruption in the ultrastructure of the IMM (Bissler et al., 2002).

Furthermore, it has been shown that CL interacts with all the complexes of the electron transport chain (ETC) (Fry and Green, 1981, Houtkooper and Vaz, 2008), playing a role in the formation of a multimolecular supercomplex that has the precise function of optimizing the flow of electrons along the ETC. This optimization function cannot be performed by other phospholipids, including MLCL (Fry and Green, 1981, Wang et al., 2014, Hoffmann et al., 1994).

Reports show that the alteration of IMM integrity due to the lower concentration of mature CL has the additional effect of causing a leakage of protons which depletes the intermembrane potential, causing further impediment to the proper function of the ETC and causing an increased production of reactive oxygen species (ROS) which aggravate the mitochondrial function (Wang et al., 2014, Gonzalvez et al., 2013).

1.1.4.2 CL balance alteration inhibits the TCA cycle

The disruption of the proton gradient in the intermembrane space causes a perturbation of NADH and FADH equilibrium (Kiebish et al., 2013). NADH and FADH are normally used as co-factors in complex I and II of the ETC. Their oxidation supplies electrons for the transport chain and protons that will be actively pumped in the intermembrane space to form the proton gradient that is necessary to power the ATP synthase supercomplex and the subsequent production of ATP.

When the ETC efficiency is disrupted, NADH and FADH are not used as substrates in the ETC and accumulate in the mitochondrial matrix. Here they cause product inhibition of the enzymes of the TCA. Isocitrate dehydrogenase, α-ketoglutarate dehydrogenase, succinate dehydrogenase and malate dehydrogenase use the oxidised forms of these compounds, NAD^+ and FAD^+, as a substrate and are efficiently inhibited by excess of the reduced species produced in the reaction (Smith et al., 1974, Gabriel and Plaut, 1984).

1.1.4.3 Inhibition of the TCA cycle causes accumulation of organic acids

Blockage of the TCA cycle leads to an accumulation of acetyl CoA and propionyl CoA in the mitochondrial matrix (Su and Ryan, 2014). When the concentration of the compounds rises above a threshold level, the enzyme T2 thiolase, responsible for the production of acetyl-CoA, reverses its direction and starts catalysing the production of Acetoacetyl-CoA. The compound undergoes a series of reactions in the organic acid metabolism pathway which lead to the production of 3-methylglutaconic acid, a dead-end metabolite that can be detected in high concentrations in the urine of BTHS patients, but is absent in non-affected males (Ikon and Ryan, 2016, Su and Ryan, 2014) (Figure 1.2).

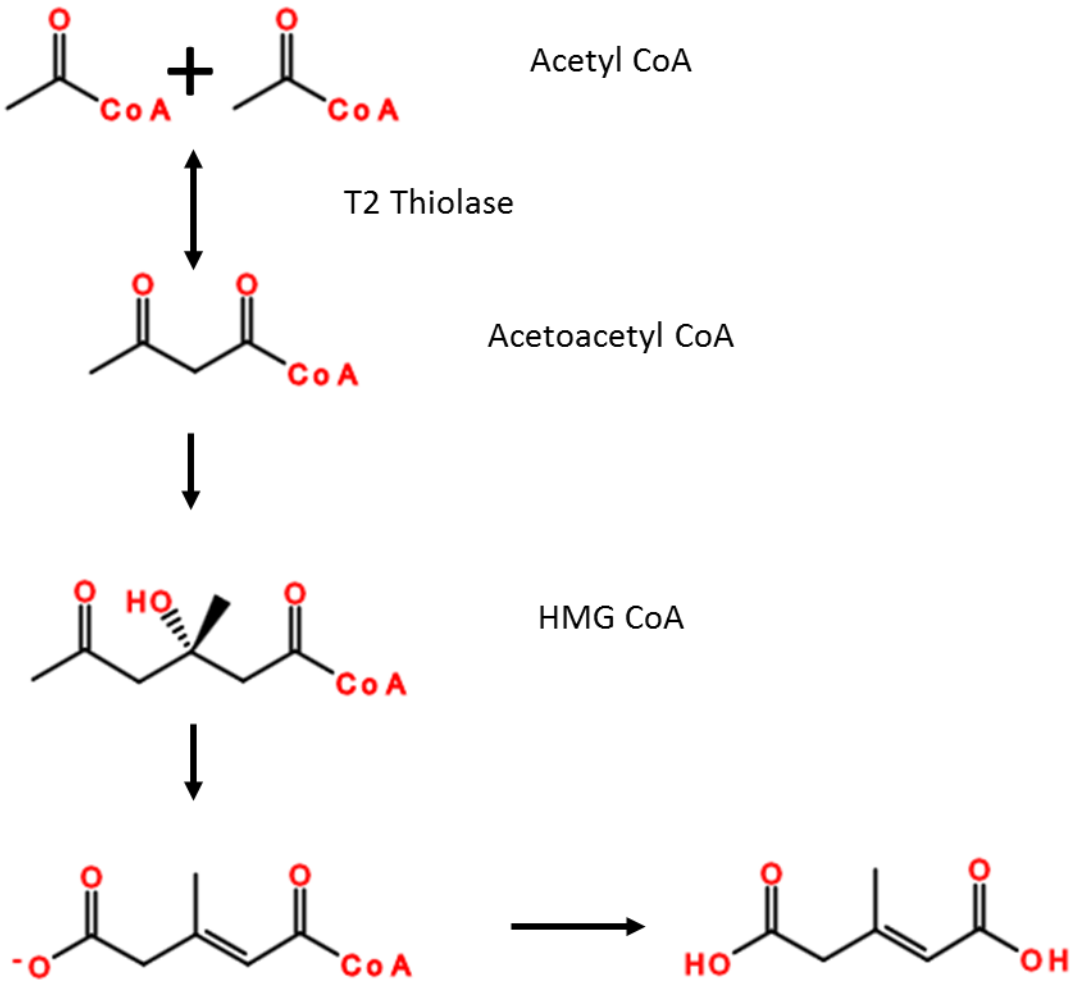

Figure 1.2: schematic representation of the metabolic pathway transforming excess Acetyl CoA to 3 methylglutaconic acid.

1.1.4.4 Cardiolipin deficiency causes abnormalities in mitochondrial ultrastructure

As previously discussed, CL is a fundamental component of the IMM: its conical shape is vital for the correct formation of the negative curvature zone of the mitochondrial cristae and its presence is necessary for correct protein/membrane interaction and the formation of protein supercomplexes of the ETC (Renner and Weibel, 2011, Bissler et al., 2002).

Its depletion has a dramatic effect on the ultrastructure of the membranes. Studies in yeast (*S. Cerevisiae*) reveal that CL depleted IMM loses its typical structure, with compactly packed reticulated cristae and show a swollen morphology with a large matrix compartment and unfolded cristae (Koshkin and Greenberg, 2002). These observations are consistent with the findings in human patients suffering from BTHS showing swollen mitochondria, presenting a mixture of normal and collapsed cristae and expanded matrix space (Barth et al., 1983, Acehan et al., 2007)

In normal conditions, defects in the mitochondrial ultrastructure result in mitophagy and recycling of the defective organelle. Mounting evidence suggests a role of CL in the initiation of the autophagy process (Chu et al., 2014, Chu et al., 2013, Li et al., 2015). Previous work in the institute revealed a role for CL as a sensor of excess ROS and in the recruitment of the mitochondrion to the autophagosome (Galbraith, 2014). Moreover, recent studies in rat cortical neurons show that upon autophagy initiation, CL is externalized to the outer mitochondrial membrane and acts as an anchoring point for the cytoskeleton. This interaction is fundamental for correct autophagy and disruption of the cytoskeleton/CL interacting site results in failed delivery of the damaged mitochondria to the autophagosome (Chu et al., 2013).

1.2 The unfolded protein response and the mitochondria

The survival of any organism in nature depends strictly on its ability to adapt to changing conditions, both at a cellular level and as a whole organism.

Maintenance of protein homeostasis (proteostasis) is a central process for the correct function and survival of cells and organisms. Perturbation of the homeostasis causes the activation of a set of response pathways aimed to restore proper function of the protein production and maturation machinery (Walter and Ron, 2011).

The major perturbant of proteostasis is the presence of unfolded peptides sensed by the cell's internal sensors. These unfolded protein species trigger the unfolded protein response (UPR) mechanism in the affected cellular compartment.

In the cytosol the main effector of the UPR is the heat shock response (HSR) network (Vabulas et al., 2010). The principal actor of the HSR is HSF1, whose activation triggers the transcription of chaperones and heat shock proteins, which help to counteract the UPR by aiding in the correct folding of cytosolic proteins (Vabulas et al., 2010).

1.2.1 Unfolded protein response in the Endoplasmic Reticulum

The endoplasmic reticulum (ER) is a major player in the secretory pathway and the site of maturation of membrane and secreted proteins. It engages in self-monitoring of its activity by quality checking the maturation of proteins through protein sensors (Schroder and Kaufman, 2005).

Chaperones are able to recognize if proteins are in their folded or unfolded form and help with the correct folding of proteins by keeping them in a folding-compatible conformation.

The best characterized sensor of the ER unfolded protein response (UPR^{ER}) is BiP. The chaperone, in its inactive state, binds the ER portion of ATF6, PERK and IRE1, transmembrane activators of the UPR^{ER}. Upon unfolded protein stimulus, BiP releases its bond to these signalling molecules and binds the unfolded proteins for retention in the folding compartment of the ER. The 3 effectors of UPR^{ER} start a cascade of events aimed at restoring proteostasis or, in case of extensive damage, to initiate apoptosis (Figure 1.3).

The UPR^{ER} pathway can be divided into 3 branches working in cooperation to reduce the damage (Bertolotti et al., 2000).

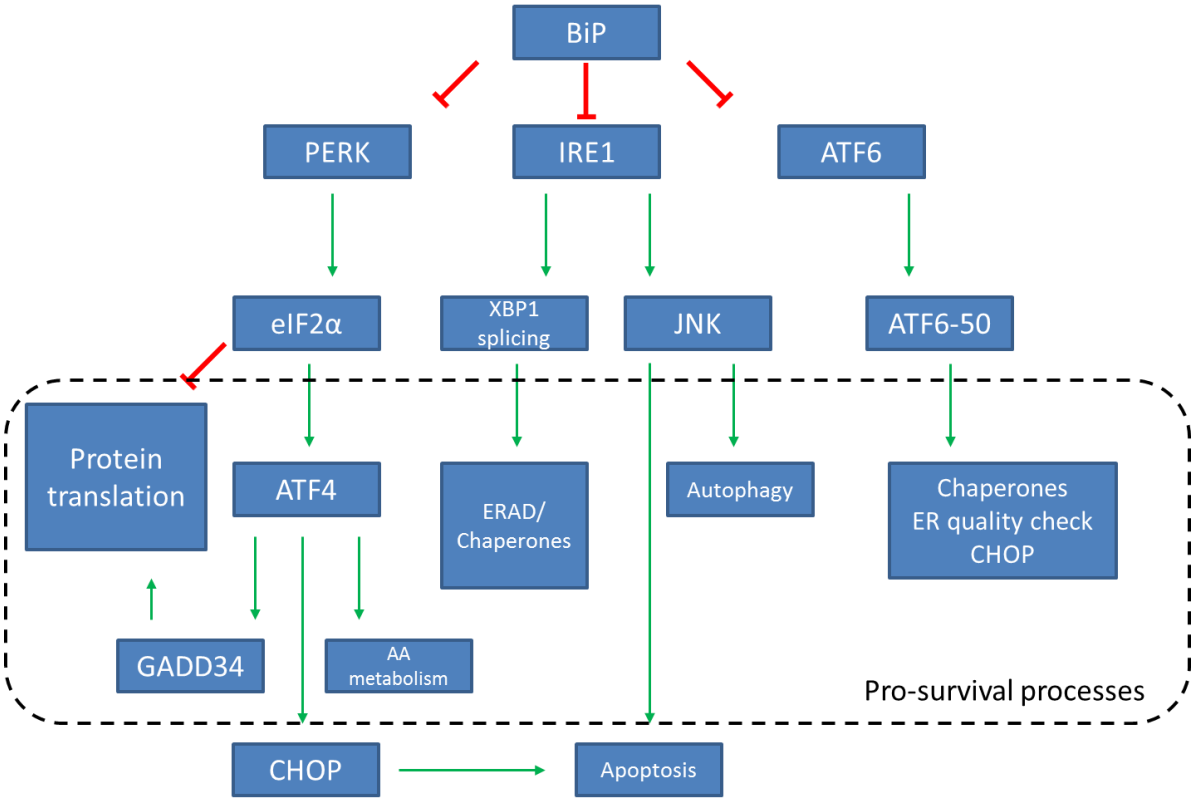

Figure 1.3: schematic representation the UPR^{ER}. The activation of the PERK, IRE1 and ATF6 signalling pathways triggers a pro-survival response aimed at recovering cell homeostasis. Failure to recover results in cells undergoing apoptosis. Green arrows: induction. Red arrows: inhibition.

1.2.1.1 ATF6 signalling cascade promotes survival of the cells

The ATF6 branch is activated when BiP releases ATF6 in the ER. ATF6 is a large protein containing a transmembrane domain and a cytosolic domain. The release from BiP binding unmasks a Golgi localization sequence located in the luminal –COOH end of the protein and promotes translocation of ATF6 to the Golgi (Shen et al., 2002). In the Golgi, ATF6 is subjected to sequential cleavage by resident proteases. The protein is first cleaved by S1P separating the transmembrane region from the membrane bound cytosolic domain. The release of the -NH2 cytosolic portion of ATF6 is then catalysed by further cleavage from S2P that releases its binding to the ER membrane (Ye et al., 2000, Shen et al., 2002). The cytosolic portion of the protein (ATF6-50) translocates to the nucleus and activates a genetic programme aimed to upregulate the transcription of BiP, HSP90 and Calnexin. These molecular chaperones aid the cell in the protein folding process and work to improve the quality check in the ER (Wu et al., 2007). ATF6-50 also induces the transcription of XBP1, a key player in the IRE1 mediated response to unfolded protein stress, suggesting a role of ATF6 in triggering subsequent phases of the UPR^{ER} (Yoshida et al., 2001).

1.2.1.2 IRE1 signalling plays a dual role in the ER stress response

IRE1 is a membrane bound kinase-endoribonuclease with a dual role as a pro-apoptotic and pro-survival signalling molecule.

IRE1's release from BiP binding starts a kinase cascade through activation of Jun kinases that activates autophagy and apoptosis (Urano et al., 2000). Autophagy has a key pro-survival role in the organism. It is, in fact, necessary for clearance of damaged organelles and recovery of building blocks for cell repair. Its activation by the UPR^{ER} suggests an attempt by the cell to recover from damage. The activation of apoptosis, on the other hand, occurs when the damage suffered by cells, in a stressed condition, is too extensive for successful recovery.

IRE1 is also responsible for the activation of the alternative splicing of XBP1. The alternative splicing produces a shorter version of XBP1 with an alternate C-

terminal motif that allows it to bind regulatory elements in the nucleus (Yoshida et al., 2001). Spliced XBP1 promotes the transcription of chaperones and activates endoplasmic reticulum-associated protein degradation (ERAD). ERAD starts the recycling process of unfolded protein and contributes to the cell's attempt to remove the unfolded protein stimulus by removing its trigger (Yoshida et al., 2003). The upregulation of XBP1 by ATF6 suggests the activation of ERAD by IRE1 is triggered in a second phase of the UPR^{ER}, when the chaperones have helped with the folding of recoverable proteins and clearance of irreparably unfolded ones is necessary.

1.2.1.3 PERK activation causes a blockade in protein translation

The final member of the transmembrane activators of the UPR^{ER} is PERK. Its luminal domain is structurally homologous to the luminal domain of IRE1 (Bertolotti et al., 2000). When released from BiP, PERK is activated through oligomerization and trans-autophosphorylation (Ariyasu et al., 2017).

Active PERK phosphorylates subunit 2α of the eukaryotic translation initiation factor complex (eIF2α). The phosphorylation inhibits the complex leading to an overall blockage of protein translation (Raven et al., 2008). The blockage of translation has the dual role of stopping the production of misfolded proteins and allowing the cell to quench the UPR stimulus by clearing unfolded protein via ERAD (Raven et al., 2008).

Phosphorylation of eIF2α stimulates the expression of transcripts containing an upstream short open reading frame (ORF) in their 5' untranslated region (Baird and Wek, 2012). This mechanism leads to upregulation of the transcription and accumulation of ATF4, a key player in the UPR (Harding et al., 2003).

The primary response activated by ATF4 promotes survival and repair of the cell via the upregulation of amino acid import, metabolism and via upregulation of chaperones and oxidation protection molecules (Harding et al., 2000, Harding et al., 2003). Upon removal of the UPR stimulus, ATF4 also negatively regulates PERK signalling through expression of GADD34, which de-phosphorylates eIF2α removing the block to protein translation (Novoa et al., 2003).

In the case of irreparable damage ATF4 plays a role in induction of apoptosis via upregulation of CHOP. CHOP is a pro-apoptotic transcription factor that triggers the expression of downstream pro-apoptotic molecules leading to activation of the cell death pathway (McCullough et al., 2001, Zinszner et al., 1998).

1.2.2 Mitochondrial unfolded protein response

Mitochondrial unfolded protein response (UPR^{MT}) is a less characterized stress response pathway activated by unfolded proteins in the mitochondria.

UPR^{MT} is involved in a number of processes in the cell: it promotes host survival during bacterial infection allowing recovery of normal cell function (Pellegrino et al., 2014); it is also involved in metabolic regulation by inhibiting the transcription of mitochondria-encoded components of the electron transport chain (ETC) and inducing expression of glycolysis-related genes (Nargund et al., 2012, Nargund et al., 2015). UPR^{MT} involvement in metabolism regulation seems to affect lifespan in both *C. Elegans* and mouse.

1.2.2.1 Mitochondria UPR in *C. elegans*

UPR^{MT} was first discovered in mammals in 1996 (Martinus et al., 1996), however its molecular mechanism has been extensively studied and characterized in *C. elegans*. The stimulus originates in the mitochondrial matrix upon accumulation of misfolded proteins. These proteins are cleaved in 6-30 amino acid peptides by ClpP peptidase (Haynes et al., 2007). The peptides are then transported into the mitochondrial intermembrane space and into the cytosol by HAF1 (Haynes et al., 2010). In the cytosol these peptides are sensed by ATFS-1 which translocates to the nucleus and activates the gene response to mitochondrial stimulus (Nargund et al., 2012).

ATFS-1 has both a mitochondrial localization sequence and a nuclear localization sequence. In normal conditions ATFS-1 is translocated to the mitochondria where it is degraded by LON peptidase. Disturbances in proteostasis impair protein

trafficking to the mitochondria, so ATFS-1 can be translocated into the nucleus and activate gene expression (Nargund et al., 2012). In the nucleus ATFS-1 improves mitochondrial protein quality control by inducing mitochondrial chaperones, reactive oxygen species protection molecules and proteases (Nargund et al., 2012) (Figure 1.4, A).

Recent reports also propose a role for UPR^{MT} in ageing. It has in fact been reported that mitonuclear protein imbalance caused by the activation of the UPR^{MT} was responsible for an extension of the lifespan of *C.elegans* (Houtkooper et al., 2013).

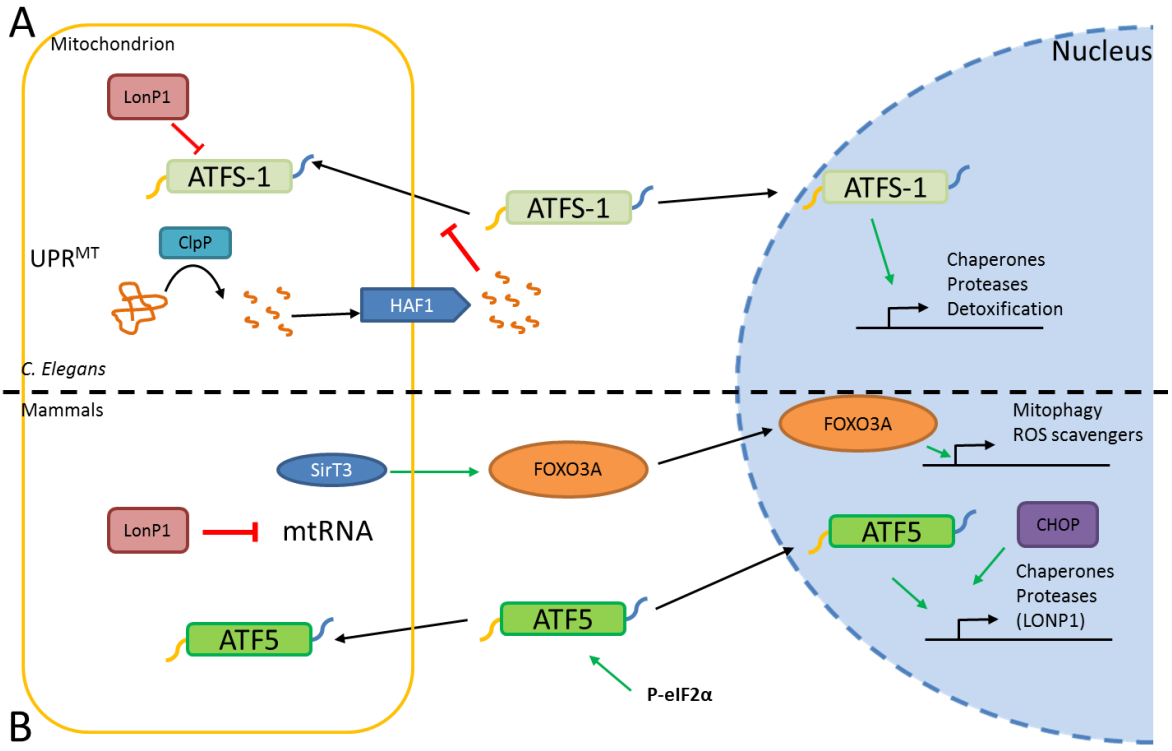

Figure 1.4: schematic representation the UPR^{MT} in C. elegans and in mammals. A: in *C. elegans* unfolded mitochondrial proteins are cleaved by ClpP and the resulting peptides are exported to the cytosol by HAF1. Peptides in the cytosol prevent mitochondrial localization of ATFS1 which migrates to the nucleus and activates the UPRMT genetic programme. B: in mammals mitochondrial stress activates translocation of ATF5 to the nucleus where it promotes expression of genes encoding proteins involved in mitochondrial homeostasis. Unfolded proteins sensed in the intermembrane space activate SirT3 which activates FOXO3A and its translocation to the nucleus, where it enacts a pro-survival genetic programme. Green arrows: induction. Red arrows: inhibition.

1.2.2.2 Mitochondria UPR in Mammals

The activation of UPR^{MT} in mammals is currently poorly understood and recent findings suggest multiple signals are needed for its activation upon unfolded protein stimulus (Zhou et al., 2008).

In 2016 Fiorese et al. identified ATF5 as a homolog of ATFS-1 in mammals by showing it could rescue UPR^{MT} in ATFS-1 null *C. elegans* (Fiorese et al., 2016).

ATF5 is induced by phosphorylation of eIF2α similarly to ATF4 by activation of its transcription through a short ORF located in the 5' UTR of the gene. Similar to ATFS-1, ATF5 has both a mitochondria localization sequence and a nuclear localization sequence and in normal proteostasis conditions it localizes in the mitochondria (Fiorese et al., 2016).

Upon UPR^{MT} stimulus ATF5 migrates to the nucleus where it activates a genetic programme aimed to improve mitochondrial quality control and protein folding capability. ATF5 induces expression of LONP1; the role of this protease in the regulation of ATF5 is still unclear, however LONP1 plays a role in inhibiting the translation of mtRNA by degrading the mitochondrial pre-RNA processing nuclease MRPP3, and thus preventing mitochondria maturation of the RNA (Munch and Harper, 2016). The inhibition of translation prevents the accumulation of further unfolded proteins, allowing the mitochondria to recovery. ATF5 also promotes the expression of mitochondrial chaperones to improve protein folding (Zhao et al., 2002, Fiorese et al., 2016). Recent works show that CHOP plays a role in aiding ATF5's induction of a genetic programme aimed to repair cellular damage (Horibe and Hoogenraad, 2007), pointing again to a collaborative activation of the UPR^{MT} via an integrated stress response.

The UPR^{MT} can also be triggered in the intermembrane space of the mitochondria. Upon unfolded protein stimulus the deacetylase Sirt3 activates FOXO3A and its translocation to the nucleus where it activates mitophagy and ROS scavenging (Papa and Germain, 2014), thus improving cell survival (Figure 1.4, B).

1.3 Models of Barth syndrome

The bulk of information on Tafazzin function has been obtained through studies using non-mammalian models (Acehan et al., 2011). Studies in yeast, Drosophila and zebrafish have provided invaluable information on the physiological role of CL and its biochemistry (Xu et al., 2006). However these models are unsuitable for clinical studies of the pathology, and its long-term and long-range effects. Recently there has been some progress in obtaining murine models of the disease that can be utilized for a systemic study of the pathology.

1.3.1 shRNA models of Barth syndrome

In 2010, TaconicArtemis GmbH generated a mouse model containing an expression cassette for a shRNA targeting Taz mRNA. The company used a recombinase-mediated cassette exchange (RMCE) strategy to insert a Doxycycline (Dox) inducible shRNA construct in the *Gt(ROSA)26Sor (ROSA26)* locus on chromosome 6 using proprietary methods. The targeting strategy uses a modified RMCE-ready *ROSA26* locus containing a recombination-acceptor sequence comprising F3 and FRT recombination sites and a FLP expression cassette. Cells bearing this modification are transfected with a plasmid carrying the shRNA and a Tetracycline promoter between F3 and FRT sites. The expression of FLP catalyses the recombination between the sites and the exchange of plasmid sequence with the sequence in the RMCE-ready site (Figure 1.5).

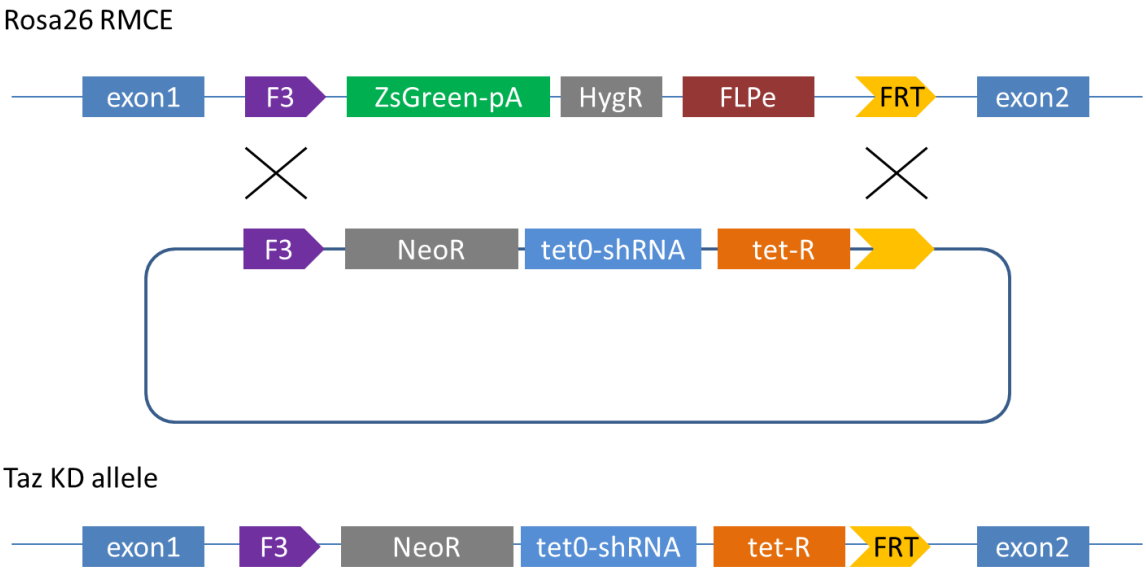

Figure 1.5: schematic representation of the production process for Tafazzin knockdown allele

To obtain animals mimicking a complete developmental loss of Taz, both the breeders and the resulting offspring were fed with chow containing Dox. Several studies report a drastic reduction in the levels of Taz mRNA in liver, brain, skeletal muscle and heart upon Dox induction, with values of Taz expression fluctuating between 3 and 10% of the original value in the examined tissues (Acehan et al., 2011, Soustek et al., 2011).

Knockdown (KD) of Taz results in a phenotype resembling that of BTHS patients: independent studies identified a switch in the concentration of CL and MLCL, with an increase in immature MLCL and a reduction in mature CL, compatible with loss of function of Taz. These studies also identified mitochondrial abnormalities, with presence of giant mitochondria and poor cristae organization and evidence of ongoing mitophagy in the heart (Acehan et al., 2011, Soustek et al., 2011).

However, Taz KD showed no visible effects on the cardiac phenotype of mice at 2 months of age. In contrast, analysis of 8 months old mice showed a well-defined cardiac phenotype with reported left ventricle dilation and reduced ventricle wall thickness (Acehan et al., 2011) resulting in a reduced ejection fraction of the ventricle (Acehan et al., 2011, Soustek et al., 2011).

Inducible alleles are a powerful tool for the analysis of genes that cannot be knocked out with conventional methods. In the case of Taz these models seem to recapitulate some of the main features of BTHS, however there is mounting evidence of a detrimental effect of prolonged Dox exposure on the heart. Vinet et al. in 2008 reported an alarming increase in left ventricular hypertrophy and heart failure in Dox treated mice exposed to cardiac stress after thoracic aorta constriction (Vinet et al., 2008). Taz KD murine model exhibits signs of cardiomyopathy only after 8 months exposure to Doxycycline. This data and the results obtained from Vinet et al. may raise doubts on the reliability of the Taz KD model for unbiased studies on BTHS, given that the cardiac phenotype showed by the inducible shRNA model could similarly be affected by prolonged exposure to Dox and therefore fabricate artefacts in the measurements. Moreover, in 2015, Moullan et al. showed a detrimental effect of tetracycline and its derived molecules on mitochondrial translation. The data showed the formation of a mitonuclear protein imbalance caused by blockage of translation in mitochondria, probably due to the evolutionary link between mitochondria and protobacteria

(Moullan et al., 2015). The detrimental effect on mitochondria was present across a range of model organisms including *Drosophila*, *C. elegans* and mouse.

1.3.2 Knockout models of BTHS

The potential problems with the Taz KD model derived from the prolonged exposure to Dox, raise some questions on the suitability of this model for accurate studies on BTHS. To solve this potential issue our lab worked on developing a murine knockout model of BTHS.

1.3.2.1 Knockout of Taz leads to sterility in male mice

In 2015 our lab produced a knockout allele of *Taz* by in vitro manipulation of HM1 embryonic stem cells (ESCs) to obtain an allele with a Neomycin (Neo) resistance cassette insertion between exon 8 and exon 9 of mouse Tafazzin. The insertion of the Neo cassette resulted in the disruption of the correct splicing pattern in Taz mRNA maturation, which in turn produced a non-functional version of the transcript (Cadalbert et al., 2015) (Figure 1.6).

The resulting targeted ESCs were used to produce chimerae via blastocyst injection in C57BL6/J background. Although being highly chimeric, mice produced using this method failed to give germline transmission of the genetic modification (Cadalbert et al., 2015).

Further analysis of the model revealed an effect of *Taz KO* on sperm cells differentiation, both *in vivo* and *in vitro*. The analysis of the testes of *Taz KO* mice showed impaired meiosis due to disruption of chromosome synapses (Cadalbert et al., 2015). Sterility is not a symptom of human BTHS; however previous studies reported Taz KO caused sterility in a *Drosophila* model of BTHS (Malhotra et al., 2009, Xu et al., 2006).

The study also revealed an increase in DNA damage in sperm cell precursors due to an increased activity of the L1 transposon, suggesting an effect of Taz on

correct function of piRNA, fundamental for regulation of transposable elements (Cadalbert et al., 2015).

No phenotype was detected in the hearts of *Taz KO* chimerae. However it was not possible to gauge ESCs contribution to the heart tissue of the chimeric animals because HPRT, expressed only in the modified ESCs and not in the host blastocyst, is not expressed in the heart (Cadalbert et al., 2015).

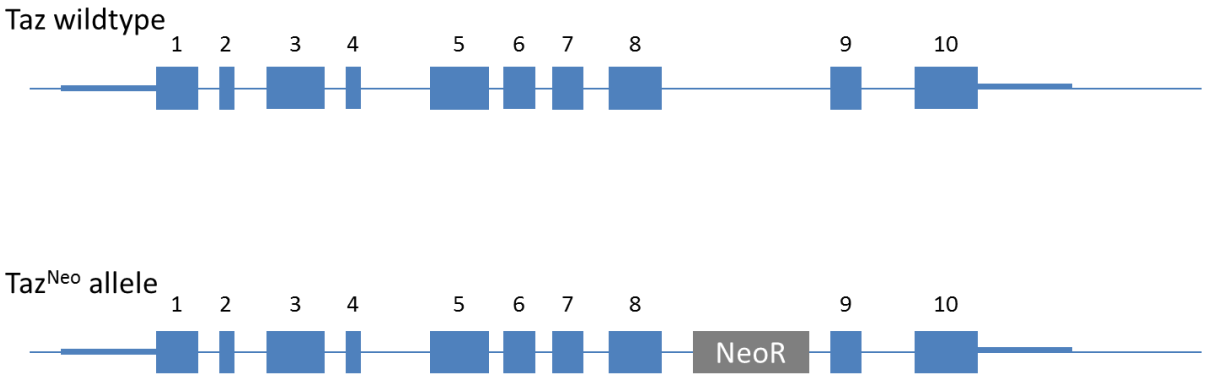

Figure 1.6: schematic representation of Taz KO allele. Blue exons; Grey Neomycin resistance cassette. Insertion of Neo cassette disrupts splicing leading to non-functional protein. Adapted from Cadalbert et al. 2015.

1.3.2.2 Conditional knockout approach results in a viable mouse model of BTHS

The issues encountered producing a Taz KO model prompted us to attempt a different approach for the generation of a usable BTHS murine model.

The lab produced a conditional allele that uses CRE recombinase to delete all the coding sequences located after exon 4 at the *Taz* locus (Figure 1.7, A).

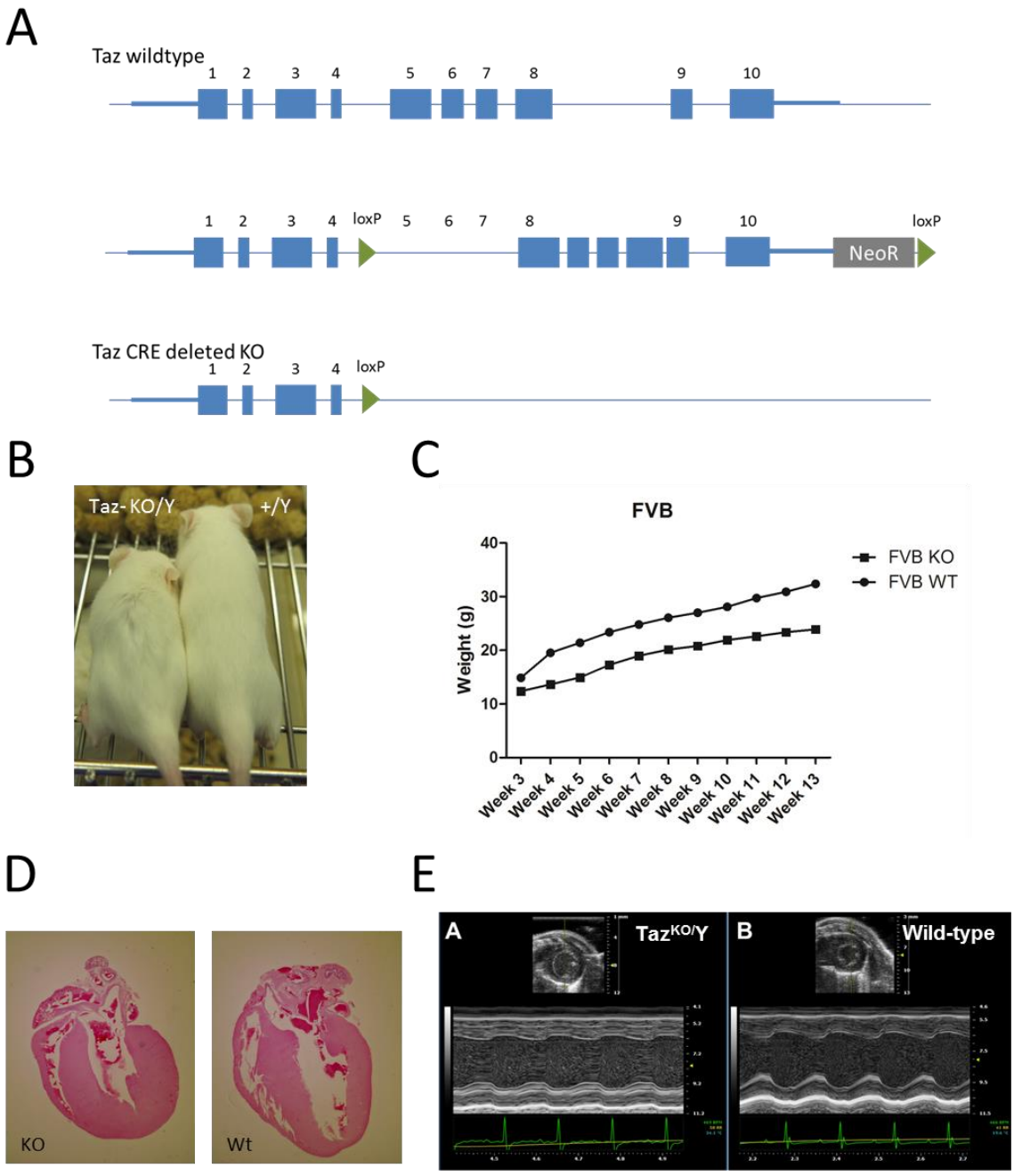

Figure 1.7: A, schematic representation of Taz conditional KO allele. Blue exons, Green loxP recombination sites, Grey Neomycin resistance cassette. Recombination with CRE produces a truncated protein. B, C, Taz KO mice are smaller than wildtype littermates. B, Taz KO mouse is clearly smaller than its wildtype littermate. C, Taz KO mice never reach the comparable size to the wildtype. D, Taz KO hearts are smaller than wildtype and exhibit thickening of the left ventricular wall. E, Heart function is compromised in TazKO when assessed by echocardiography.

The construct carrying the modified allele was targeted into recipient G4 ESCs which were in turn used for microinjection in recipient blastocysts derived from mice of the C57BL6/J genetic background.

The resulting mice were crossed with a CMV CRE deletor mouse line to obtain whole body deletion of CRE.

To overcome male sterility derived from *Taz KO*, females heterozygous for the deleted allele were crossed to wildtype males to obtain viable *Taz KO* mice.

Characterization of the KO mice showed that the model recapitulated part of the phenotype of human BTHS. *Taz KO* mice were exhibiting growth delay compared to the wildtype littermates, with an average 30% reduction in average weight of the KO males compared to the wildtype counterparts. Ultrasound scans of the heart showed a reduction in fractional shortening, increased left ventricle end systolic dimension and increased QT interval (Figure 1.7, B, C, D and E).

Taken together, these data suggest a cardiomyopathy phenotype with reduced contractility of the left ventricle and an overall problem in the repolarization of the membranes after the action potential discharge. Histology of the testis shows a situation similar to the one that was detected in the chimerae, with lack of terminal differentiation and sterility (data not shown).

This model offers new perspectives to the study of BTHS in a mammalian model organism, granting us a new tool for a better understanding of the phenotypes underlying the loss of Taz in the organism.

1.4 Aim of the study

Barth syndrome (BTHS) is a rare monogenic disorder caused by loss of function of the Tafazzin gene, resulting in defective production of the membrane phospholipid cardiolipin.

Official data from the Barth syndrome foundation database put its prevalence at 1/300000-400000 live births, but recent advancements of the diagnostic protocols suggest gross under-diagnosis problem with the pathology and that the figure

should be adjusted to 1/140000 live births, making BTHS much more relevant to the clinical landscape than it was in the past.

Comprehensive study of Barth syndrome is rendered difficult by the current lack of optimal murine models of the disease. The bulk of knowledge we possess of Tafazzin derives from studies in yeast, zebrafish and Drosophila, with just a few studies on a knockdown murine model of BTHS.

In this study we present a novel murine model for BTHS displaying many of the founding features of the human pathology. The aim of this study is to better characterize the mouse model to verify how closely the murine phenotype resembles the clinical characteristics of human patients. We believe an accurate model of BTHS would be an invaluable tool in the understanding of the disease and identifying new possible treatments for the improvement of patients' quality of life.

2. Materials and methods

2.1 Materials

2.1.1 Reagents

Product	Supplier	Cat. No.
19mm Coverslips	VWR	631-0154
Agarose	Sigma-Aldrich	A2790
Antimycin A	Sigma-Aldrich	A8674
CCCP	Sigma-Aldrich	C2759
Collagenase, type II	Thermo Fisher	17101015
CoverGrip coverslip sealant	Biotium	23005
DNase I	Thermo Fisher	18047019
DyNAmo HS SYBR Green qPCR Kit	Thermo Fisher	F410L
ECL	GE Healthcare	RPN2232
Ethidium bromide	Sigma-Aldrich	E7637
Folin & Ciocalteu's phenol reagent	Sigma-Aldrich	F9252-1L
Glutamine	Thermo Fisher	25030081
GOTaq polymerase mastermix	Promega	M7808
HBSS	Thermo Fisher	14025092
Laminin	Thermo Fisher	23017015
MACS LS Column	Miltenyi Biotec	130-042-401
MidiMACS separator	Miltenyi Biotec	130-042-302
neonatal cardiomyocyte isolation kit	Miltenyi Biotec	130-100-825
NuPAGE 4-12% Bis-Tris protein gels	Thermo Fisher	NP0321BOX
Oligomycin A	Sigma-Aldrich	75351
QuantiTect reverse transcription kit	Qiagen	205310
red blood cells lysis solution	Miltenyi Biotec	130-094-183
RNase free DNase set	Qiagen	79254
RNeasy RNA extraction kit	Qiagen	74104
Rotenone	Sigma-Aldrich	R8875
Trypsin	Thermo Fisher	15090046
Vectashield hard set with DAPI	Vector	H-1500
XF base medium	Agilent	102353-100
XFe96 FluxPak	Agilent	102416-100
αMEM	Thermo Fisher	32561094

Table 2.1: List of reagents

2.1.2 Equipment

Equipment	Supplier
710 Confocal microscope`	Zeiss
CFX connect Real Time system	BIO-Rad
easycast2	Thermo Fisher
Gene Genius Gel doc	Syngene
Microscope slides	VWR
Nanodrop 2000c	Thermo Fisher
Olympus FV1000 fluorescent microscope	Olympus
Seahorse XF96	Agilent
Tetrad 2 termocycler	BIO-Rad
Xcell-II blot module	Thermo Fisher

Table 2.2: List of equipment

2.1.3 List of antibodies

Product	Supplier	Cat. No.
Donkey anti mouse-HRP conjugated	Jackson	715095-150
Donkey anti rabbit-HRP conjugated	Jackson	711-035-152
Mouse anti α-actinin	Abcam	ab9465
Phalloidin	Thermo Fisher (Gift from Alvaro Roman)	A12380
Rabbit anti Tom20	Cell signalling technologies	424065
Rabbit anti α-tubulin	Abcam (Gift from Joel Riley)	ab18251

Table 2.3: List antibodies and dyes

2.1.4 List of primers

Primer name	Sequence
dloop FW	AATCTACCATCCTCCGTGAAACC
dloop REV	TCAGTTTAGCTACCCCCAAGTTTAA
SRY FW	TAGTGTTCAGCCCTACAGCC
SRY REV	TGTCCCACTGCAGAAGGTTG
Taz GT KO U1	CCAAGTTGCTAGCCCACAAG
TAz GT WT-flox D1	CAGGCACATGGTCCTGTTTC
TAz GT WT-flox U1	CTTGCCCACTGCTCACAAAC
Tert FW	CTAGCTCATGTGTCAAGACCCTCTT
Tert REV	GCCAGCACGTTTCTCTCGTT

Table 2.4: List of primers

2.1.5 Buffers and solutions

Buffer/Solution	Components
Blocking buffer	5% BSA or 5% milk in TBST or PBS
Blotting buffer	25mM Tris, 192mM Glycine, 0.01% SDS, 20% Methanol pH8.3
laemmli buffer	4% SDS, 20% Glycerol, 120 mM Tris-HCl (pH 6.8) in water
Lowry solution A	4mg/mL NaOH, 20mg/mL Na2CO3 in water
Lowry solution B	10 mg/mL Potassium Sodium Tartrate, 5 mg/ mL CuSO4 in water
Phosphate buffered saline (PBS)	137mM NaCL, 2.7mM KCl, 10mM Na_2HPO_4, 2mM KH_2PO_4, pH7.4
RIPA Buffer	10 mM Tris-HCl (pH 8.0), 1 mM EDTA, 0.5 mM EGTA, 1% Triton X-100, 0.1% sodium deoxycholate, 0.1% SDS, 140 mM NaCl
SDS PAGE running buffer	25mM Tris, 192mM Glycine, 0.1% SDS, pH8.3
TBST	TBS + 0.05% Tween-20
Tris Buffered saline (TBS)	50mM Tris-Cl, 150mM NaCL, pH7.6
Tris-acetate-EDTA (TAE)	40mM Tris-acetate, 1mM EDTA

Table 2.5: List of buffers and solutions

2.2 Experimental procedures

2.2.1 Mice

Mice used in this study were obtained by genetically modifying a strain of C57BL6/J mice by blastocyst injection of genetically modified G4 embryonic stem cells as described in the introduction. The mice were bred with a CRE deletor strain to remove a portion of Tafazzin and obtain a non-functional truncated Taz protein. Heterozygous females from the CRE deleted strain were crossed with wildtype males to obtain Taz KO males. Mice used in the study have been backcrossed into FVB strain for 6-8 generations to reduce genetic variability between specimens. All mice used in the study were humanely sacrificed at either postnatal day 1 or 8-10 weeks of age.

2.2.2 Embryonic Stem Cells

Cells used in for *in vitro* assays belonged to the G4 mixed background (129S6/SvEvTac x C57BL/6Ncr) and were provided by Andreas Nagy's lab at the Samuel Lunenfeld Research institute Mount Sinai Hospital (600 University avenue, Toronto, Ontario, M5G1X5, Canada).

Wild type cells were treated with Tafazzin (Taz) directed CRISPR/Cas9 to obtain a knockout cell line for Taz. Cells were screened and tested to identify the mutations occurred in the cell line following CRISPR/Cas9 transfection and showed a ~100bp deletion in exon 3 of the gene.

2.2.3 Cardiomyocytes derivation

Cardiomyocytes were derived from postnatal day 1 (P1) mice's whole hearts. Mice are sacrificed by cervical dislocation and tail tipped for genotyping. The hearts were explanted, washed in cold HBSS buffer and then incubated overnight in ice cold 0.05% trypsin in PBS/EDTA. The next day, hearts are washed in ice cold HBSS and then in ice cold αMEM. Hearts were then incubated in αMEM containing 50U/mL type II collagenase and 1U/mL DNase I for 45 minutes at 37^0.

Digested tissue was then disrupted mechanically using a 1mL pipette and the suspension was strained through a 70μm cell strainer. The cell preparation was incubated with red blood cells lysis solution and centrifuged following manufacturer instructions. The pellet was then incubated with neonatal cardiomyocyte isolation kit for magnetic separation. The kit operates negative selection of cardiomyocytes from the total population. It contains a cocktail of magnetic micro-beads conjugated to antibodies directed to surface markers for all of the heart's cell populations except for cardiomyocytes. Application of a magnetic field causes separation of the relevant cells from a mixed population

Beads-conjugated lysates were loaded on a MACS LS column and separated magnetically using a MidiMACS separator.

The purified cells were counted and seeded on Laminin coated plates for further use.

2.2.4 Fibroblast derivation

Fibroblast were derived from primary skin samples of P1 wildtype and knockout littermates. Mice were sacrificed and a portion of skin was explanted from their back. The pieces of tissue were washed thoroughly in PBS. The samples were laid, skin side down, on a sterile petri dish and the dermis was scraped off with a scalpel together with any fat residues. The resulting tissue was cut in 1-2mm pieces using a sharp surgical scalpel. The pieces were then placed in a 6cm petri dish and covered with a sterile glass coverslip to create a micro-chamber in which the cells were free to outgrow from the tissue.

When the fibroblasts were confluent, the coverslips were removed and the plate was washed with PBS. The residual pieces of tissue were discarded and the cells were incubated with 0.05% trypsin for 5 minutes to dissociate the cells.

Cells were then counted and plated on a suitable cell culture vessel for further use.

2.2.5 Genotyping

Cells and tissue were lysed by incubation with a lysis buffer (100mM Tris-HCl (pH8.5), 5mM EDTA, 0.2%SDS, 200mM NaCl, 100µg Proteinase K/ml). The lysates were centrifuged and the pellet was discarded, the supernatant was added to pure isopropanol which precipitated nucleic acids. The solution was centrifuged and the supernatant was discarded. The pellet formed by nucleic acids was washed 3 times in 70% ethanol to eliminate excess salt and then re-suspended in TE buffer.

The genomic DNA was then used for PCR with the relevant primers, using GOTaq polymerase mastermix with the protocol described in table 2.6.

The PCR products were then run on a 2% agarose gel containing 0.002% ethidium bromide. Bands were imaged using a UV transilluminator.

STEP	**Temperature**	**Time**
1. Initial Denaturation	95°	2’
2. Denaturation	95°	30’’
3. Annealing	62°	1’
4. Extension	72°	1’
5. GOTO 2	34 cycles	
6. Final extension	72°	5’
END		

Table 2.6: thermic protocol for genotyping

2.2.6 Intracellular metabolites extraction

Heart, liver and skeletal muscle tissue was harvested from mice and snap-frozen in liquid N_2. Intracellular metabolites were extracted by tissue homogenization in an ice-cold solution of methanol, acetonitrile and water (5:3:2). The extracts were centrifuged at 16,000g for 10 min at 4°C and the supernatants were used for LC-MS analysis

2.2.7 LC-MS analysis

Mass spec was performed using a Q-Exactive Orbitrap mass spectrometer (Thermo Scientific) together with a Thermo Scientific Accela HPLC system. The HPLC setup consists of a ZIC-pHILIC column (SeQuant, 150x2.1 mm, 5 µm, Merck KGaA , with a ZIC-pHILIC guard column (SeQuant, 20x2.1 mm) and an initial mobile phase of 20% 20 mM ammonium carbonate, pH 9.4, and 80% acetonitrile.

Cell extracts (5 µl) were injected and metabolites were separated over a 15 min mobile phase gradient, decreasing the acetonitrile content to 20%, at a flow rate of 200µL/min and a column temperature of 45°C. Metabolites were detected

across a mass range of 75-1000 m/z using the Q-Exactive mass spectrometer at a resolution of 25,000 (at 200m/z), with electrospray ionization and polarity switching. Lock masses were used and the mass accuracy obtained for all metabolites is below 5 ppm. Data were acquired with Thermo Xcalibur software.

The peak area of different metabolites was determined using Thermo LCquan software which identifies metabolites using the exact mass of the singly charged ion and their known retention time on the HPLC column. Intracellular metabolite content was normalized to sample mass.

2.2.8 Lipid extraction and analysis

Tissue from wildtype and Taz KO mice of identical genetic background and similar ages, was harvested and snap-frozen in liquid nitrogen. Tissues were then homogenised using a Precellys evolution homogeniser and sonicated with a tip sonicator.

Lipids were extracted using the method described in (Vaz et al., 2003). In brief 0.4 nmol of CL (C14: 0)4 (Avanti Polar Lipids, Alabaster, AL) was added to the equivalent of 1 mg/mL protein in distilled water, the solution was extracted twice with chloroform/methanol (2:1 v/v) followed by centrifugation at 1000 × g. The organic phases were evaporated under a nitrogen stream, and the residue was resuspended in 100 µl of chloroform/methanol/water (50:45:5 v/v/v) containing 2.5 ml/L NH4OH.

Five µL of this lipid extract was injected into a straight-phase high pressure liquid chromatography system, and cardiolipin analysis was performed by on-line electrospray tandem mass spectrometry.

2.2.9 Mitochondrial respiration assay

Mitochondrial respiration assays were performed on the SeahorseXF96, the materials used for cell culture and the assay are contained in the Seahorse XFe96

FluxPak. Seahorse medium is composed of: XF base medium; Glucose 50mM; Glutamine 650µM and it is adjusted to pH 7.4 with NaOH. The drugs used to test mitochondria respiration and their final concentrations are described in table 2.7.

Compound	**Final Concentration**
Oligomycin A (Sigma-Aldrich Cat. No. 75351)	1.2 µM
CCCP (Sigma-Aldrich Cat. No. C2759)	4µM
Rotenone (Sigma-Aldrich Cat. No. R8875	2µM
Antimycin A (Sigma-Aldrich Cat. No. A8674)	2µM

Table 2.7: drugs used in the Seahorse experiment and their final concentrations.

Cells were plated in seahorse specific 96well plates in a cell type-specific density, so that they got to 80% confluence for the assay. One hour prior to the assay the cartridge was hydrated with the XF calibrant solution at 37^0 in a normal atmosphere incubator. Cells were then incubated for 1 hour at 37^0 in normal atmosphere incubator with seahorse medium.

Next drugs for the assay were prepared in seahorse medium and loaded in the appropriate ports in the cartridge.

The assay consists of serial measures of pH and oxygen concentration in a micro-chamber containing the cells. The machine performs three measures to set a baseline respiration rate, then the drugs are injected sequentially and pH and oxygen consumption are measured three times after each injection.

After the assay the readings were normalized against protein content of each well measured with a Lowry colorimetric assay.

2.2.10 Lowry protein assay

Cells were incubated with solution A (4mg/mL NaOH, 20mg/mL Na_2CO_3 in water) for 20 minutes on a plate shaker. Then solution B (10 mg/mL Potassium Sodium

Tartrate, 5 mg/ mL $CuSO_4$ in water) was added to the mix and incubated for 20 minutes. Folin & Ciocalteu's phenol reagent was added to each sample and incubated for 10 minutes. The Absorbance values of the samples were then read on a spectrophotometer at 750nm. Protein content was determined using known concentrations of bovine serum albumin (BSA) to produce a standard concentration curve.

2.2.11 Immunostaining

Cell samples were seeded on glass coverslips and cultured to desired confluence. The cells were then fixed in 4% Paraformaldehyde (PFA) in phosphate buffered saline (PBS) for 15 minutes at room temperature. PFA was removed and the sample was incubated for 5 minutes at room temperature with 5% BSA and 0.01% TritonX100 in PBS for membrane permeabilization. The sample was then incubated with 5% BSA in PBS for 40 minutes at room temperature to block aspecific protein-protein interactions.

The samples were then incubated for 1 hour in a fresh aliquot of the blocking solution containing the primary antibody. After this time the cells were incubated for a further hour with the appropriate secondary antibody.

After each step, 3 washes are performed, by rinsing the coverslips face down in drops of PBS placed on parafilm.

Slides were mounted using a hard set Vectashield containing DAPI to avoid photobleaching and stain nuclei. Coverslips were then sealed using CoverGrip coverslip sealant.

2.2.12 IF data analysis

Immunostained samples were imaged using a Zeiss LSM710 confocal microscope, using a 64x oil lens. Images were taken keeping the acquisition parameters consistent between the different fields and the different samples.

Each channel was then analysed separately and processed with ImageJ software: a threshold was set to cut out any background signal and the intensity of fluorescence in the sample was calculated as a function of the total area occupied by fluorescent signal. Values were normalized to total nuclei area. Parameters for the analysis were kept consistent between samples.

One mouse per genotype was harvested to produce MSF cell lines, 3 parallel slides were stained from each cell line and 25 fields were examined for each slide.

2.2.13 RNA samples production

Samples were processed for RNA using the RNeasy extraction kit (Qiagen) following the manufacturer's instructions, adding a genomic DNA clean-up step using a RNase free DNase set (Qiagen).

2.2.14 RNAseq

RNA extracted with the method above was tested for quality on an Agilent 2200 Tapestation using RNA screentape.

Libraries for cluster generation and DNA sequencing were prepared according to the method adapted from Fisher et al. (Fisher et al., 2011) using Illumina TruSeq RNA LT Kit v2. Quality and quantity of the DNA libraries were assessed on an Agilent 2200 Tapestation and Qubit (Thermo Fisher Scientific) respectively. The libraries were run on the Illumina NextSeq500 using a High Output 75 cycles kit (2x36cycles, paired end reads, single index).

2.2.15 Mitochondria quantification

The DNA produced using the method above was quantified using a NanoDrop 2000c (Thermo fisher). 10ng of the DNA for each sample was then used in the RTqPCRs.

The PCR reaction was performed in the presence of the DyNAmo Sybr Green fluorescent probe which intercalates the DNA molecules produced by the PCR reaction, offering a readout of the amount of cDNA in the sample. The reaction was performed using the protocol described in table 2.8

The CT data obtained was normalized to a housekeeping gene and represented as relative expression level (ΔCT).

STEP	**Temperature**	**Time**
1. Polymerase activation	95°	10'
2. Denaturation	95°	15''
3. Annealing/extension	60°	45''
Plate read		
4. GOTO 2	39 cycles	
5. Melt Curve	60° to 95° with 0.5°/5 sec	increments
Plate read		
END		

Table 2.8: thermic protocol for Real time PCR

Mitochondria quantification was performed by comparing the amount of genomic DNA, quantified by measuring the amount of telomerase reverse transcriptase (Tert) sequence, against the amount of mitochondrial DNA, measured by quantifying the amount of mitochondrial displacement loop (D-loop) sequence. D-loop is a triple strand structure located at the mitochondrial origin of replication and it is present in single copy on each copy of the mitochondrial circular DNA.

The comparison between the amount of genomic DNA and the amount of mitochondrial DNA gives us a measure of the relative abundance of mitochondria.

The primers used for the real-time RT-qPCR are listed in table 2.4.

2.2.16 Western Blotting

Specimens were prepared by lysing tissue and cells using RIPA buffer (10 mM Tris-HCl (pH 8.0), 1 mM EDTA, 0.5 mM EGTA, 1% Triton X-100, 0.1% sodium deoxycholate, 0.1% SDS, 140 mM NaCl). The samples were then quantified by

Bradford spectrophotometric assay, using known concentrations of BSA to produce a standard concentration curve. A working solution containing 1mg/µL protein was prepared from the stock in laemmli buffer (4% SDS, 20% Glycerol, 120 mM Tris-HCl (pH 6.8) H2O).

10µL of the working solution were resolved using pre-cast 4-12% Bis-Tris acrylamide gel. The gels were then blotted onto nitrocellulose membranes for antibody staining.

The membranes were blocked with a hyperproteic solution (5% milk or 5% BSA) to minimize non-specific protein-protein interactions that could interfere with assay sensitivity. Then the membranes were incubated with the relevant primary and peroxidase conjugated secondary antibodies. The bands were revealed using ECL producing chemiluminescecnt staining that was than exposed on a photographic film using an x-ray processor.

Protein levels were measured using densitometric analysis and normalized against protein levels of a housekeeping gene.

2.2.17 Electron microscopy

Heart samples were harvested post mortem from adult and newborn mice, 3 adults per genotype and 3 newborn per genotype were used in this experiment, two samples of heart tissue were harvested from each animal. The hearts were sectioned and a 2mm cubic section of the left ventricle wall was harvested using a surgical scalpel and washed in a 0.2M sodium cacodylate buffer solution. Samples were then fixed using 2.5% Glutaraldehyde in sodium cacodylate buffer. Fixed samples were immersed in sodium cacodylate solution to preserve them for shipping to the University of Aberdeen for sectioning and imaging using the electron microscope.

3 Results

3.1 Taz Knockout mice exhibit striking changes in cell ultrastructure

3.1.1 Tafazzin Knockout affects lipid composition in multiple tissues

Cardiolipin (CL) is a major structural building block of the inner mitochondria membrane (IMM), where it represents ~20% of the total lipid component. Taz catalyses the addition of a linoleic acid side chain to monolysocardiolipin (MLCL) to form the mature form of the molecule tetralinoleoylcardiolipin (4L-CL) (Houtkooper and Vaz, 2008). Studies performed in model organisms and in samples from BTHS patients reveal a striking shift in the concentration of 4L-CL and MLCL, proving that the knockout of Taz prevents the formation of mature CL and causes the accumulation of MLCL.

Starting with this information we tested how the lack of Taz and the consequent impairment in cardiolipin maturation was influencing the global lipid composition of the cells.

We performed Lipid content analysis on multiple tissues in collaboration with Dr. Frederic Vaz of the AMC of Amsterdam.

Samples of heart, liver and skeletal muscle tissue all showed a reduction in mature CL species (72:5 and 72:8) with an accumulation of more saturated species with lower number of carbons (56:0) in Taz KO animals compared to the wildtype counterparts (Figures 3.1, A; 3.2, A; 3.3, A). CL 72:8 is the lipid species of 4L-CL, which represents more than 90% of the CL present in the IMM. This data is consistent with an impaired action of Taz, preventing the formation of mature 4L-CL.

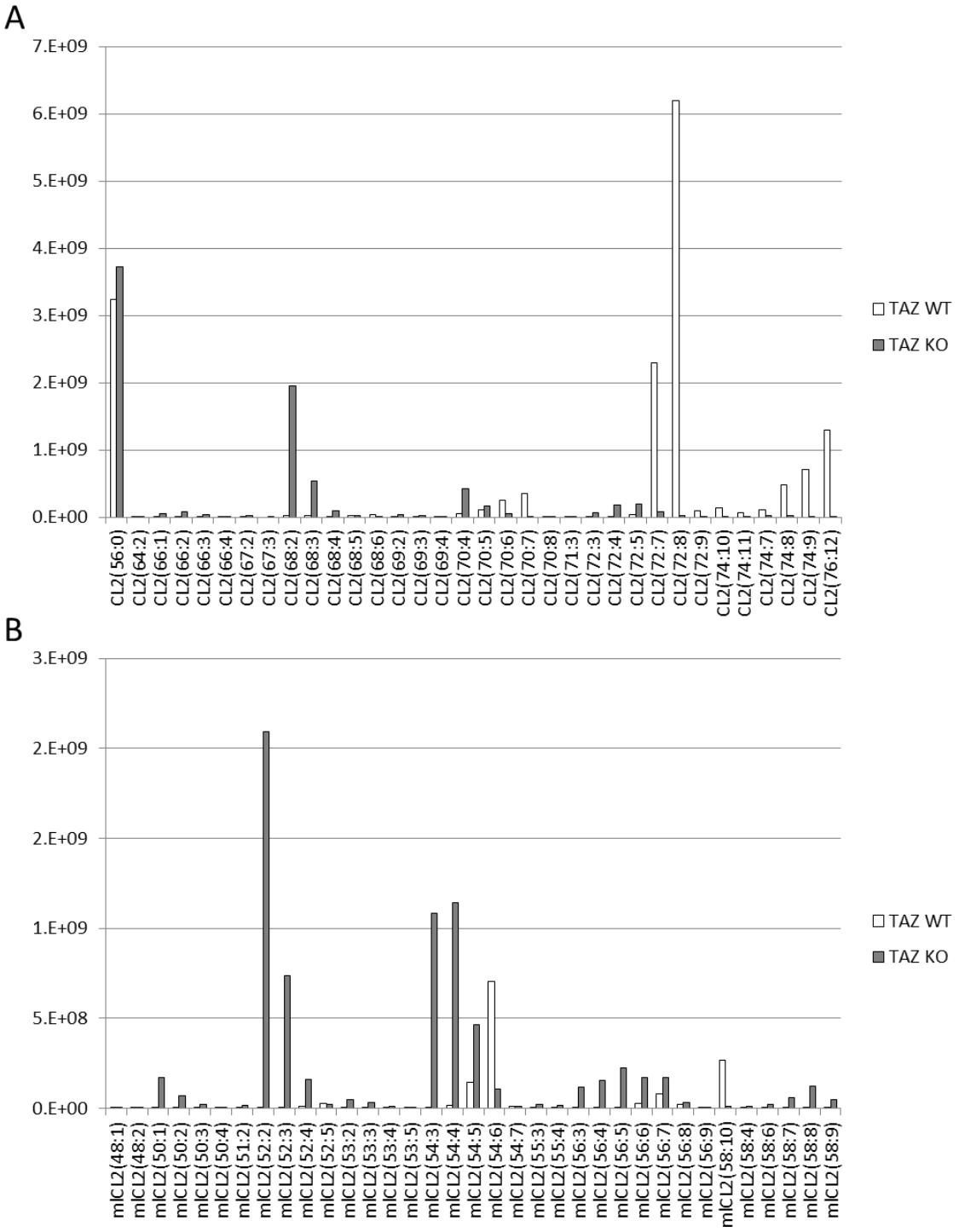

Figure 3.1: effects of Taz KO on lipids relative abundance in the heart. A, relative abundance of cardiolipin species (CL) in Taz KO (grey) compared to the wildtype (white). B, relative abundance of monolysocardiolipin species (MLCL) in Taz KO (grey) compared to the wildtype (white)

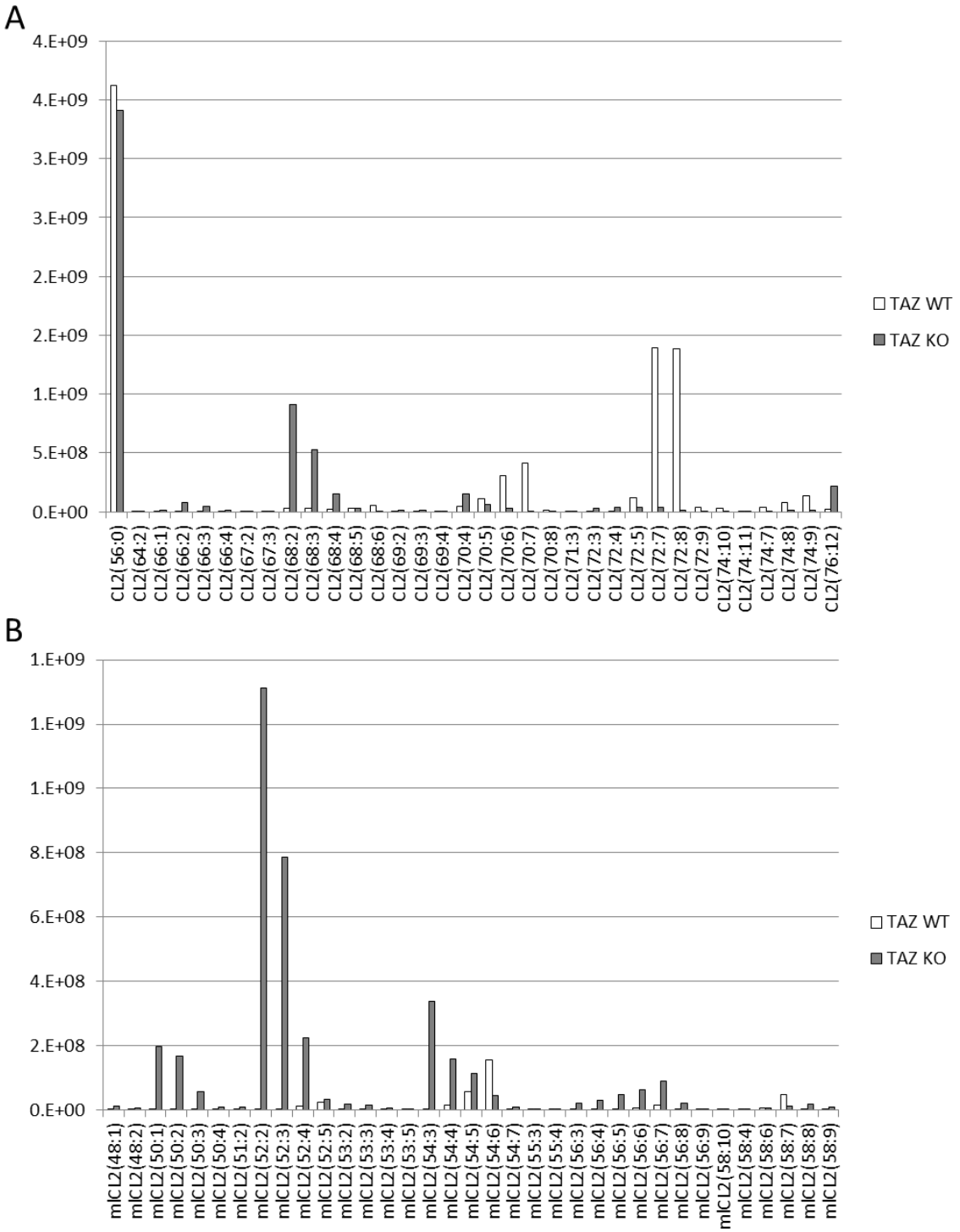

Figure 3.2: effects of Taz KO on lipids relative abundance in the liver. A, relative abundance of cardiolipin species (CL) in Taz KO (grey) compared to the wildtype (white). B, relative abundance of monolysocardiolipin species (MLCL) in Taz KO (grey) compared to the wildtype (white)

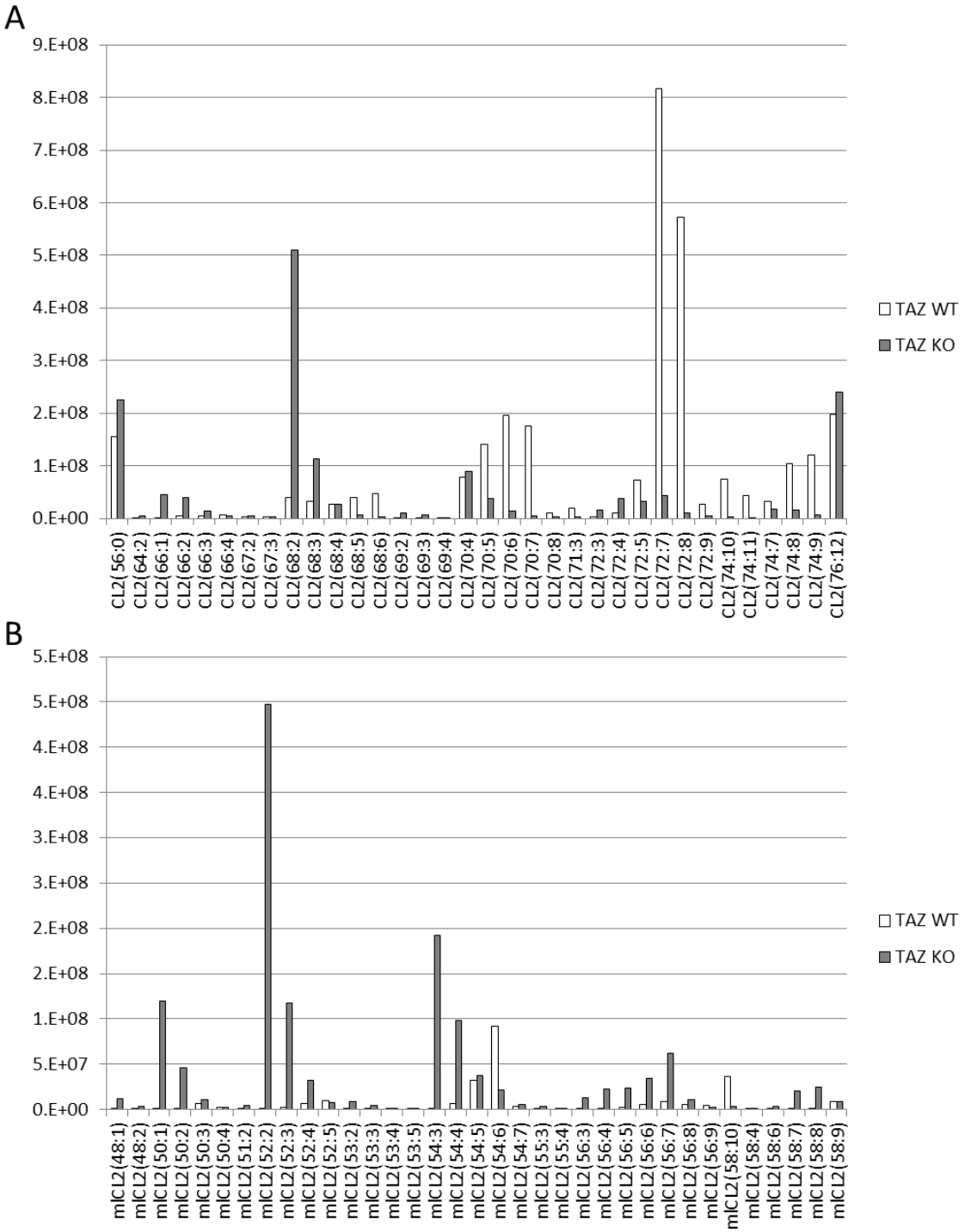

Figure 3.3: effects of Taz KO on lipids relative abundance in skeletal muscle. A, relative abundance of cardiolipin species (CL) in Taz KO (grey) compared to the wildtype (white). B, relative abundance of monolysocardiolipin species (MLCL) in Taz KO (grey) compared to the wildtype (white)

As expected, in parallel to the reduction in mature CL, we identified an increase in the levels of MLCL, the immature precursor of the fully formed CL molecule. As previously shown with CL, MLCL species levels indicate a striking difference between Taz KO and wildtype mice, with an overall increase in MLCL which is particularly evident in more saturated, lower carbon content species (52:2, 52:3) (Figures 3.1, B; 3.2, B; 3.3, B).

Coincidentally to the changes in CL and MLCL we detected an increase in both positively and negatively charged 18:2 fatty acid species in the heart, in particular Lyso-Phosphatidylcholines (LPC) and Lyso-Phosphatidylethanolamines (LPE). These 18:2 alkyl acids are the main components of CL side chains in most animal tissue and the donors of linoleic acid for the transacylation catalysed by Taz.

CL and MLCL alterations are readily identifiable in heart, skeletal muscle and liver, pointing to a whole-body loss of function of Taz.

Interestingly, other than the described difference in the concentration of CL/MLCL, easily identifiable in all examined tissue, differences in other membrane lipids concentration are much less pronounced in liver compared to heart and almost non-existent in muscle which shows a surprisingly normal lipid phenotype.

3.1.2 Taz knockout alters mitochondria morphology

The alteration in membrane composition detected in the heart of Taz KO mice stems directly from the inability of the cells to produce mature cardiolipin, the condition leads to an imbalance in the total lipid composition that is likely to affect other aspects of the mitochondria physiology. As was previously discussed, studies in model organisms revealed that CL plays a fundamental role in the integrity of the membrane and in their capability to achieve an efficient ultrstructural organization (Renner and Weibel, 2011, Bissler et al., 2002, Koshkin and Greenberg, 2002).

With this in mind it was decided to assess whether the structural integrity of the mitochondria was preserved in a Taz KO environment. To this end heart samples

were prepared for electron microscopy (EM) imaging in collaboration with the microscopy and histology facility at the University of Aberdeen.

3.1.2.1 Taz knockout alters mitochondria morphology

In normal conditions (Figure 3.4 A, B) the heart tissue presents well organized muscle fibres composed by parallel sarcomeres divided by the Z-lines (dark stripes in the picture). The muscle fibres are surrounded by clusters of mitochondria. The structure of the mitochondria is neatly organized, with tightly packed cristae (Figure 3.5 A, B).

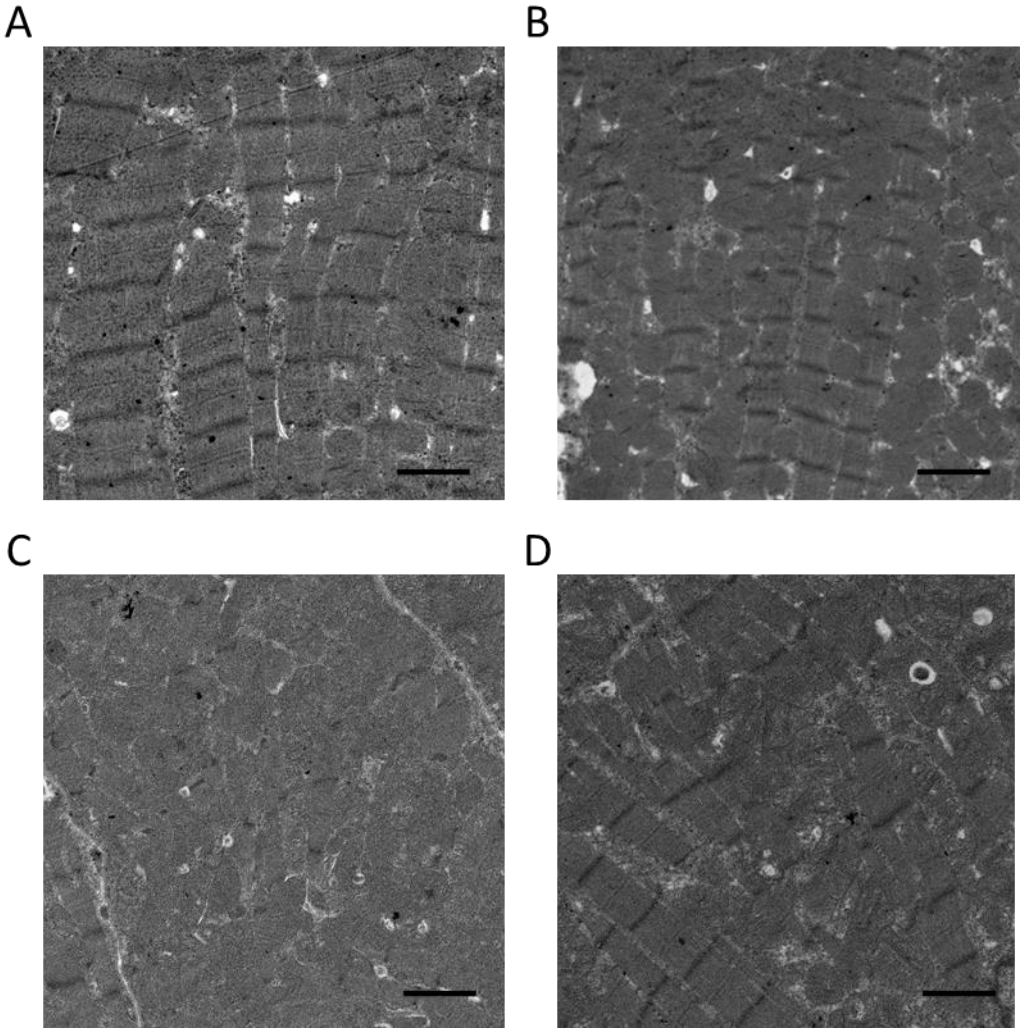

Figure 3.4: Smooth muscle fibres in the heart imaged using electron microscopy. A, B wildtype; C, D Taz KO. Dark bands represent the Z-discs of the sarcomere (scale bar 2µm). Pictures taken by Gillian Milne at the histology and microscopy facility of the university of Aberdeen.

The structure of the muscle fibres does not seem to be affected in Taz KO hearts (Figure 3.4 C, D). The muscles appear to be normal, with neatly organized parallel fibres and clearly recognizable Z-lines.

However, when observed at higher magnification we can clearly distinguish differences in the mitochondria structure. The organelles appear to be enlarged with fewer cristae and larger matrix filled cavities (Figure 3.5 C, D, E, and F).

These differences in mitochondria structure are compatible with the lack of Cardiolipin caused by the knockout of Tafazzin and are consistent with the

mitochondrial phenotype observed in histologic samples from BTHS patients (Barth et al., 1983, Clarke et al., 2013).

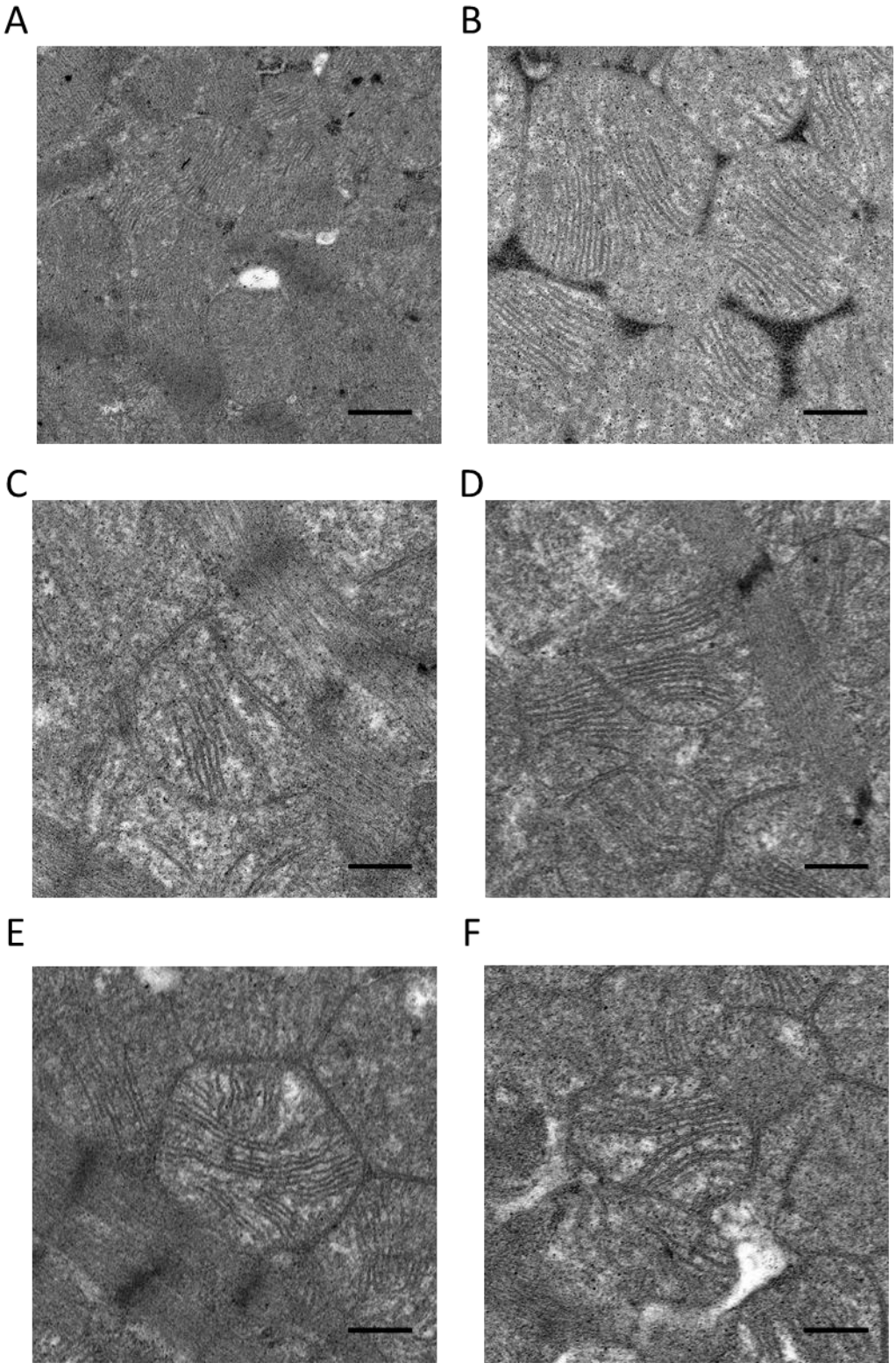

Figure 3.5: Mitochondria in the heart imaged using electron microscopy. A, B wildtype cardiac mitochondria; C, D, E and F Taz KO mitochondria (scale bar 500nm). Pictures taken by Gillian Milne at the histology and microscopy facility of the university of Aberdeen.

3.1.2.2 Taz KO does not impair cardiac muscle fibre formation

As stated above, EM imaging of the heart tissue shows no detectable differences in muscle fibre organization in Taz KO hearts compared to the wildtype.

The images clearly show a well-organized structure of the muscle fibre in both Taz KO and wildtype with the Z-discs clearly visible as darker streaks in the fibre (Figure 3.6 A, B). Fluorescent staining of the muscle structural protein α-actinin was performed; confirming the EM data. α-actinin is a structural protein belonging to the spectrin superfamily. In the smooth muscle it is located at the Z-discs where it acts as an anchoring point for f-actin and it is necessary for muscle contraction.

Antibody staining of the molecule in isolated cardiomyocytes, derived from the heart of mice sampled at post-natal day 1 (P1), shows no distinguishable differences between Taz KO hearts (Figure 3.6 C) and their wildtype counterparts (Figure 3.6 D). In both samples a well-ordained structure can be easily identified, with the staining forming a banded pattern corresponding to the Z-discs.

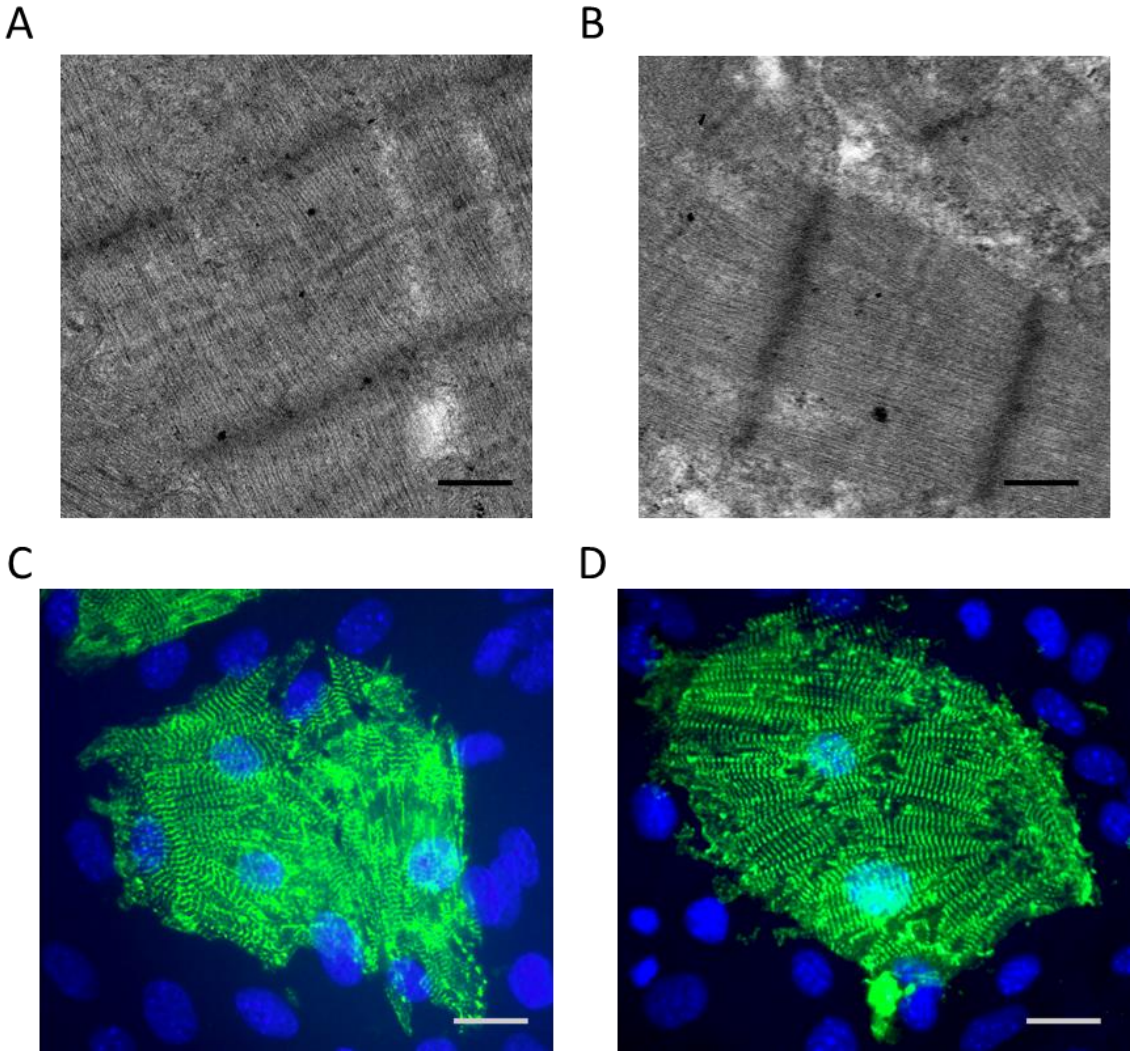

Figure 3.6: Muscle organization is not affected by knockout of Taz. A, EM image of wildtype smooth muscle fibre (scale bar 500nm). B, EM image of Taz KO smooth muscle fibre (scale bar 500nm). C, fluorescent image of wildtype smooth muscle cells isolated from P1 mouse hearts. Blue: nuclei; green: Z- discs stained with α-actinin (scale bar 20μm). D, fluorescent image of Taz KO smooth muscle cells isolated from P1 mouse hearts. Blue: nuclei stained with DAPI; green: Z- discs stained with α-actinin (scale bar 20μm). EM pictures taken by Gillian Milne at the histology and microscopy facility of the university of Aberdeen.

3.1.2.3 Taz KO reduces the number of mitochondria in the heart

The EM images show a clear modification in mitochondria morphology caused by Taz KO, with the mitochondria of KO hearts showing fewer cristae and larger matrix compartment. To better assess the mitochondrial phenotype we performed a fluorescent staining using a Tom20 antibody as a mitochondrial surface marker (Figure 3.7 A, B, C, D). Tom20 is a translocase of the outer mitochondrial membrane, central component of the complex responsible for the recognition and translocation of mitochondrial proteins synthesized in the cytosol. Murine skin fibroblasts (MSF) derived from the dorsal skin of Taz KO and wildtype P1 mice were utilised for the experiment.

Overall this staining does not reveal any macroscopic differences between Taz KO and wildtype MSFs. However, when I performed a quantification of the fluorescence using ImageJ, we detected a non-significant 35% reduction in Tom20 fluorescence in Taz KO (Figure 3.7 E). This method offers a rough quantitative estimation of the mitochondrial content of the cells based on the surface area of the image covered by the fluorescent signal associated with the secondary antibody. Normalization to nuclei area helps us ensure fluctuations in the values of mitochondrial fluorescence are not due to the number of cells, but a result of the phenotype.

The technique can be influenced by multiple factors which can invalidate the result, such as a selective upregulation of the specific protein used for mitochondrial detection, which would result in an increase in the fluorescent signal without an actual increase in the number of mitochondria.

This technique, although imperfect, offers an interesting insight in mitochondria biology.

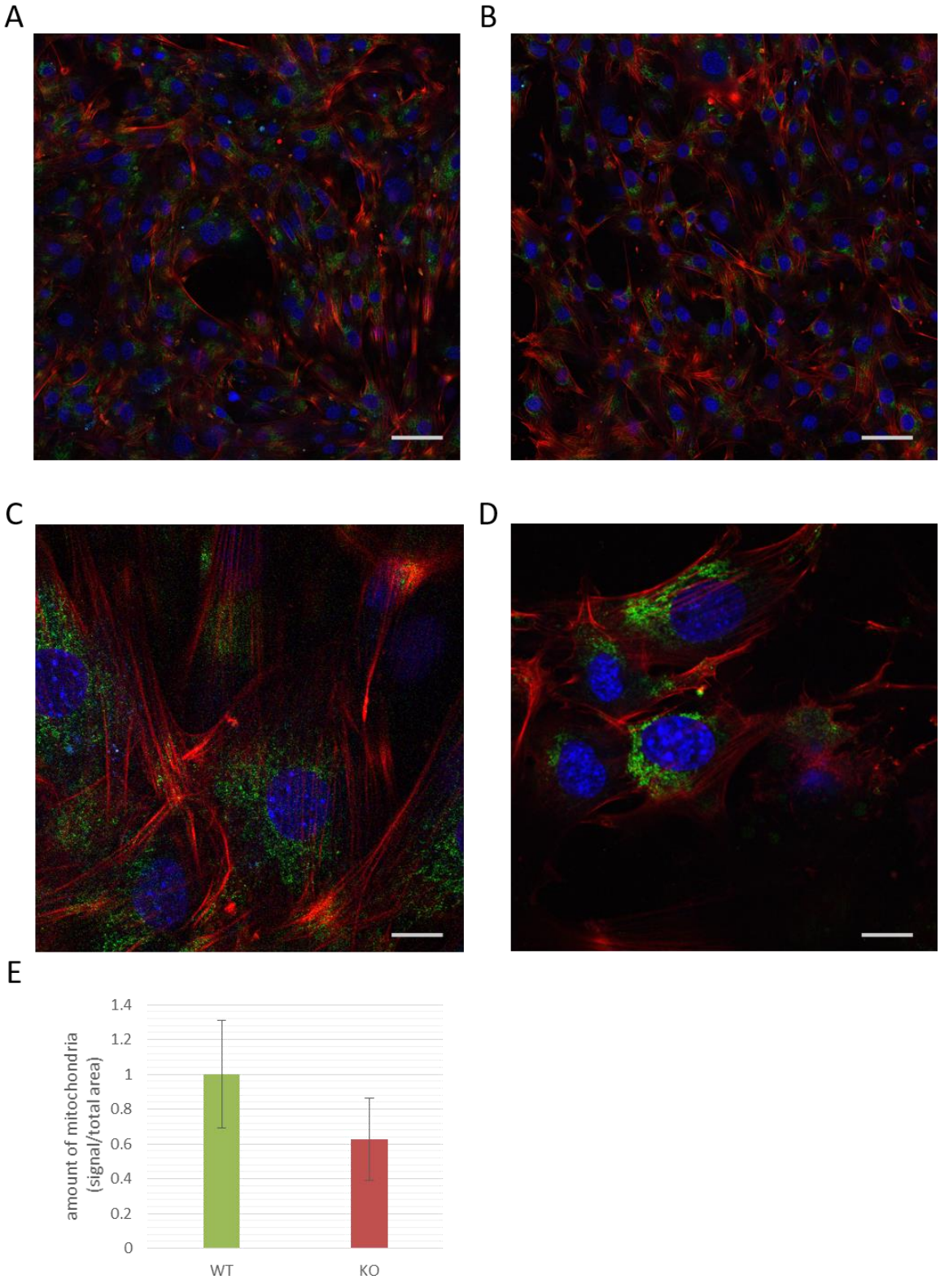

Figure 3.7: Mitochondria numbers are affected by knockout of Taz in skin fibroblasts. A, fluorescent image of wildtype mouse skin fibroblasts (MSF) isolated from P1 mice (scale bar 100µm). B, fluorescent image of Taz KO MSF isolated from P1 mice (scale bar 100µm). C, magnification of A (scale bar 20µm). D, magnification of B (scale bar 20µm). A to D Blue: nuclei stained with DAPI; green: mitochondria stained with Tom20. Red: f-actin

stained with phalloidin E, quantification of the fluorescent signal for mitochondria staining (p=0.891).

Lipid composition data suggests the modifications in phenotype derived from Taz knockout are more pronounced in the heart tissue compared to the rest of the organism. So we performed Tom20 analysis using heart samples.

To obtain a more quantitative measure of Tom20 a western blot on cardiac protein extracts was performed (Figure 3.8 A). The densitometric analysis of the bands identified a 50% reduction of Tom20 in Taz KO cardiac tissue (Figure 3.8 B).

The reduction identified, although non-significant, suggests a reduction in the number of mitochondria caused by the knockout of Taz. However, this reduction could also be related to a downregulation of the expression of Tom20 at a translational and post-translational level, or to a heightened activity of the proteasome. It was decided to perform a quantification of mitochondrial DNA, which would allow us to obtain a measure of the number of mitochondria which would only be dependent on the actual copy number of the mtDNA.

Real-time qPCR was used to test the abundance of mitochondria DNA copies compared to a sequence located in the nuclear DNA. The nuclear DNA probe was designed to anneal with the sequence encoding for the telomerase reverse transcriptase (Tert), mapped on chromosome 5. The mitochondrial probe recognizes the displacement loop (D-loop) sequence located as a stable structure at the origin of replication of mitochondrial DNA.

The data shows a significant ($p \leq 0.05$) 60% reduction in copy number of the mitochondrial DNA in Taz KO hearts, confirming the reduction identified via the quantification of Tom20 (figure 3.8 C).

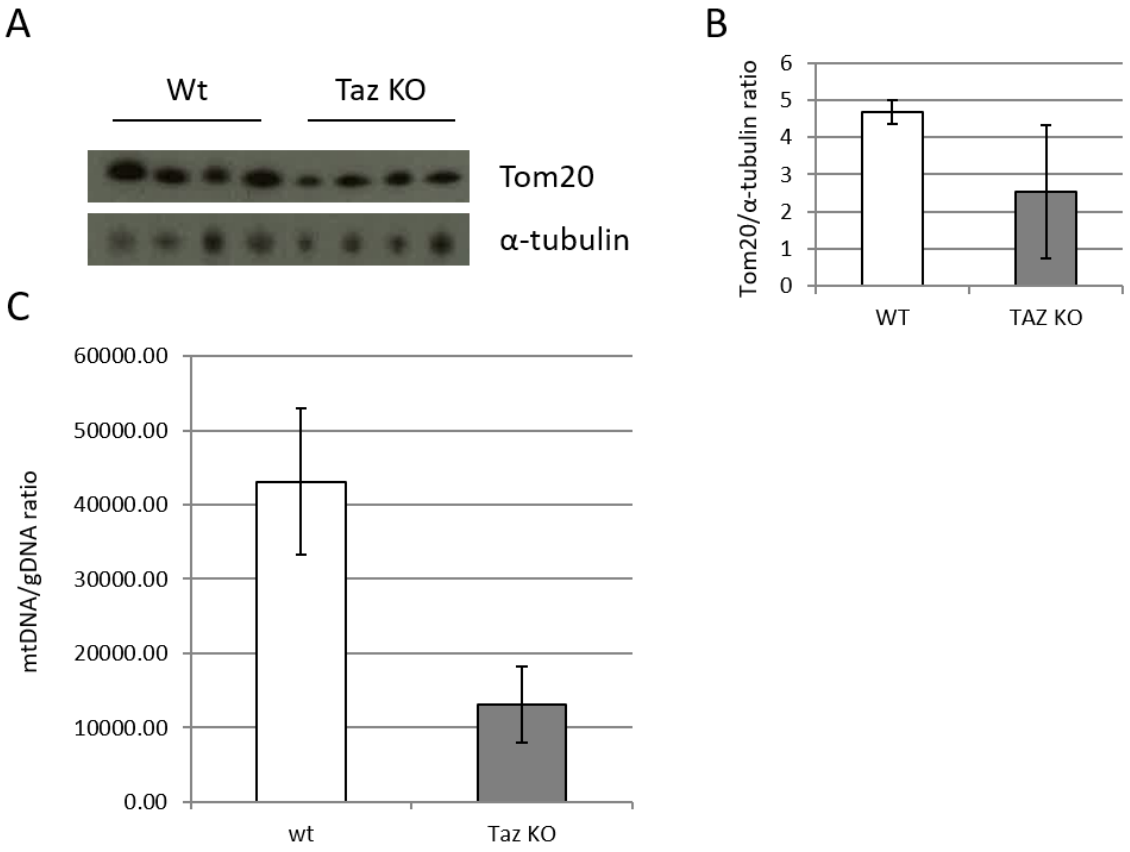

Figure 3.8: Mitochondria numbers are affected by knockout of Taz in the heart. A, western blot for mitochondrial outer membrane Tom20, performed on protein extracts from Taz KO and wildtype hearts. B, Densitometric quantification of A, performed with ImageJ software using α-tubulin as a housekeeping protein ($p=0.94$). C, quantification of mitochondrial DNA in the heart tissue of Taz KO (grey) and wildtype (white) mice using real-time qPCR ($p \leq 0.05$). Statistical significance is calculated using a two-tailed unpaired student T-test.

3.3 Discussion

The data shown in this chapter reveal that knockout of Tafazzin influences lipid maturation and membrane composition. As expected Taz KO results in a reduction of mature cardiolipin and an accumulation of its immature form monolysocardiolipin, accompanied by an increased concentration of the side chains lipid species that are not being used for the production of mature cardiolipin.

The mitochondrial membrane is especially affected by the lack of mature cardiolipin which composes almost 20% of the total lipid portion of the organelle. EM images of the heart tissue show a marked difference in structure between Taz KO and wildtype hearts, with a defect in the ultrastructure of the organelle which is much less densely packed with cristae and much richer in matrix space.

Mitochondria numbers are also affected in our system, with a significant reduction of total mitochondria in Taz KO hearts, measured comparing the amount of mitochondrial DNA to the amount of genomic DNA.

The data presented in this chapter are in partial concordance with observations in BTHS patients and model organisms. Our model shows a significant effect of Taz KO membrane lipid composition, with a dramatic shift in the CL/MLCL ratio. This observation is coherent with the data obtained both in the model organisms and in BTHS patients. Cell ultrastructure is also modified in the heart, resulting in defects of the mitochondria structure, coherent with the data from BTHS patients (Barth et al., 1983). However, in contrast with the data obtained from human patients (Barth et al., 1983), we were not able to identify any defect in cardiac muscle fibre organization. There is no consensus over the number of mitochondria in BTHS samples. Phoon et al. produced a study using the Taz KD model in which they detected an approximate 50% reduction in the embryonic number of mitochondria ($p<0.0001$) that was however lost in the newborn which exhibited normal mitochondria numbers (Phoon et al., 2012). However, more recent works have shown an approximate 60% increase in mtDNA ($p<0.05$) in Taz KD compared to the wildtype (Huang et al., 2017). Our data is in sharp contrast with this report, showing an approximate 60% reduction of the mtDNA content in Taz KO hearts.

This result could be due to the substantial difference of the two model systems and further investigation of this matter is required.

3.2. Metabolic profiling of Taz mice shows alterations in the heart but not in other tissues

3.2.1 Taz Knockout alters multiple metabolic pathways in the adult heart

Data gathered in model organisms suggested a recognizable effect of Taz KO on the metabolic pathways of yeast, with disruption of the TCA cycle and the electron transport chain (Smith et al., 1974, Wang et al., 2014, Gonzalvez et al., 2013).

To understand whether defects in mitochondria organization, detected in our model, affected the normal metabolic pathways in knockout mice tissue, it was decided to measure the concentration of several intracellular metabolites via mass spectrometry (mass spec) using samples derived from heart, liver and skeletal muscle of adult Taz KO mice.

We performed targeted analysis of hydro soluble metabolites of the cells and analysed a representative selection of the main metabolic pathways. The mass spec. data reveal a very recognizable phenotype, which is, surprisingly, extremely specific to the heart tissue (Figure 3.9).

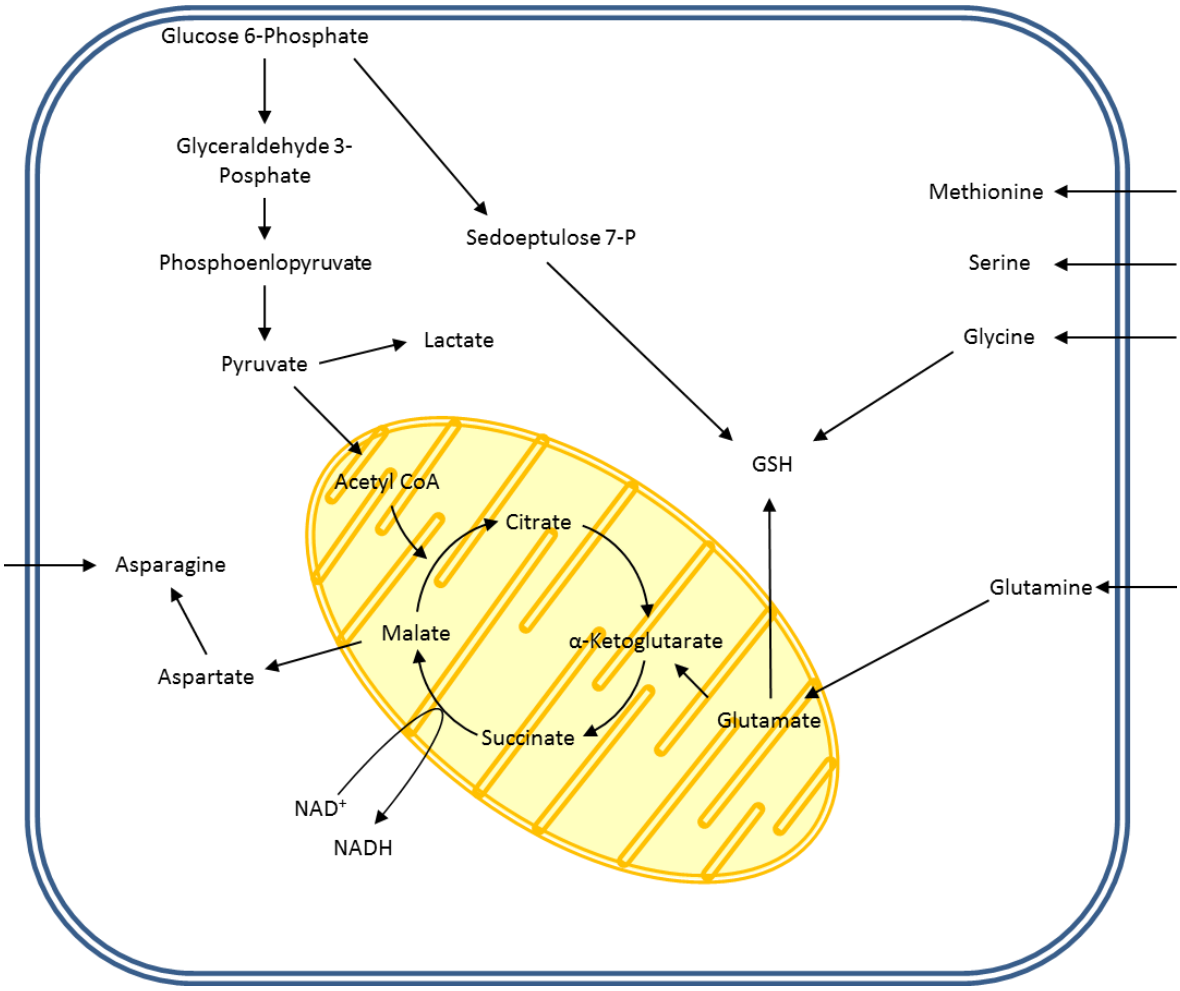

Figure 3.9: Schematic representation of a cell with the principal metabolites influenced by Taz knockout for the principal metabolic pathways. Blue double line: cell limit. Yellow organelle: mitochondrion.

3.2.1.1 Alterations in Glycolysis do not affect carbon content entering TCA cycle

Mass spec data revealed an extensive alteration in most intermediates of the glycolytic pathway. The measurable intermediates in heart tissue appear to be strongly downregulated for the initial phases of the pathway with glucose 6-Phosphate (G6P) concentration measured to be 1/4 in Taz knockouts compared to the wildtype ($p=0.0040$). This trend is respected in skeletal muscle with a ~3 fold decrease in measured levels of G6P, while it does not appear to be present in liver tissue (Figure 3.10, A).

The trend of downregulation for glycolysis metabolites in heart is respected in subsequent intermediates of the pathway with Glyceraldehyde 3-Phosphate (G3P) concentration halved in the knockouts compared to the wildtypes ($p=0.0181$). No significant variation is however detected for G3P concentration in either skeletal muscle or liver (figure 3.10, B).

Phosphoenolpyruvate (PEP) levels were also measured in Taz knockout tissues compared to wildtype and again the concentration is halved in heart ($p=0.0002$) and skeletal muscle and unchanged in liver (Figure 3.10, C).

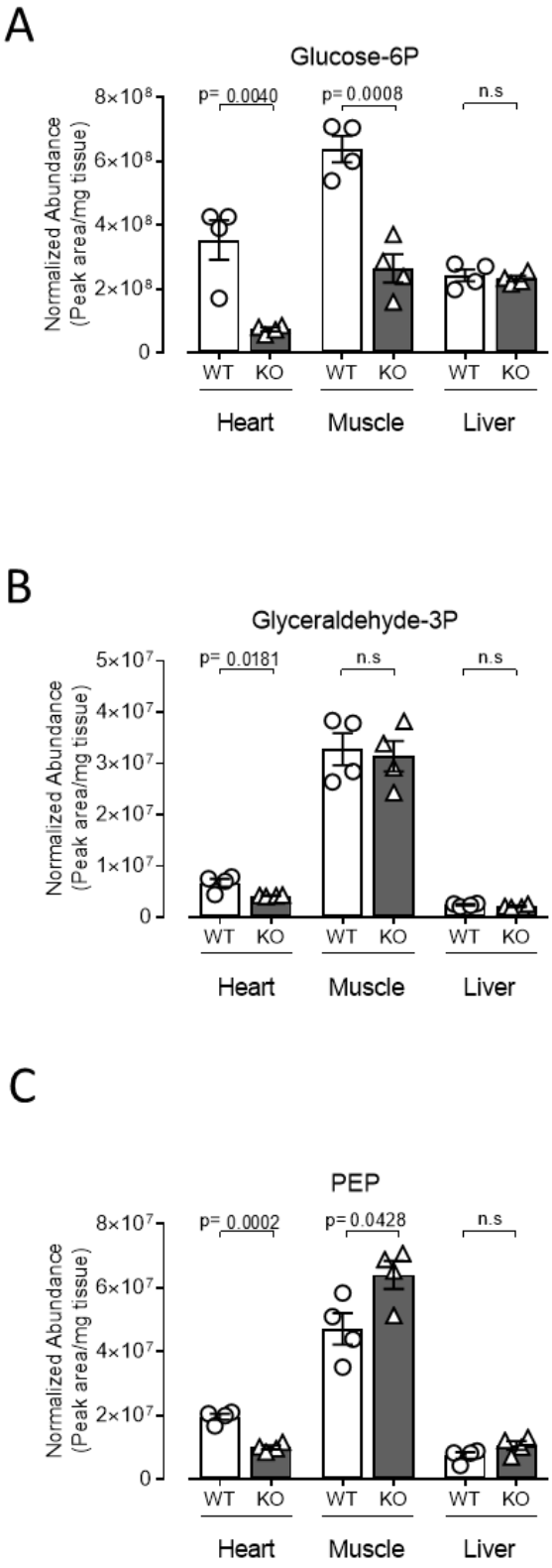

Figure 3.10: Taz Knockout significantly affects Glycolysis in Taz mice hearts, but not in other tissues. Relative abundance of key intermediates of the glycolytic pathway measured via mass spectrometry and normalized. A Glucose 6-Phospate; B Glyceraldehyde 3-Phosphate; C Phosphoenolpyruvate. Significance is measured using an unpaired two-tailed student T Test.

These changes however are not carried on to the end of the pathway. The data clearly show that the amount of pyruvate (Pyr) produced in both knockouts and wildtypes is unvaried in all examined tissues, with non-significant fluctuations of the concentration levels (Figure 3.11, A). The levels of Pyr are probably kept constant by an augment in the activity of the lactate dehydrogenase, which converts lactate into pyruvate and vice versa. Consistently the measured levels of lactate are significantly diminished in knockout mice hearts ($p=0.0142$), however this trend is conserved across all the tissues examined, hinting to a more widespread de-regulation of lactate dehydrogenase activity, directly linked to the knockout genotype (Figure 3.11, B).

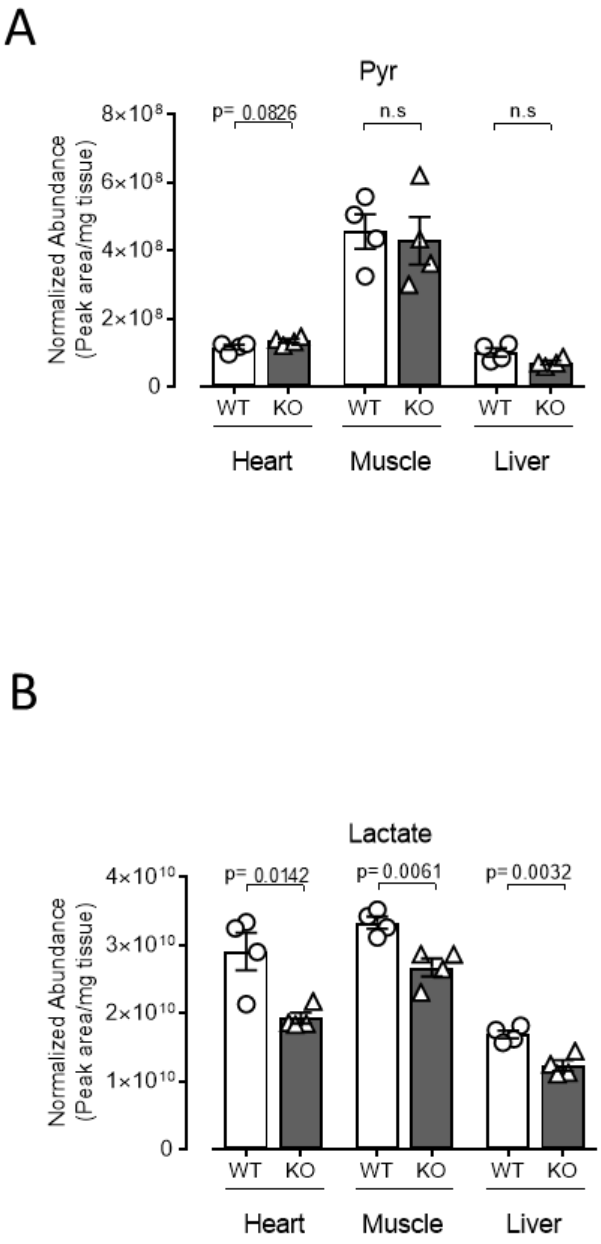

Figure 3.11: Taz Knockout does not alter the carbon intake into TCA cycle compensating lower overall glycolysis rate with diminished production of lactate. Relative abundance of A Pyruvate and B Lactate in heart, skeletal muscle and liver samples from adult mice. Measures obtained via mass spectrometry and normalized. Significance is measured using an unpaired two-tailed student T Test.

3.2.1.2 Tricarboxylic acid cycle is widely deregulated in Taz KO mice

In depth analysis of the metabolic intermediates of the Tricarboxylic acid (TCA) cycle reveals a widespread deregulation of the levels of most metabolites involved. The amount of carbon entering the cycle as Acetyl-CoA (AcCoA) is not significantly changed in all the examined tissues (Figure 3.12, A), however we detected a significant rise in the concentration of the first two detectable metabolites of the pathway with a 30% increase in Citrate and αKetoglutarate (αKG) concentration in the heart of KO animals ($p=0.0002$ and $p=0.0147$ respectively) (Figure 3.12, B, C). The 30% increase in citrate levels is also detected in the liver, but there are no significant changes in liver concentration of αKG. Skeletal muscle levels, for both metabolites, are unchanged.

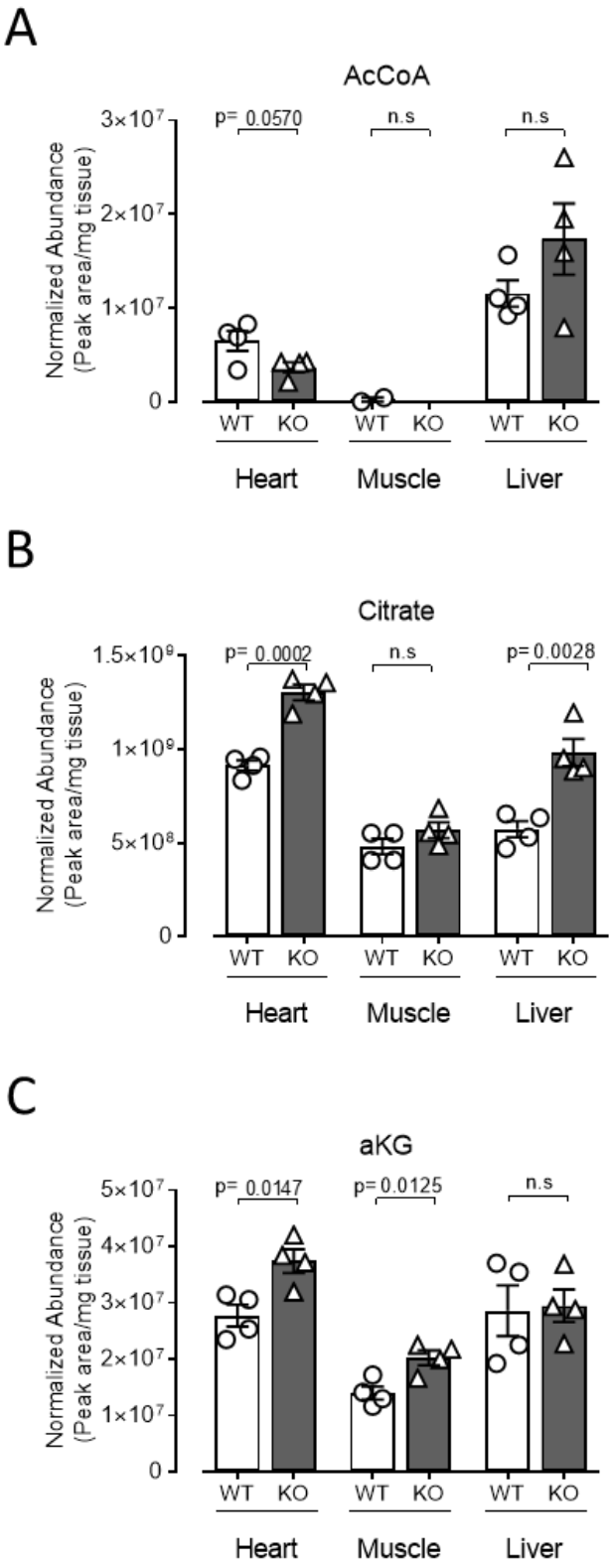

Figure 3.12: unchanged carbon intake in TCA cycle results in upregulated metabolic intermediates for the first part of the cycle. Relative abundance of A Acetyl CoA, B Citrate and C αKetoglutarate in heart, skeletal muscle and liver samples from adult mice measured via mass spectrometry and normalized. Significance is measured using an unpaired two-tailed student T Test.

αKG proceeds through the TCA cycle and it is transformed in Succinate by αKG-dehydrogenase. We measured the levels of this metabolite and detected an inversion of the upregulation trend, 30% reduction in the levels of succinate in the heart of the KO mice compared to the wildtype, the reduction is not present in the other examined tissue (Figure 3.13, A).

Concentration of the following intermediate of the TCA cycle, malate, is unchanged in the KOs compared to the wildtypes (Figure 3.13, B).

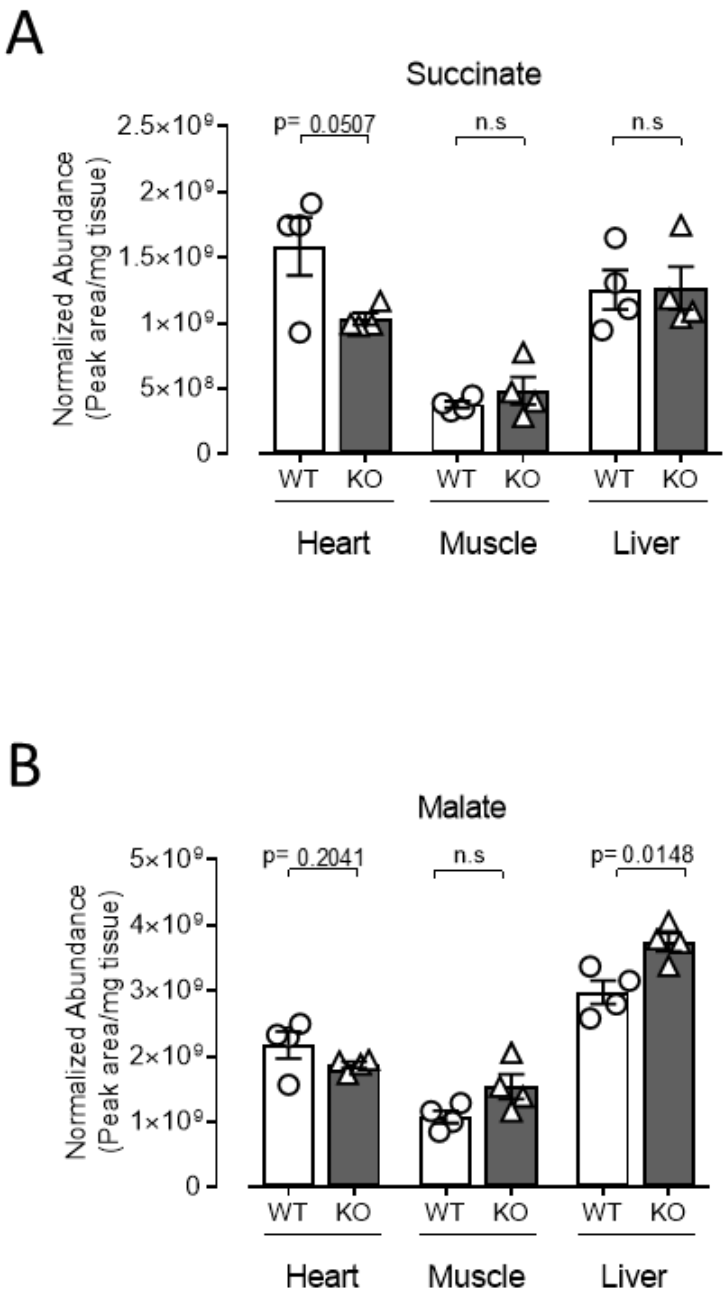

Figure 3.13: Regulation of the TCA cycle shift in final intermediates of TCA cycle. Relative abundance of A Succinate and B Malate in heart, skeletal muscle and liver samples from adult mice, measured via mass spectrometry and normalized. Significance is measured using an unpaired two-tailed student T Test.

These changes in the metabolic balance of the TCA cycle, however, do not reflect in a difference in the energy charge of the cells. The adenylate charge (measured using the equation in figure 3.14, A.), remains unchanged in all tissues examined, suggesting ATP production is somehow not affected by the metabolic changes (Figure 3.14, A).

$NADH/NAD^+$ ratio is sharply reduced in KO hearts compared to the wildtype but unchanged in the other tissues examined (Figure 3.14, B). The measurement correlates with the increase in concentration of αKG. αKG-dehydrogenase catalyses the reduction of NAD^+ to NADH as a by-product of its conversion of αKG to succinyl-CoA. It has been reported that the action of the enzyme is inhibited by decrease of the $NADH/NAD^+$ ratio through a product inhibition mechanism (Smith et al., 1974, Gabriel and Plaut, 1984). $NADH/NAD^+$ ratio does not seem to be affecting the concentration of other NAD^+-dependent metabolites, this suggests additional mechanisms are contributing to the inhibition of the αKG-dehydrogenase.

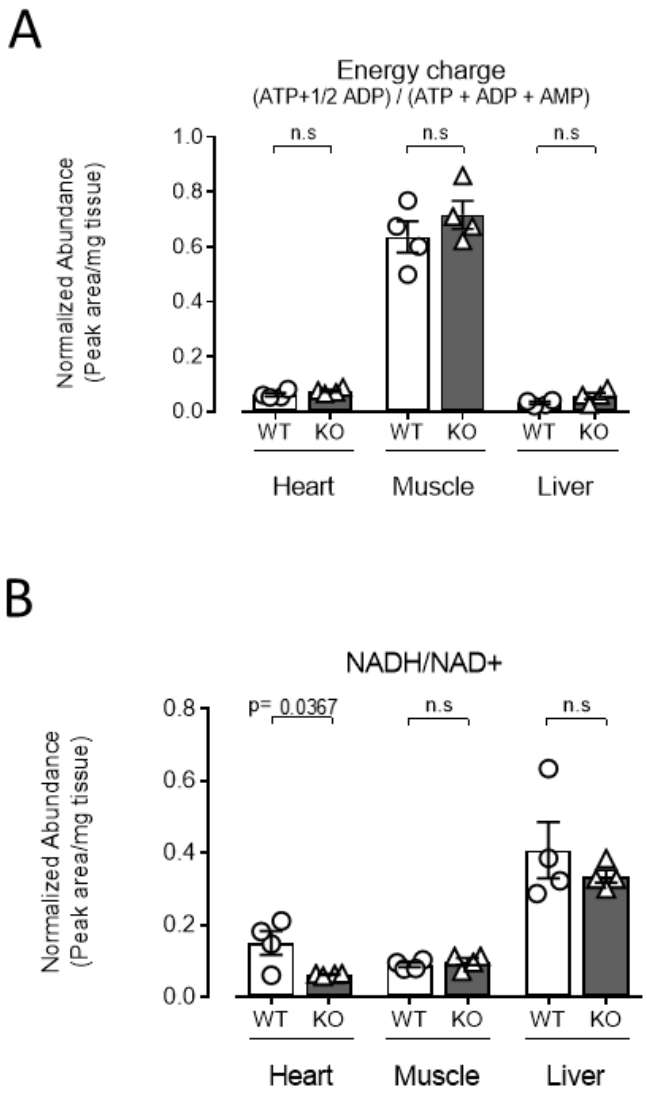

Figure 3.14: Taz Knockout does not alter Energetic balance in heart, muscle or liver tissue (A). NADH production is affected in heart and liver. A ATP balance measured as the ratio of ATP+1/2ADP / ATP+ADP+AMP, B NADH/NAD+ ratio. Relative abundance of the metabolites is measured via mass spectrometry and normalized. Significance is measured using an unpaired two-tailed student T Test.

3.2.1.3 Neutral amino acid balance is altered in Taz KO hearts

Mass spec data also reveals a sharp increase in the concentration of several neutral amino acids: Methionine (Met), Serine (Ser) and Glycine (Gly) are strongly upregulated across all examined tissue, with the highest level of upregulation in the heart (Figure 3.15, A, B and C). Within this group, Ser and Gly present the most striking upregulation 2 and 3 fold respectively, showing significant alteration in amino acid metabolism across all tissue.

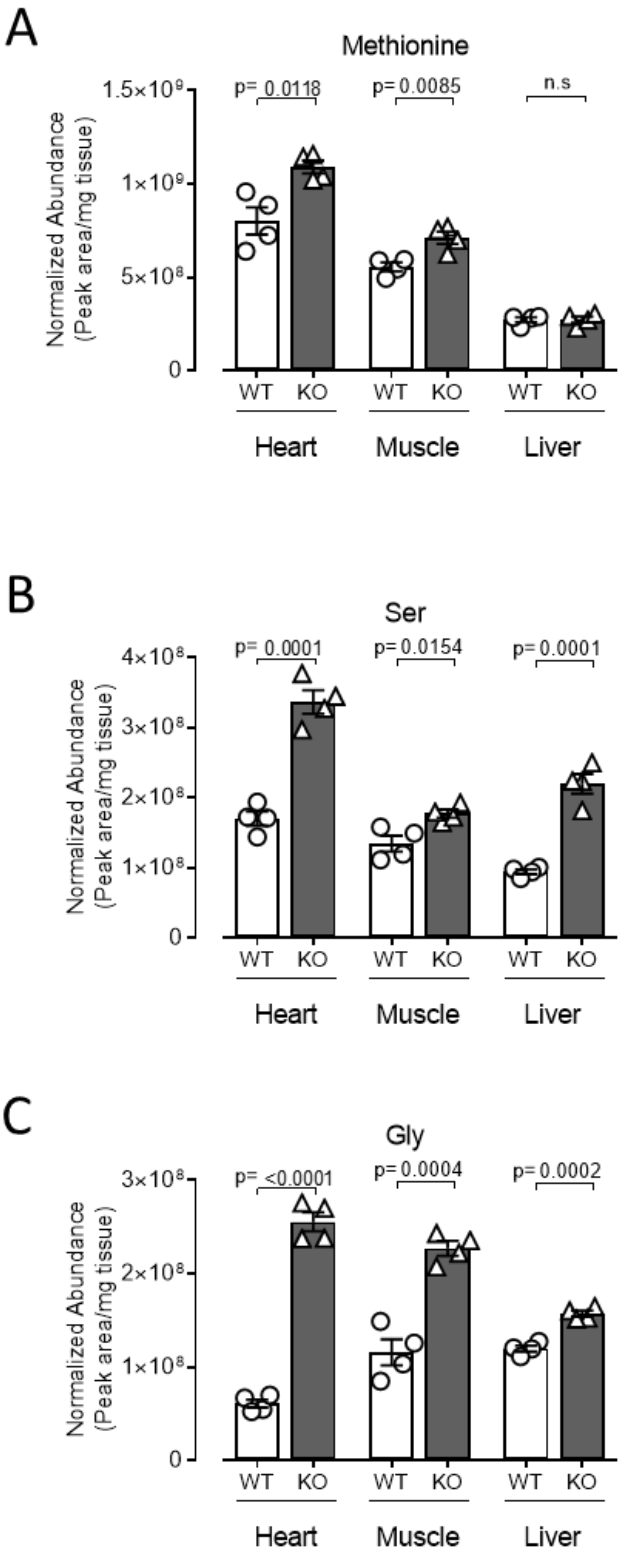

Figure 3.15: Neutral aminoacid concentration is increased in Taz knockouts compared to the wildtype in several tissue samples. Relative abundance of A Methionine, B Serine and C Glycine in heart, skeletal muscle and liver samples from adult mice, measured via mass spectrometry and normalized. Significance is measured using an unpaired two-tailed student T Test.

Asparagine (Asn), another member of the neutral amino acid group, presents a 3 fold augmented concentration in KO hearts, but not in any other examined tissue (Figure 3.16, A). Aspartate (Asp), which is derived from Asn via Asparagine synthase (Asns), is even more significantly upregulated with a 4 fold increase of its already high levels. Similarly to Asn data, Asp deregulation in KO mice is also only present in heart tissue, with no variation at all in skeletal muscle and liver (Figure 3.16, B).

Finally we examined Glutamine (Gln) levels which showed no alteration in any of the tested tissue (Figure 3.16, C). Conversely the heart-specific deregulation is again significant in Gln's derived amino acid, Glutamate (Glu) which shows a 30% increase in the heart of KO mice compared to the wildtype (Figure 3.16, D).

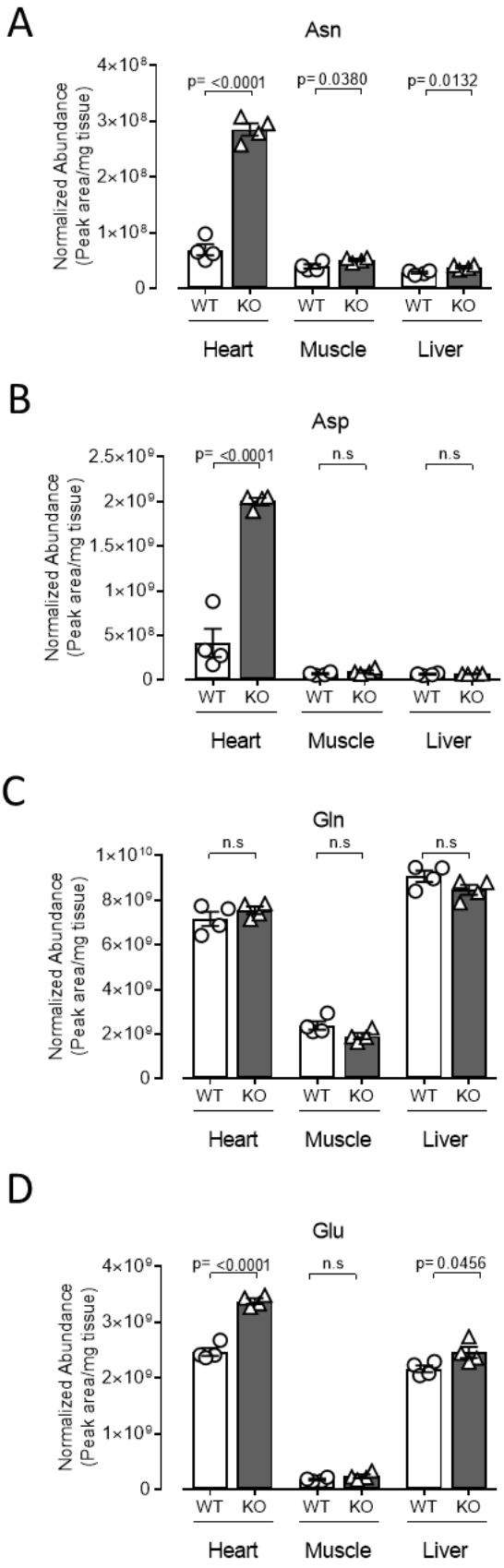

Figure 3.16: Asparagine and Aspartate levels are sharply increased in Knockout vs wildtype hearts, but not in other tissue (A and B). Glutamine levels are constant, but Glutamate is significantly increased in heart (C and D). Relative abundance measured via mass

spectrometry and normalized. Significance is measured using an unpaired two-tailed student T Test.

3.2.1.4 Redox potential does not seem to be affected by knockout of Taz gene

Mass spec data allowed us to measure Glutathione (GSH) global concentration in our tissues of reference. Data shows no detectable alteration in GSH concentration (Figure 3.17, A). We then proceeded to examine the ratio of GSH and its reduced form Glutathione disulphide (GSSG). The measure is slightly decreased in Taz KO hearts even though the difference does not appear significant (Figure 3.17, B).

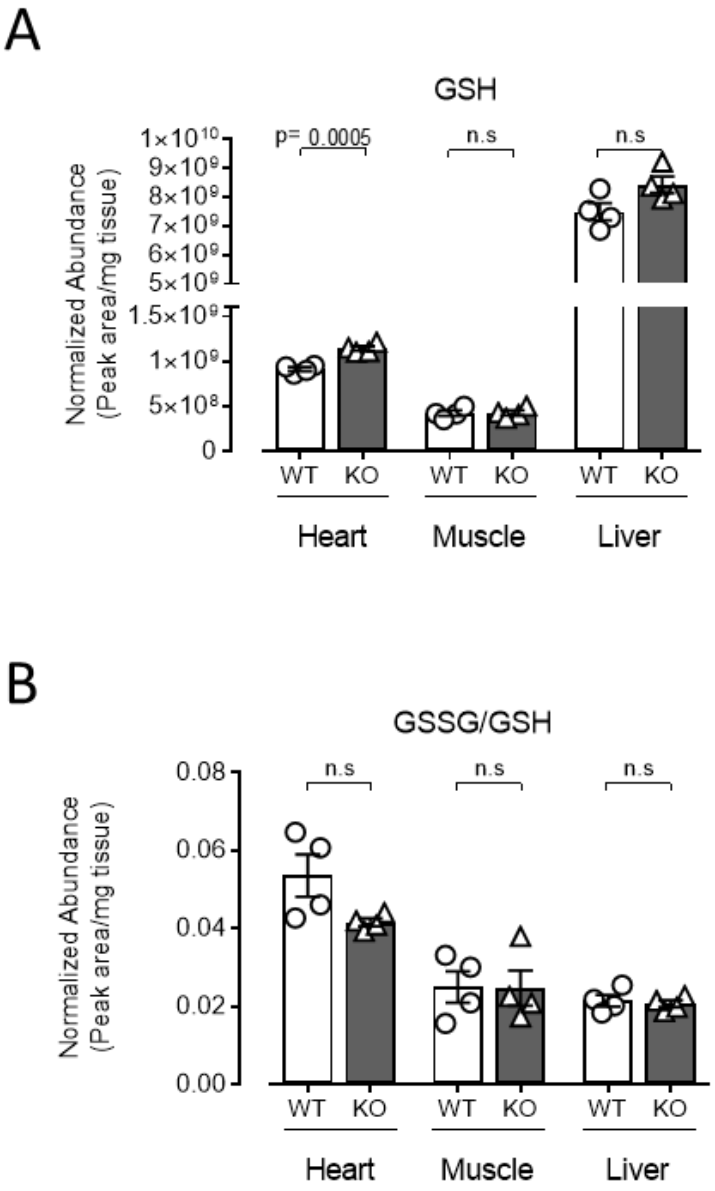

Figure 3.17: Glutathione concentration remains constant in all examined tissue (A). Glutathione disulfide/ Glutathione ratio is not significantly altered in knockout mice's hearts. Relative abundance of the metabolites is measured via mass spectrometry and normalized. Significance is measured using an unpaired two-tailed student T Test.

3.2.2 Alterations in the metabolism do not seem to affect respiration in cardiac cells

Mitochondria are central to the energetic production of the cell. ATP is produced via various metabolic and electrochemical processes and is then utilized as an energy supply for many reactions in the cell.

Taz KO mice show an altered mitochondria membrane composition and in the previous sections we showed the alterations to the metabolism caused by the mutation. However, we also showed that the total ATP balance in substantially unchanged.

Our results point to a very specific influence of Taz KO on cardiac-specific phenotypes.

Neonatal rat cardiomyocytes are a well-established system for the study of cardiomyopathies and heart defects (Louch et al., 2011), so we decided to adapt this model to our transgenic mice to investigate whether cardiolipin defects caused by the knockout of Taz were affecting the mitochondrial respiration rate in heart tissue.

3.2.2.1 Taz KO hearts do not show any detectable change in mitochondrial respiration rate

To analyse mitochondria respiration rate, we performed the Agilent Seahorse assay using cardiomyocytes extracted from postnatal day 1 (P1) Taz KO and wildtype mice.

The assay consists of multiple automated readings of pH and oxygen concentration performed both in native state and after the injection in the culture wells of drugs that interfere with components of the electron transport chain apparatus. The system performs repeated readings of the oxygen concentration and pH of the culture medium then elaborates the readings and presents the data as oxygen consumption rate (OCR) and extracellular acidification rate (ECAR).

The readings surprisingly show no significant difference between KOs and wildtypes. Both OCR and ECAR are not significantly altered, showing that mitochondria respiration does not seem to be affected by the mitochondrial phenotypes (Figure 3.18).

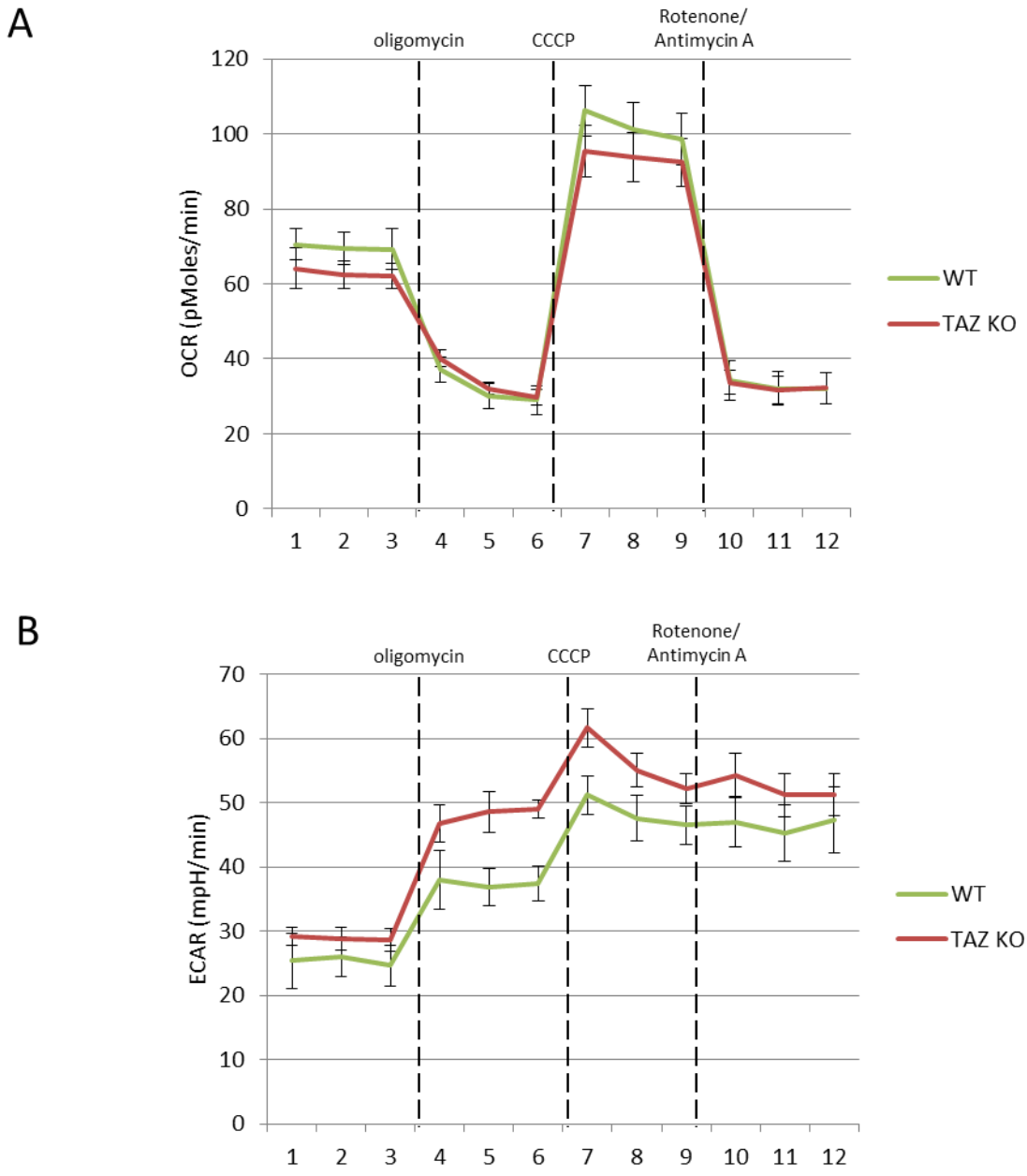

Figure 3.18: Mitochondria respiration rate is not altered in wildtype vs Taz KO cardiomyocytes. (A) Oxygen consumption rate measured over time (pMoles/min) in wildtype (green) vs Taz KO (red). (B) Extracellular acidification rate measured over time (mpH/min) in wildtype (green) vs Taz KO (red) ($p>0.05$).

To assess whether the lack of variation was a heart specific phenotype we performed Seahorse assays using different cell populations.

Firstly, skin fibroblasts obtained from the back of P1 Taz KO and wildtype mice were used as a representative line for differentiated cell types. Consistently with the cardiomyocytes results, fibroblasts did not show any difference in the OCR and ECAR readings (Figure 3.19 A, B).

Then wildtype embryonic stem cells and their Taz KO counterparts were used, but again there was no difference between the 2 populations (Figure 3.19, C, D).

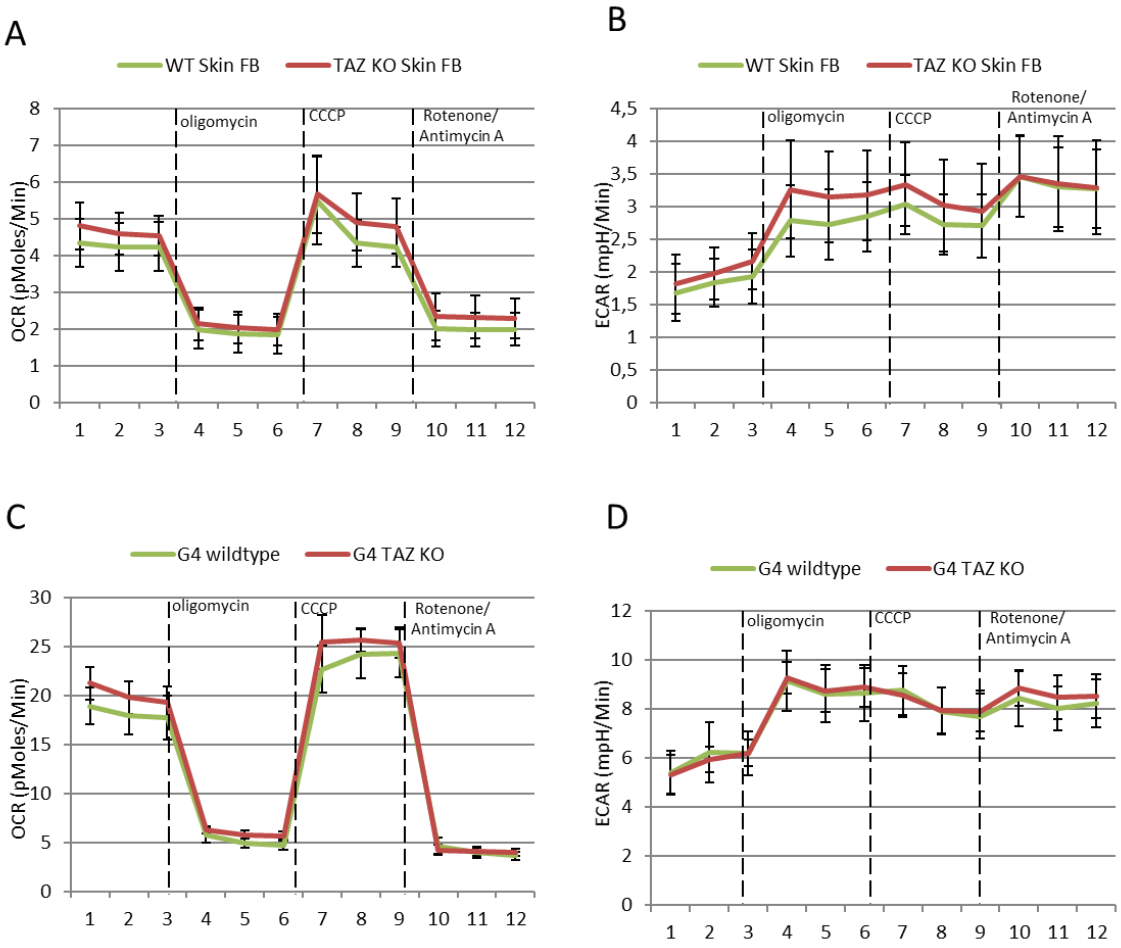

Figure 3.19: Mitochondria respiration rate is not altered in wildtype vs Taz KO cells. (A) Oxygen consumption rate measured over time (pMoles/min) in wildtype (green) vs Taz KO (red) mouse skin fibroblasts. (B) Extracellular acidification rate measured over time (mpH/min) in wildtype (green) vs Taz KO (red) mouse skin fibroblasts. (C) Oxygen

consumption rate measured over time (pMoles/min) in wildtype (green) vs Taz KO (red) G4 ESCs. (B) Extracellular acidification rate measured over time (mpH/min) in wildtype (green) vs Taz KO (red) G4 ESCs.

3.2.3 The metabolic signature of neonatal heart is different from adult

Seahorse results are in contrast with our previous observations of a striking metabolic and energetic phenotype in the heart of Taz KO mice.

To investigate the mechanisms behind this anomaly we decided to test P1 mice hearts and livers for metabolic content using mass spectrometry. For this experiment we decided to focus on these tissues as, based on the adult's metabolomics and the lipid composition analysis, it was our opinion that heart and liver would yield more convincing results compared to the skeletal muscle.

Surprisingly neonatal hearts of Taz KO mice show less significant changes in metabolites content compared to their wildtype littermates.

3.2.3.1 Glycolysis is less impacted from Taz Knockout in the P1 mice compared to the adults

Metabolic content of glycolytic intermediates in P1 Taz KO mice shows a reduction in the trends exhibited by the adults.

Glucose-6 Phosphate (G6P) maintains the trend for reduction in the KO hearts compared to the wildtype, with roughly 50% downregulation of the metabolite in the KOs. However, this reduction of the metabolite is not as striking as it was in the adults where G6P content in the wildtypes was 4 times higher than in the controls (Figure 3.20, A).

The trend of reduction is maintained also for Glyceraldehyde-3 Phosphate (G3P) which is reduced by 50% in Taz KO hearts compared to their wildtype littermates (Figure 3.20, B). This downregulation is coherent with the observation in the adult hearts.

The trend is then lost in the last 3 metabolites examined, in fact we cannot detect any significant change in the levels of Phosphoenolpyruvate (PEP), Pyruvate (Pyr) and Lactate (Lac) (Figure 3.20, C, D, E).

Levels of the metabolites in liver samples remain substantially unchanged for all the metabolites measured, showing again a difference between the P1 mice and their adult counterparts where we could detect a deregulation in Lac content across all tissues examined which is not present in the newborn mice.

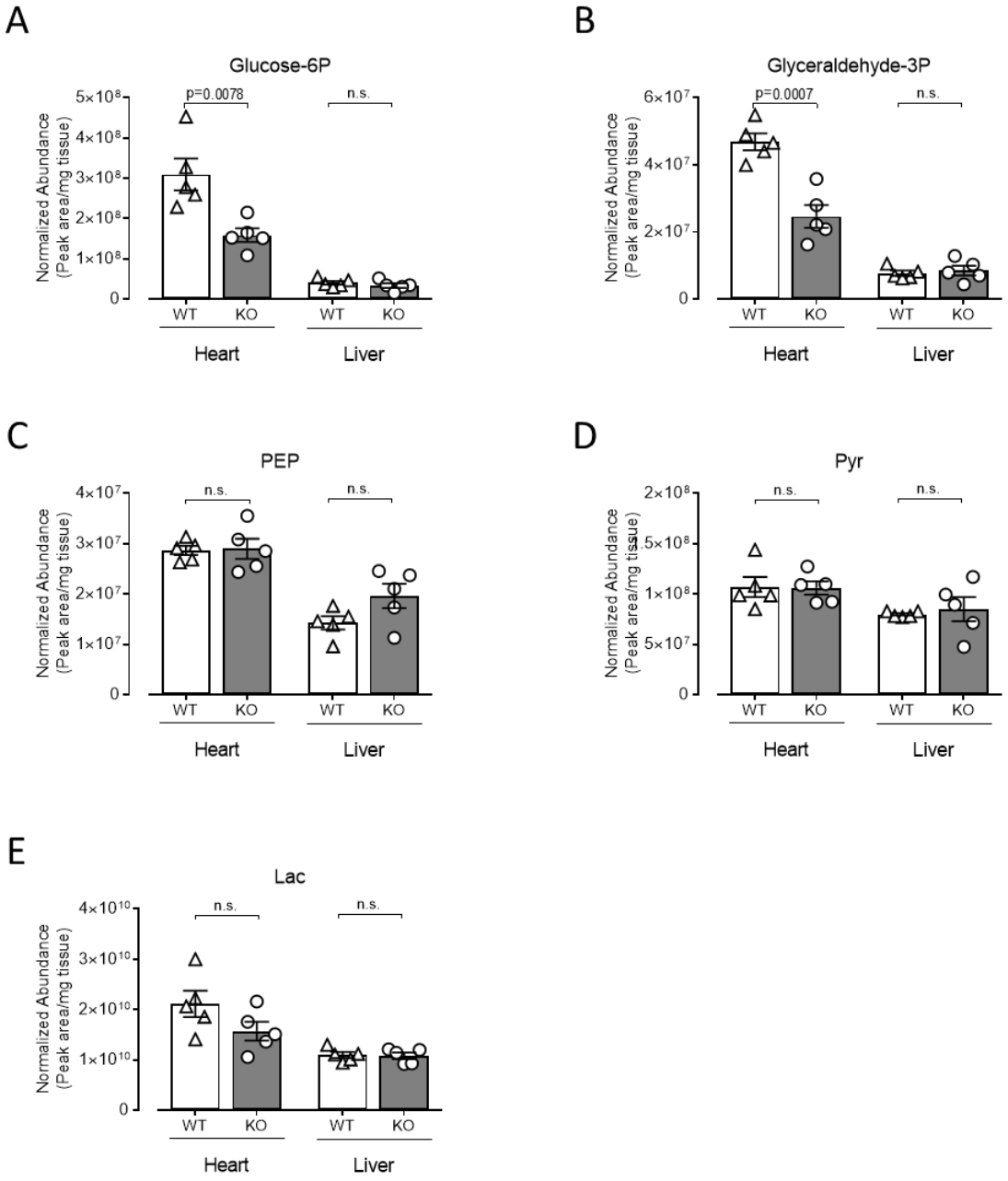

Figure 3.20: Effect of Taz Knockout on the glycolytic pathway in newborn mice. Relative abundance of metabolites of the glycolytic pathway. Abundance is measured via mass spectrometry and normalized. Significance is measured using an unpaired two-tailed student T Test.

3.2.3.2 TCA cycle metabolic profile in P1 mice shows fewer alterations than in the adults

Analysis of the metabolite content for TCA cycle intermediates shows a wide difference between P1 mice and the adults.

Citrate levels are unchanged in Taz KO mice compared to the wildtype (Figure 3.21, A). This data differs from the readings in the adult which showed a 30% increase in Citrate levels for Taz KO hearts and livers.

α-Ketoglutarate (α-KG) levels are also not significantly changed in the hearts of P1 KO mice. Conversely, we detected a sharp 25% increase in α-KG levels for the KOs compared to the wildtypes in adult hearts.

Liver levels of the metabolite are unchanged for both the adults and the P1 mice (Figure 3.21, B).

Succinate levels were remarkable in the adults because they inverted the upregulation trend we had in our results for the first metabolites of the TCA cycle, with a 30% reduction of the abundance of succinate in Taz KO mice compared to the wildtype.

This change is somehow reversed in P1 mice with a 30% upregulation of Succinate content in the Knockout hearts compared to the wildtype. No significant changes were detectable in the liver levels in concordance with what was observed in the adults (Figure 3.21, C).

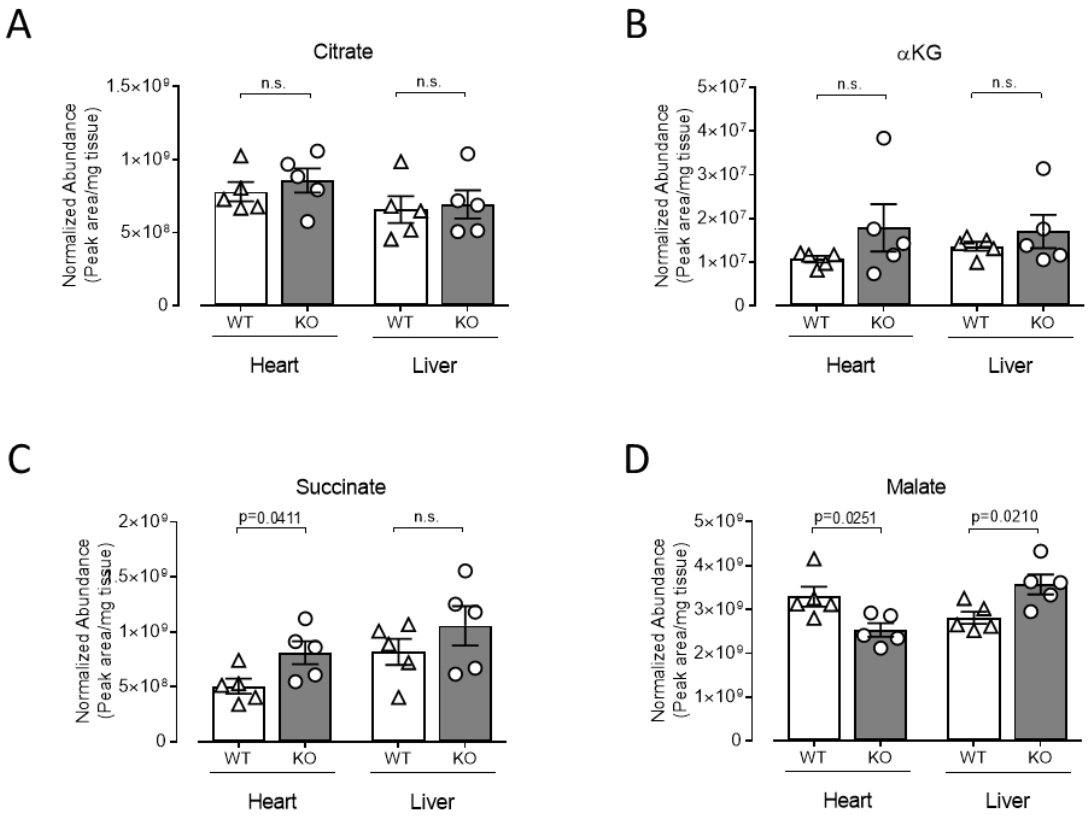

Figure 3.21: knockdown of Taz in newborn mice has minor effects on TCA cycle intermediates concentration. Relative abundance of the metabolites is measured via mass spectrometry and normalized. Significance is measured using an unpaired two-tailed student T Test.

Malate content is again different in adult vs P1 mice with the levels being unchanged in the former and a 20% reduction in the Kos in the latter (Figure 3.21, D). Liver metabolic content of the metabolite is increased by 25% in the knockouts. The measure fits with what was observed in the adults.

3.2.3.3 Neutral amino acid balance presents minor alterations in Taz KO hearts for P1 mice

Methionine (Met), Serine (Ser) and Glycine (Gly) content was sharply increased in adult mice's hearts (30%, 2 fold and 3 fold respectively). However, P1 mice show a different expression profile between Taz KO and wildtype hearts, with Met unchanged, Ser reduced by 40% and Gly increased by 40% (Figure 3.22, A, B, C).

The most striking difference between Taz KO and wildtype readings in the adult was found in the levels of Asparagine (Asn) and Aspartate (Asp) which were increased by 3 and 4 fold respectively. This change was not present in P1 mice with levels of the metabolites being not significantly altered between the two genotypes examined (figure 3.23, A, B).

Glutamine levels in P1 mice are unchanged between the 2 genotypes in concordance with the adult readings (Figure 3.23, A). Glutamate levels show a reversion in the trend observed in the adult heart with a 20% reduction in the levels in P1 mice in contrast with the 20% augment in the relative abundance detected in the adults (Figure 3.23, D).

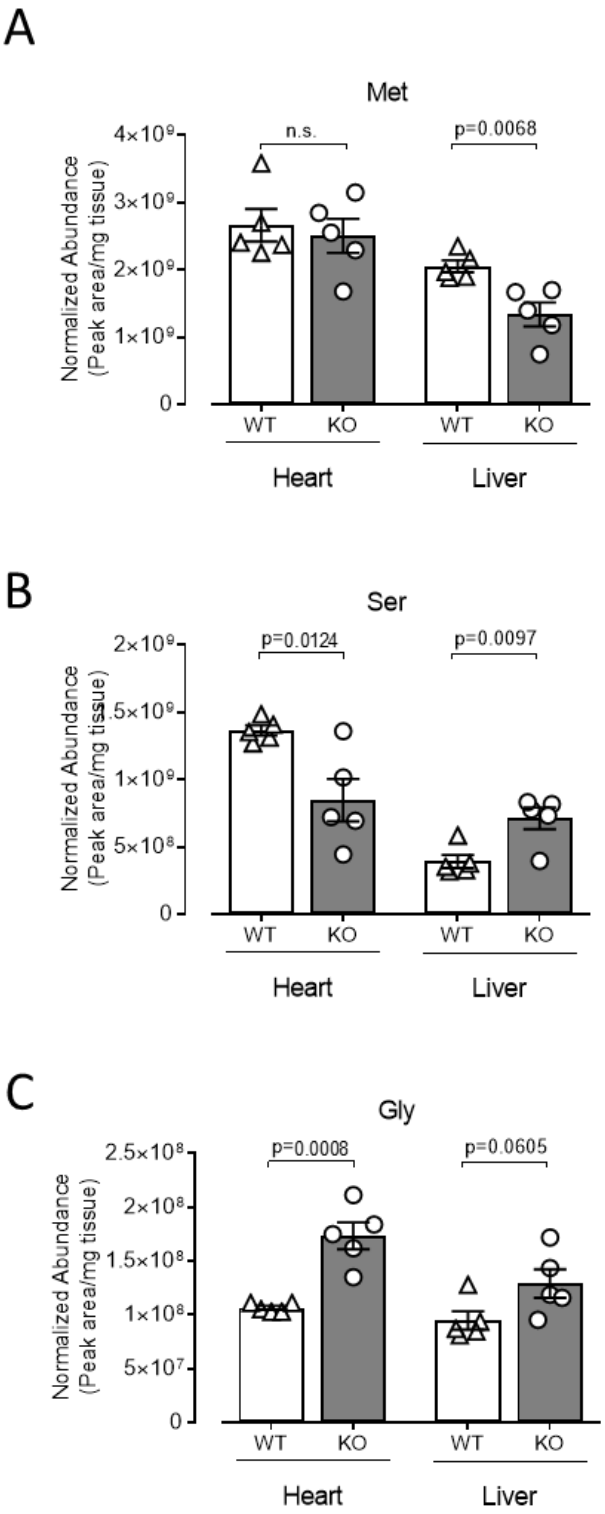

Figure 3.22: Neutral amino acid concentration in tissue from P1 mice shows variable regulation of the metabolites. Relative abundance of A Methionine, B Serine and C Glycine in heart, skeletal muscle and liver samples from adult mice, measured via mass spectrometry and normalized. Significance is measured using an unpaired two-tailed student T Test

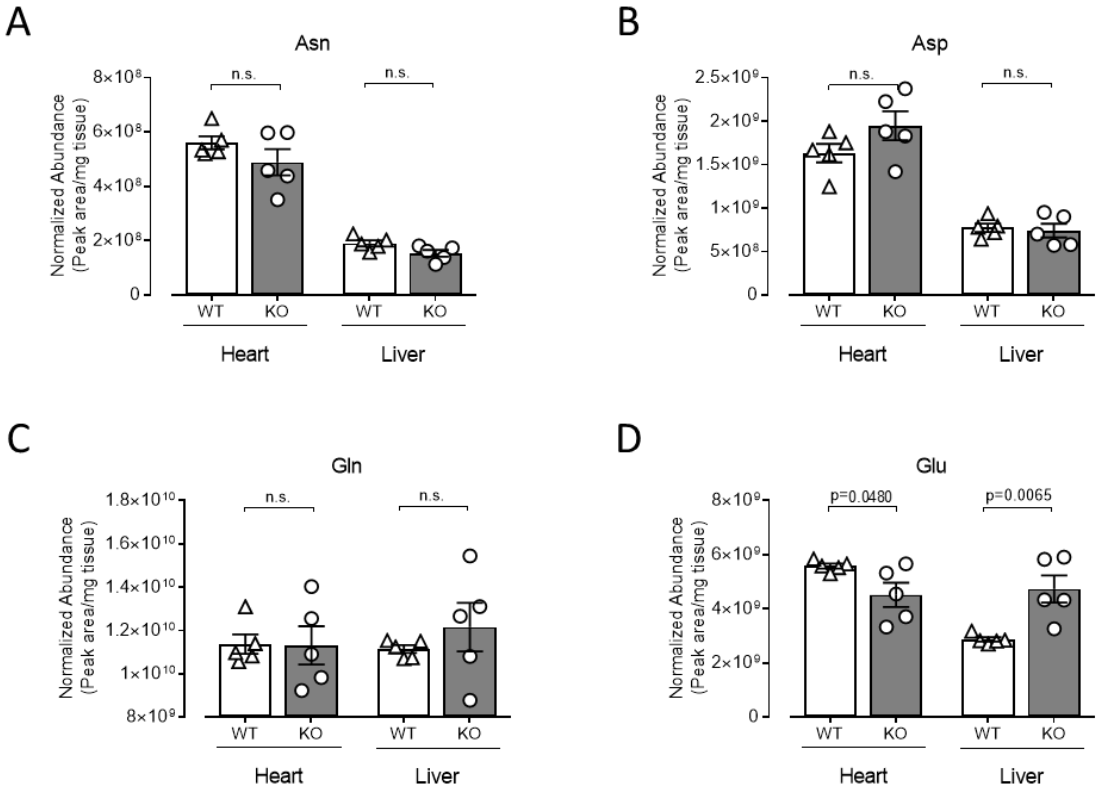

Figure 3.23: Asparagine and Aspartate levels are unchanged in P1 Knockout vs wildtype tissue (A and B). Glutamine levels are constant, but Glutamate is significantly reduced in heart and increased in liver (C and D). Relative abundance measured via mass spectrometry and normalized. Significance is measured using an unpaired two-tailed student T Test.

3.2.3.4 Redox potential is affected by knockout of Taz in P1 mice

Glutathione (GSH) levels in the heart and liver of P1 Taz Knockout mice are reduced by 30% compared to their wildtype counterparts (Figure 3.24, A). This differs from what was observed in the adults where there was no change in the levels between the 2 genotypes.

The change in GSH levels reflects in a change in the ratio between GSH and its reduced form, Glutathione disulphide, which is increased by 50% in P1 Taz KO mice compared to the wildtype (Figure 3.24, B), pointing to a lower oxidative potential in the heart and liver.

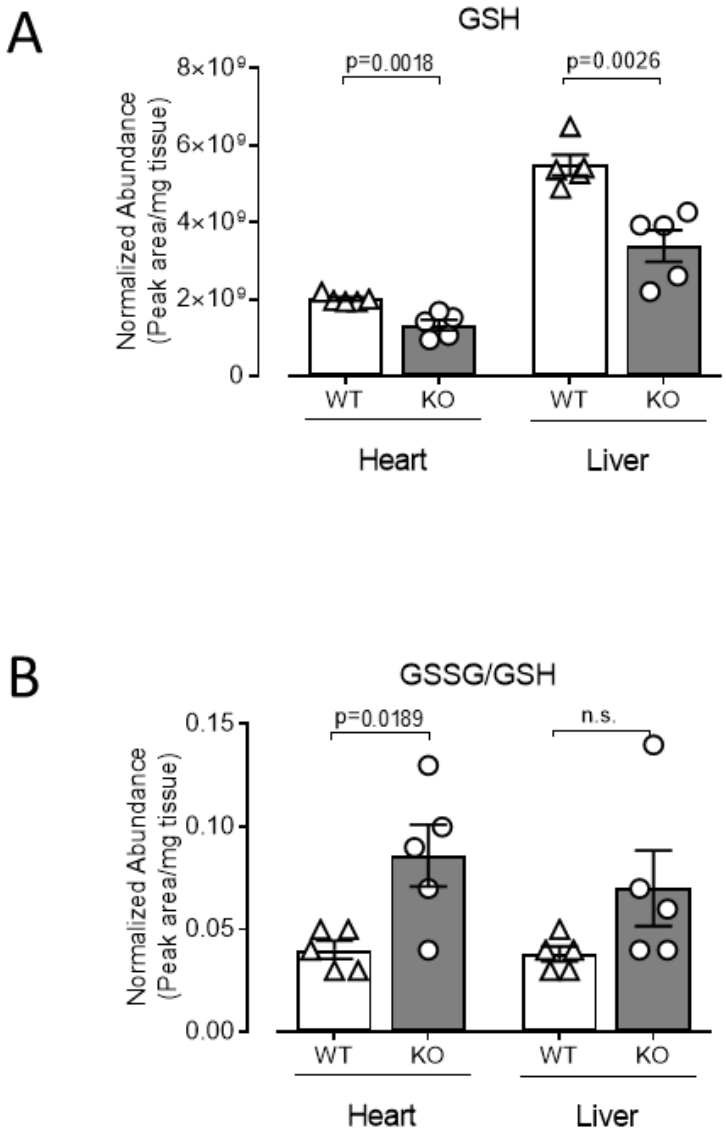

Figure 3.24: Glutathione concentration is reduced in all examined tissue (A). Glutathione disulphide/Glutathione ratio is significantly altered in knockout mice's heart and liver. Relative abundance of the metabolites is measured via mass spectrometry and normalized. Significance is measured using an unpaired two-tailed student T Test.

3.2.4 Mitochondria ultrastructure in the neonatal hearts does not present alterations compared to the wildtype

The differences in metabolic signatures between the heart of newborn mice and that of the adults, prompted us to a closer examination of the mitochondria phenotype present at birth.

To assess the mitochondrial integrity, we prepared heart samples from newborn mice at postnatal day 1 (P1) for sectioning and imaging via electron microscopy.

The results show no distinguishable difference between Taz KO hearts and the wildtypes (figure 3.25), suggesting the differences observed in the adult are occurring at some later time point probably after substitution of the postnatal/foetal mitochondrial apparatus with the mature mitochondria.

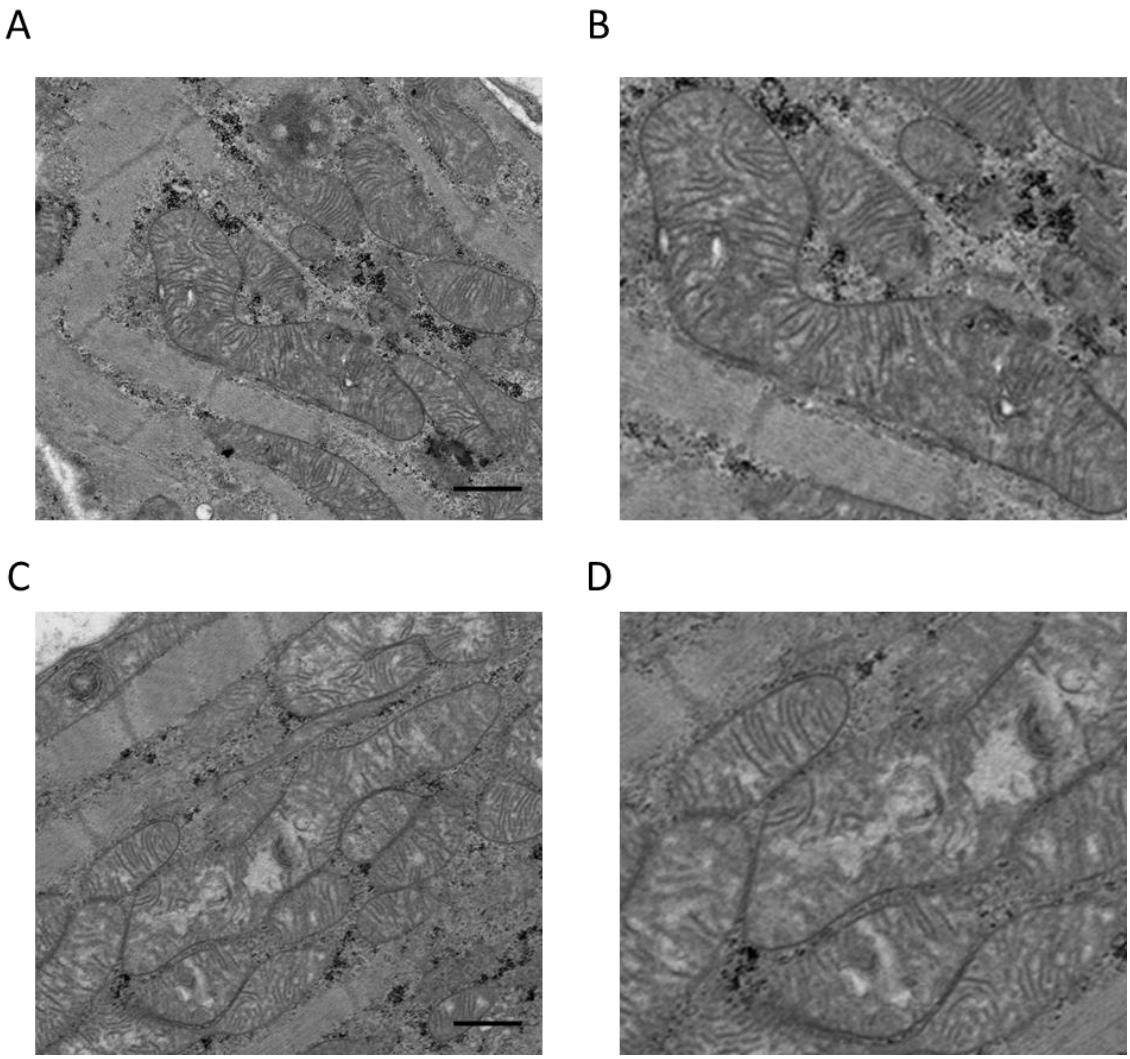

Figure 3.25: Electron microscopy images of wildtype (A, B) and Taz KO (C, D) neonatal heart tissue. A, mitochondria in the heart of wildtype P1 mice (scale bar 500nm). B, magnification of A. C, mitochondria in the heart of Taz KO P1 mice (scale bar 500nm). D, magnification of C. Pictures taken by Gillian Milne at the histology and microscopy facility of the university of Aberdeen.

3.2.5 Discussion

In this chapter we show how the knockout of *Taz* widely affects cellular metabolism in a tissue specific fashion.

The results point to a wide deregulation of metabolite content in the heart resulting in a clear change in major metabolic pathways. Glycolysis is only minimally affected: we detected widespread changes in the concentration of the initial intermediates of the pathway, with a 50-80% reduction in metabolites concentration for G6P, G3P and PEP. However, this downregulation of the abundance of these metabolites do not result in an altered carbon introduction to the TCA cycle with the amount of Pyruvate produced by the pathway remaining unchanged. This could be explained by the reduction of the content of lactate in the examined tissues which could be resulting from an upregulation of the Lactate-Pyruvate conversion ratio. Further experiments are required to examine carbon flux through the cells to pinpoint pressure points in the carbon metabolism pathway that could explain the differences in metabolic content in Taz KO hearts compared to the wildtype.

Despite having regular carbon intake in the TCA cycle, our results show an increased production of citrate and αKG in Taz KO tissue, pointing to a heightened activity of the pathway, this upregulation is, surprisingly, reversed in Succinate, which is in fact 30% less present in Taz KO compared to the wildtype. This shift from upregulation to downregulation could be explained by a reduced activity of αKG-dehydrogenase (αKG-DH). The enzyme is part of a complex multi-enzyme complex that converts αKG to Succinyl-CoA and is a critical checkpoint of the TCA cycle and regulates the energy production by the electron transport chain (Tretter and Adam-Vizi, 2005). It is inhibited via negative feedback by high levels of ATP, NADH and Succinyl-CoA (McLain et al., 2013). It is also considered to be a redox sensor of the cell and it is reversibly inhibited by free radicals. The role of this enzyme in our phenotype is currently under investigation through an assessment of the enzymatic activity of αKG-DH.

Neutral amino acid balance is also strikingly skewed in Taz KO hearts with Met, Ser and Gly content strongly increased in heart and muscle, and Glu which is 20%

increased in the heart. The most evident upregulation is however that of Asn and Asp, with a highly significant ($p<0.0001$) ~4 fold heart specific upregulation.

The deregulation of the metabolism seems not to impact energy production in the heart: ATP balance is not significantly changed in any of the tissue analysed. NADH production is however reduced.

To further investigate the energy production profile, we performed seahorse assays to assess mitochondria respiration rates. Using P1 mice derived cardiomyocytes we measured the respiration ability of the heart cells. Surprisingly the readings offered no significant difference between the genotypes, showing the respiration is not affected by the phenotype in P1 mice.

We also performed seahorse assays on different cell population to assess if the phenotype would present itself on a different cell type. However, both skin-derived fibroblasts and embryonic stem cells (ESCs) offered no difference in both OCR and ECAR.

Results in skin fibroblasts and ESCs were not unexpected, in fact our previous results pointed towards a phenotype that was very much heart-specific. Neonatal cardiomyocytes, however, delivered a surprising lack of difference between Taz KO and wildtype hearts. Our observations are in contrast with data on the respiratory activity of the cardiomyocytes produced by differentiation of patient-derived induced pluripotent ES cells (iPSCs), showing a severe reduction in respiration likely caused by an impairment in the organisation of the respiratory chain complexes (Dudek et al., 2016). These differences could be caused by several factors.

Firstly, it could depend on the mitochondria composition of the newborn mice. It is in fact known that mammals undergo a recycling of their mitochondrial apparatus perinatally (Gong et al., 2015), losing foetal mitochondria and producing adult mitochondria. Foetal mitochondria present a widely different morphology and gene expression profile compared to the adult (Gong et al., 2015), this is likely to affect the overall metabolic profile of the cells, leading to a stark difference in the effects of Taz KO in the newborn animals compared to the adult.

Secondly, it could be due to experimental conditions: previous reports show how a different carbon source can affect the results for the mitochondrial respiration rate in a iPSCs model of Barth Syndrome (Wang et al., 2014). This hypothesis will need further investigation in the future.

To test the first hypothesis described, we performed mass spec. analysis for the metabolic content in P1 mice. The results portray a vastly different situation in the newborn mice compared to the adults (Figure 3.26), with some cases in which the expression profile of the metabolite is completely reversed between adults and P1 mice. While, in some instances, being barely significant (succinate downregulation p=0.0411) these differences between the adults and the newborn contributes to highlight how metabolic profiles are dramatically different in different phases of Taz KO mice life cycle.

	Adult			P1	
	Heart	Liver	S. Muscle	Heart	Liver
Acetyl CoA					
Asparagine					
Aspartate					
Citrate					
Glucose 6-Phosphate					
Glutamate					
Glutamine					
Glyceraldehyde 3-Phosphate					
Glycine					
GSH					
GSSG/GSH					
Lactate					
Malate					
Methionine					
NAD+/NADH					
Phosphoenolpyruvate					
Pyruvate					
Serine					
Succinate					
αKetoglutarate					

	>30% up
	>10% up
	<10% up
	unchanged
	<10% down
	>10% down
	>30% down

Figure 3.26: Heat map overview the principal metabolite concentrations in Taz knockout vs wildtype in adults and P1 mice.

Metabolic differences in the adult heart point to an extremely interesting phenotype that could offer a new insight in the mechanism of action of Barth syndrome. The upregulated presence of neutral amino-acids in the tissue is particularly interesting. This increased presence is in fact an indicator of the upregulation of transport and/or production of these metabolites. This upregulation, in particular regarding Asn, is a typical unfolded protein response-induced phenotype marker. The potential presence of an unfolded protein response will be addressed in the next chapter.

3.3. Tafazzin Knockout modifies the gene expression profile of adult mouse hearts

The previous chapter showed that knockout of *Taz* causes a significant overhaul of many cardiac phenotypes in the adult mouse. It is reasonable to hypothesise that the changes observed in the morphology of the mitochondria and in the metabolism, are accompanied by a general change in the gene expression signature of the tissue. To determine whether Taz knockout was affecting general gene expression in the mouse heart we ran an RNAseq experiment comparing the gene expression in wildtype vs KO mice.

We compared the gene expression in tissue harvested from 8 weeks old mice and detected a dramatic genome wide gene expression modification between our examined genotypes with about 3000 genes with significant differences fold change in the KO compared to the wildtype. Our analysis identified 1506 genes that were upregulated more than 1.5 times and 1411 downregulated more than 1.5 times showing a dramatic gene expression pattern divergence caused by depletion of Taz (Figure 3.27).

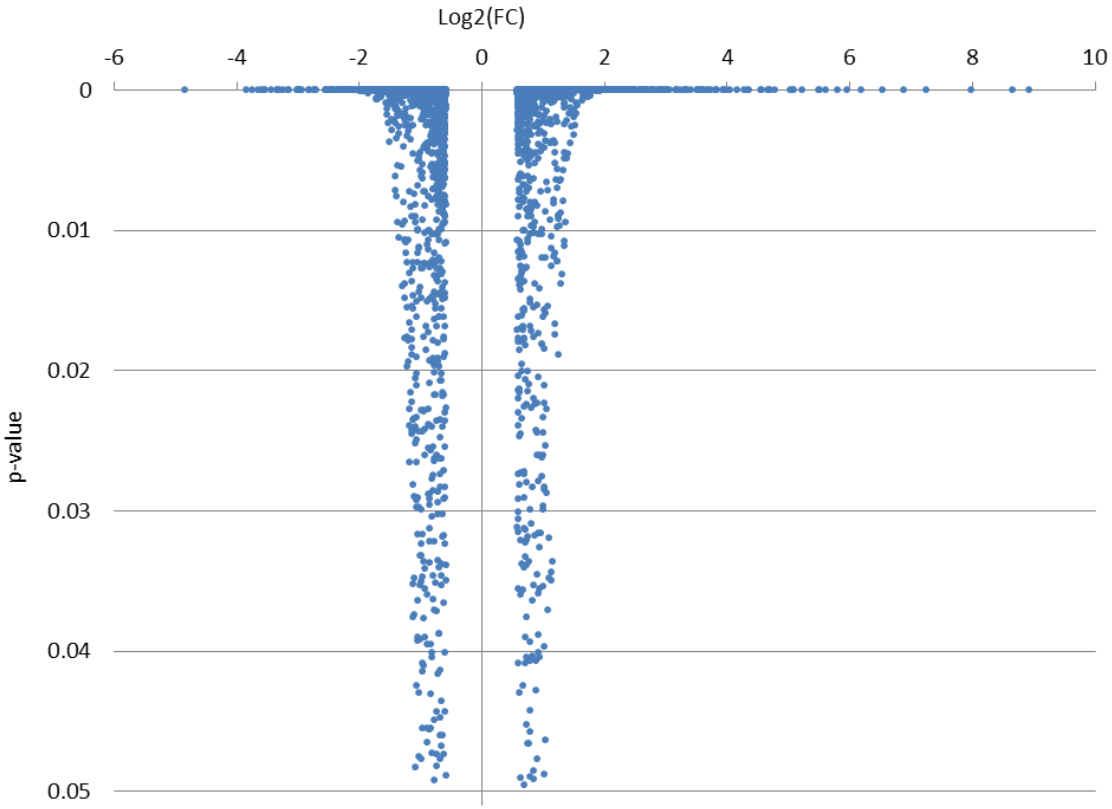

Figure 3.27: overview of differential gene expression in Taz KO mice' hearts compared to the wildtype. Data is expressed as Log2 of the Fold change and organized in order of significance.

3.3.1 The expression of genes regulating cardiac function is greatly influenced by Taz knockout

RNAseq data shows extensive alterations in cardiac gene expression signature for Taz KO mice hearts. Analysis of the dataset show a general downregulation of structural components of the cardiac muscle (Figure 3.28) with members of both heavy and light chain family of myosin (Myh11, Myl9) strongly depleted and suggesting an impaired contractility. Myotilin and Tcap are components of the Z line of the sarcomere and control stability of the thin filaments the general assembly of the sarcomere; they also are strongly downregulated suggesting a general impairment of sarcomere organizational ability in the KO mice. The most significant changes in gene expression however, are Smoothelin and Mybpc2, structural proteins which play a role in the regulation of the contractility of the smooth muscle.

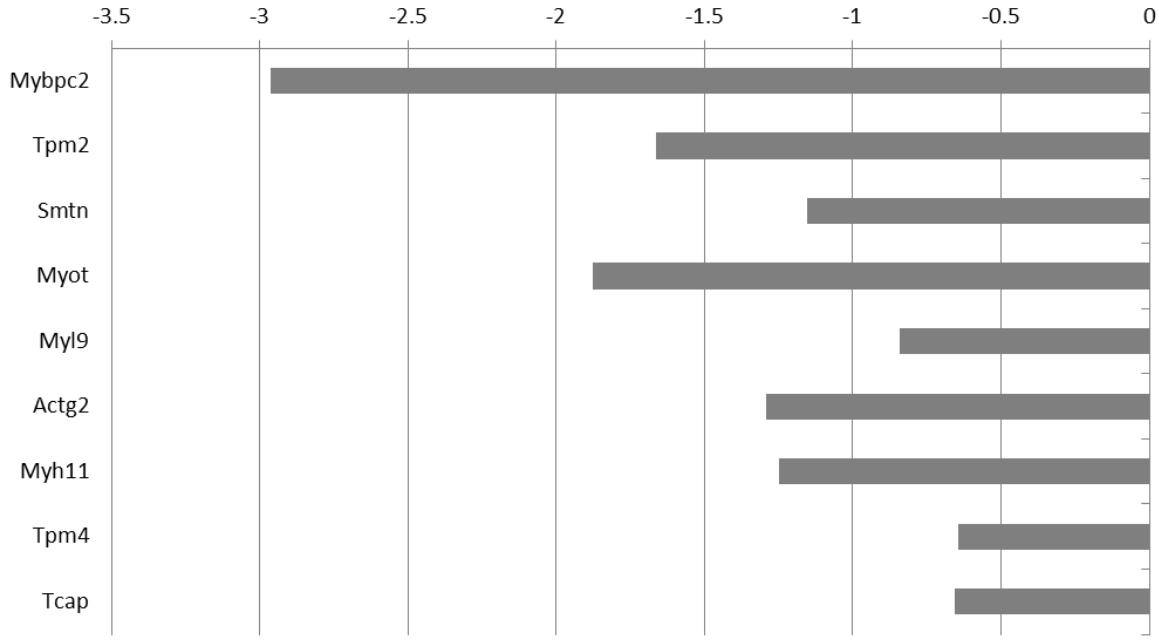

Figure 3.28: Taz KO causes a downregulation of structural components of the contractile mechanism of the heart. Data is expressed as Log2 of the Fold change, the 0 represents level of expression in the wildtype. Data is organized in order of significance.

We also identified changes in gene expression in the calcium homeostasis machinery, with downregulation of several genes encoding for proteins involved in calcium sensing, storage and mobilization from the sarcoplasmic reticulum (Figure 3.29). Calcium dependent regulators of the cardiac function are also affected in our system, with downregulation of Tnni2 and Mylk (Figure 3.30). Muscle contractility regulation genes also show signs of deregulation of the expression in Taz KO hearts with all member of the cardiac Troponin complex (Tnni2, Tnni3, and Tnnt1) downregulated. Tnni3 encodes the cardiac isoform of Troponin I, which act as an inhibitory subunit in the complex, helping with muscle relaxation after contraction. Interestingly the downregulation of this gene is counterbalanced by a strong upregulation of Tnni1, encoding the skeletal muscle isoform of the protein. Skeletal muscle Troponin I is expressed in both the skeletal and cardiac muscle in the developmental stage of these tissues, but is then lost in the cardiac muscle, when its expression is replaced by the cardiac version Tnni3. This data offers an interesting point of speculation on the cardiac phenotype suggesting a defect in the cardiac maturation, with an adult phenotype resembling, in some respects, the foetal and perinatal phenotype.

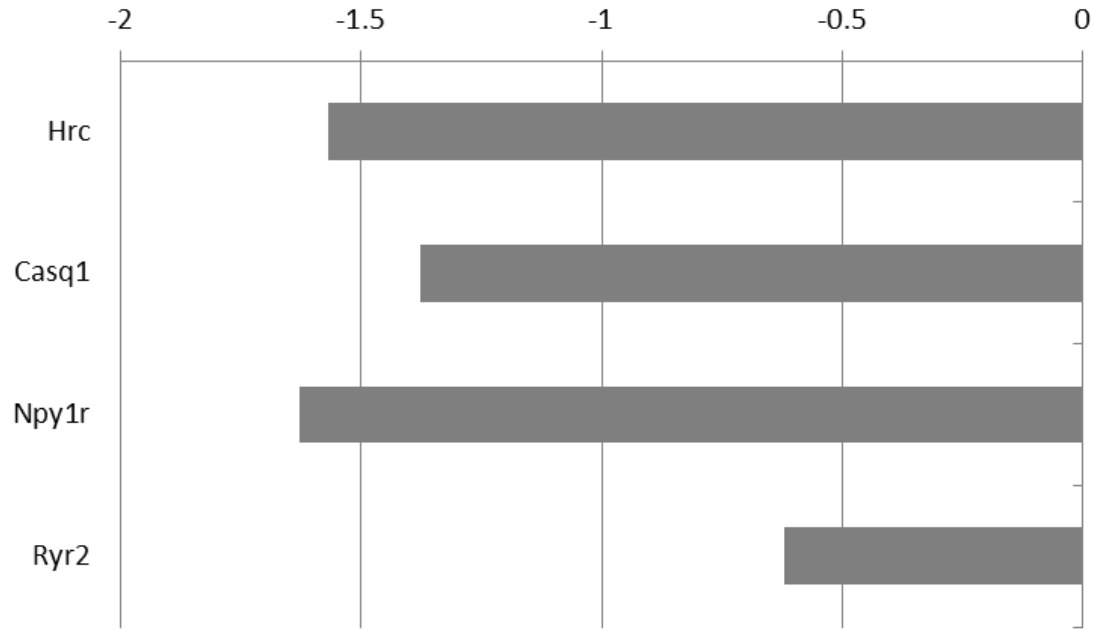

Figure 3.29: Taz KO causes a downregulation in the calcium homeostasis machinery. Data is expressed as Log2 of the Fold change, the 0 represents level of expression in the wildtype. Data is organized in order of significance.

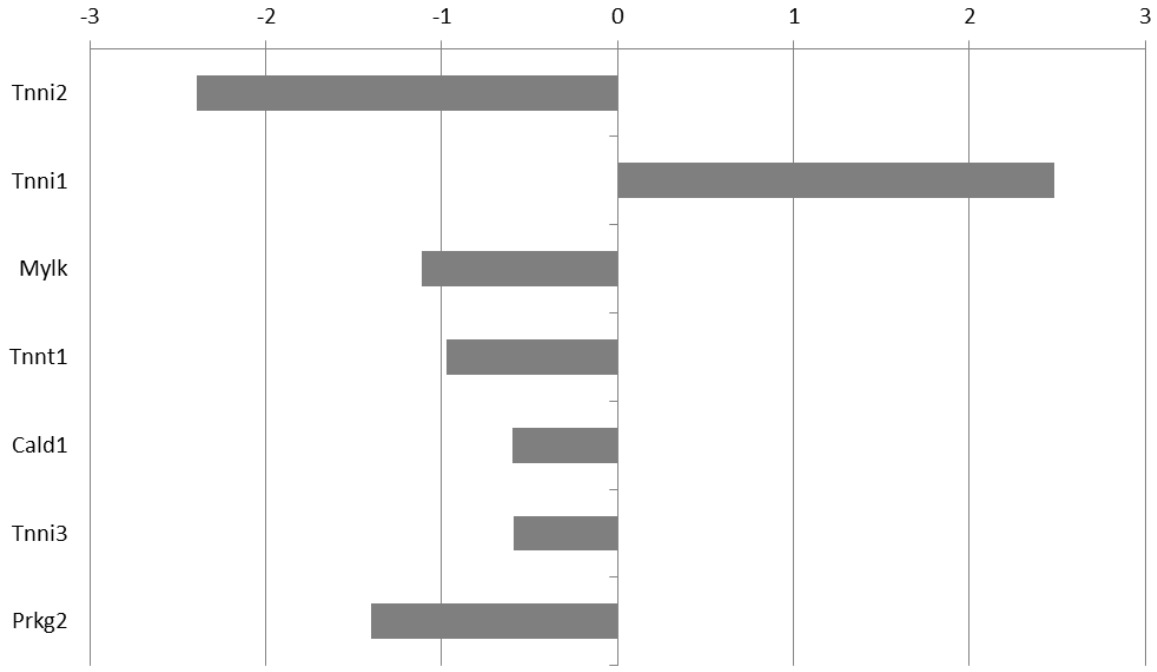

Figure 3.30: Taz KO modifies the expression of several elements of the cardiac regulatory network. Data is expressed as Log2 of the Fold change, the 0 represents level of expression in the wildtype. Data is organized in order of significance.

Calcium transport is not the only ionic trafficking affected by Taz KO. The data indicate a widespread deregulation of components for chlorine, potassium and sodium channels (Figure 3.31). The dysregulation of these genes fits with the hypothesized defects in contractility offering a more detailed picture of the affected steps in the contraction chain of events. From the graph we can infer impairment in repolarization, caused by a reduction in the levels of Kcnq1 and Kcnb1, and a reduction in the upward stroke of the action potential caused by the downregulation of Scn5a which acts as the main effector of this section of the action potential spike. Moreover, the reduction in Hcn4, partially compensated by the upregulation of Hcn2 suggests a defect in the intrinsic pace making of the heart.

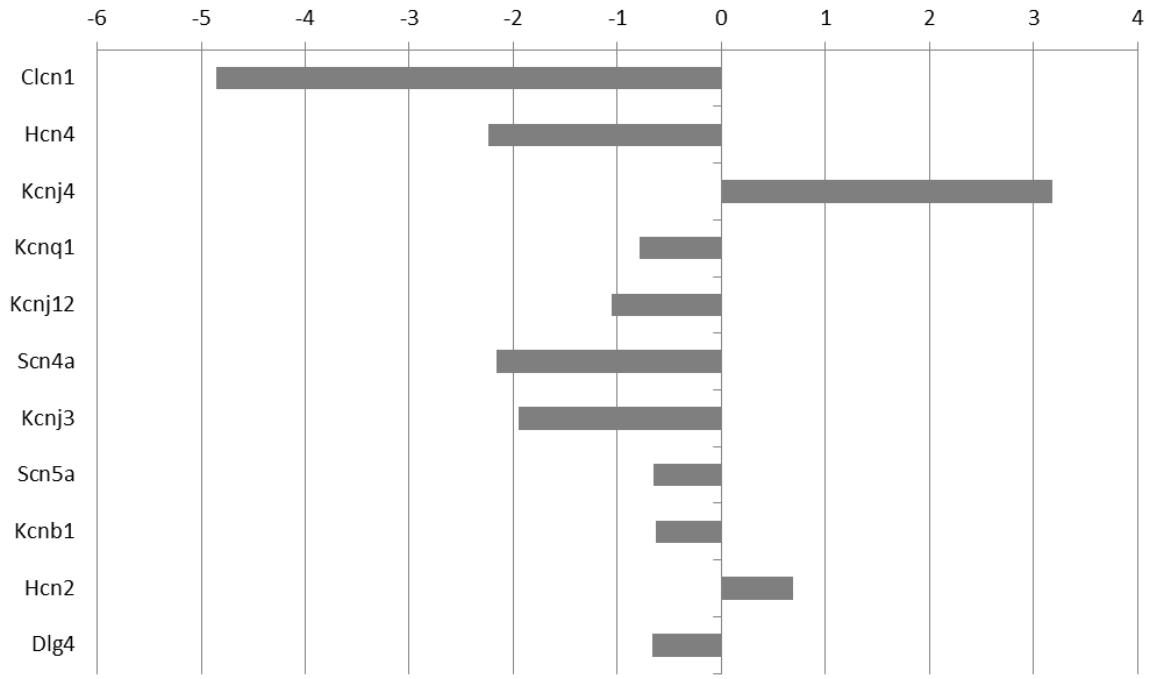

Figure 3.31: Taz KO causes a downregulation of the expression of various ion channel components. Data is expressed as Log2 of the Fold change, the 0 represents level of expression in the wildtype. Data is organized in order of significance.

3.3.2 Taz KO induces an unfolded protein response in mice's hearts

As discussed in the previous chapter, the upregulation of certain metabolites in our samples led us to hypothesize an unfolded protein response-type situation in the heart of KO mice. The first step into the verification of this hypothesis was to identify a genetic validation of the metabolic data. We analysed our RNAseq data set looking for elements of the amino acid metabolism pathway which could confirm that the alterations in the metabolites' presence was due to an alteration of the genetic signature.

3.3.2.1 The amino acid metabolism pathways are highly enriched in Taz KO tissues

The amino acid synthesis and modification pathways are generally de-regulated in Taz KO hearts compared to the wildtype (Figure 3.32). Asparagine Synthetase (Asns) is the 8th most significantly enriched gene in our RNAseq data (p=1.7E-133). The graph shows an increased amino acid metabolising ability in Taz KO hearts compared to the wildtype, with higher synthesis (Asns), higher modification potential (Psat1, Psph, Cth) and higher processing (Bcat1, Dtd1). The data also shows an increase in the expression levels of all enzymes dedicated to production of charged tRNAs (Figure 3.33).

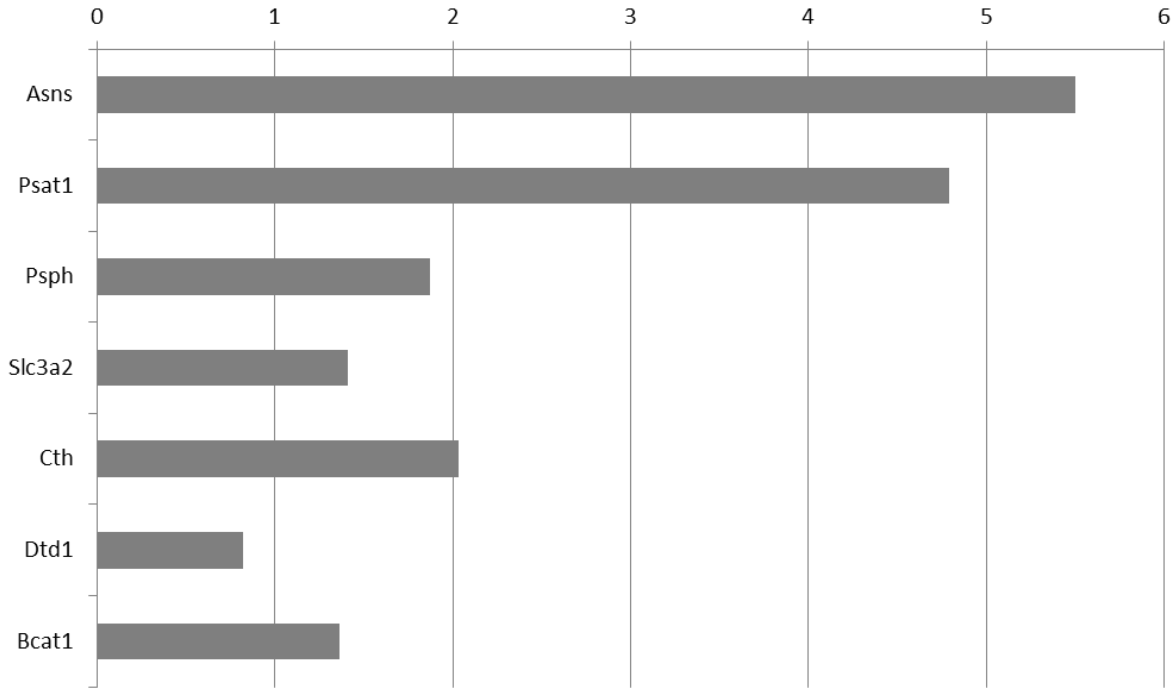

Figure 3.32: Amino acid metabolism is upregulated in Taz KO hearts. Changes in the expression levels of key members of the amino acid modification machinery. Data is expressed as Log2 of the Fold change, the 0 represents level of expression in the wildtype. Data is organized in order of significance.

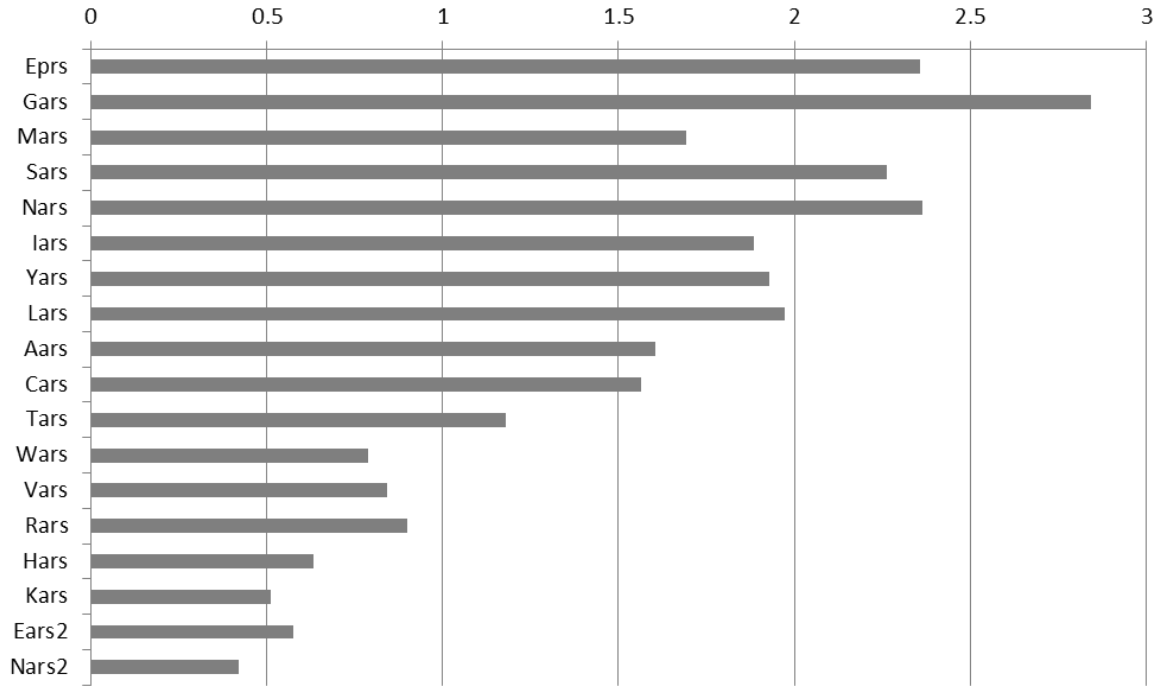

Figure 3.33: Amino acid metabolism is upregulated in Taz KO hearts. Changes in the expression levels of major aminoacyl tRNA Synthetase enzymes. Data is expressed as Log2

of the Fold change, the 0 represents level of expression in the wildtype. Data is organized in order of significance.

Amino acid import/export machinery also exhibits an altered expression level. We then analysed the solute carrier encoding genes and found a mixed situation with a majority of components of the cationic transport system upregulated (Figure 3.34), showing an augment in the amino acid trafficking with the extracellular environment.

Taken together this data strongly suggests an amino acid starvation response triggered by ATF4 signalling.

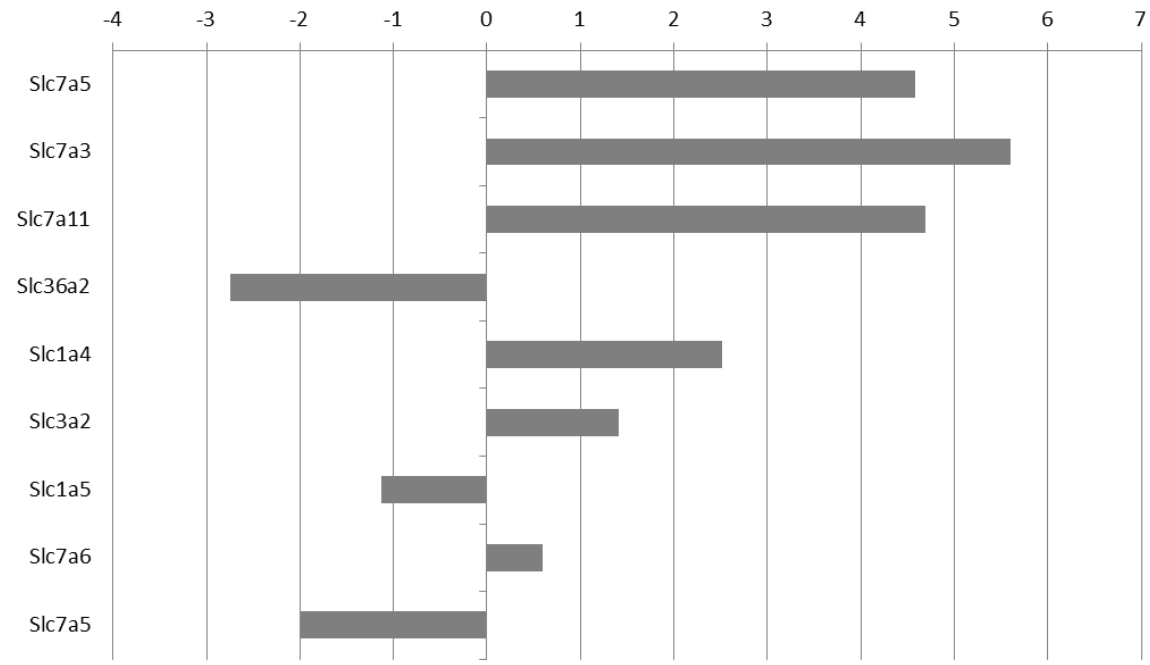

Figure 3.34: Amino acid metabolism is upregulated in Taz KO hearts. Changes in the expression levels of amino acid carriers in Taz KO hearts compared to the wildtype. Data is expressed as Log2 of the Fold change, the 0 represents level of expression in the wildtype. Data is organized in order of significance.

3.3.2.2 ATF signalling triggers an unfolded protein response in Taz KO hearts

ATF4 is a downstream transcription factor activated by a cascade of events known as the endoplasmic reticulum (ER) unfolded protein response (UPR^{ER}).

The pathway is comprised of 3 parallel activation mechanisms, which react to the sensing of the presence of unfolded proteins in the cells.

We analysed our RNAseq data to verify if Taz KO induced changes in gene expression profile were consistent with the genetic signature of the UPR^{ER}. The initiating factors in the UPR^{ER} are ATF6, IRE1 (Ern1) and PERK (eiF2ak3), these molecules are anchored to the membrane of the endoplasmic reticulum and inactivated by binding with BiP (Hspa5).

According to RNAseq data all of the initiating factors are significantly upregulated (Figure 3.35), with ATF6 expression doubled and Ern1 expression more than tripled in the KO hearts compared to the Wildtype. BiP expression is unchanged in our samples.

A

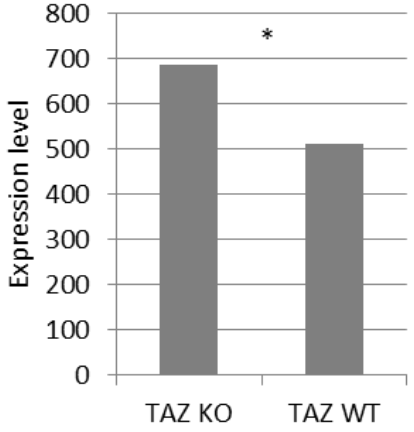
Eif2ak3
800
700
600
500
400
300
200
100
0
Expression level
*
TAZ KO
TAZ WT

B

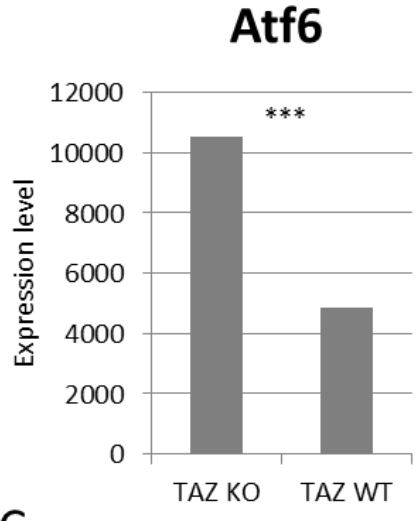
Atf6
12000
10000
8000
6000
4000
2000
0
Expression level
***
TAZ KO
TAZ WT

C

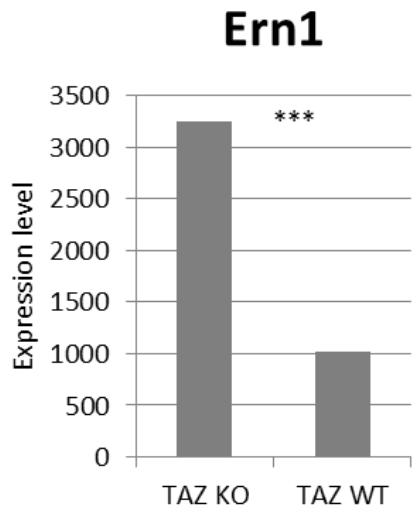
Ern1
3500
3000
2500
2000
1500
1000
500
0
Expression level
***
TAZ KO
TAZ WT

Figure 3.35: Taz KO induces an upregulation of the expression of the initiators of ER unfolded protein response. A, expression of PERK (eIF2ak3) ($p \leq 0.05$). B, expression of ATF6 ($p \leq 0.001$). C, expression of Ire1 (Ern1) ($p \leq 0.001$).

In the presence of unfolded proteins BiP releases its binding with ATF6, IRE1 and PERK to bind the unfolded polypeptides and retain them in the folding compartment of the ER.

Subsequently ATF6 is cleaved in the Golgi and translocated to the nucleus where it acts as a transcription factor inducing CHOP (Ddit3), several molecular chaperones and Xbp1. Xbp1 is then spliced by IRE1 and induces the endoplasmic reticulum-associated protein degradation (ERAD).

Our data show an overall upregulation of the genes encoding for molecular chaperones, 300% augment in the levels of CHOP (Ddit3), but no significant changes in the levels of Xbp1 (Figure 3.36).

The IRE1 branch of the UPR^{ER} pathway seems not to be involved in our response, with no detectable difference in the expression of components of the ERAD complex and only a modest downregulation of the IRE1 target p58IPK (data not shown).

Conversely the PERK branch of the UPR^{ER} appears to be highly active in Taz KO hearts. The main function of PERK is the phosphorylation of eIF2-α (eIF2s1) which activates a cascade of events mediated by ATF4.

In our system eIF2s1 is upregulated with high significance together with many members of the eukaryotic translation initiation factor complex (Figure 3.37).

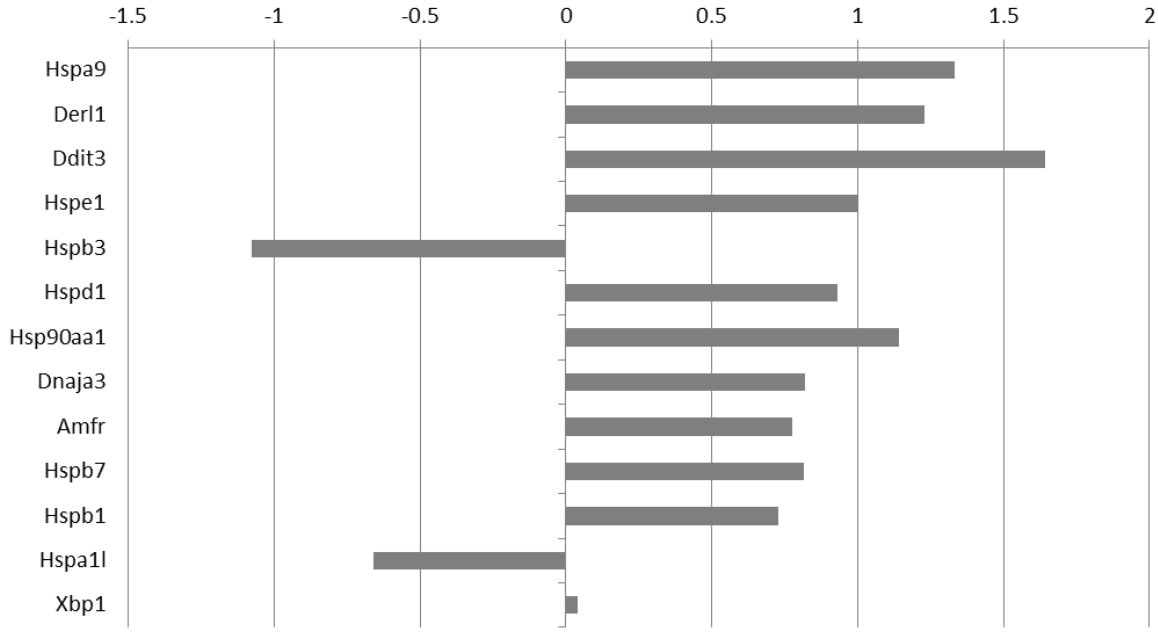

Figure 3.36: Taz KO induces the upregulation of key molecular chaperones, through induction of the transcription by ATF6. Data is expressed as Log2 of the Fold change, the 0 represents level of expression in the wildtype. Data is organized in order of significance.

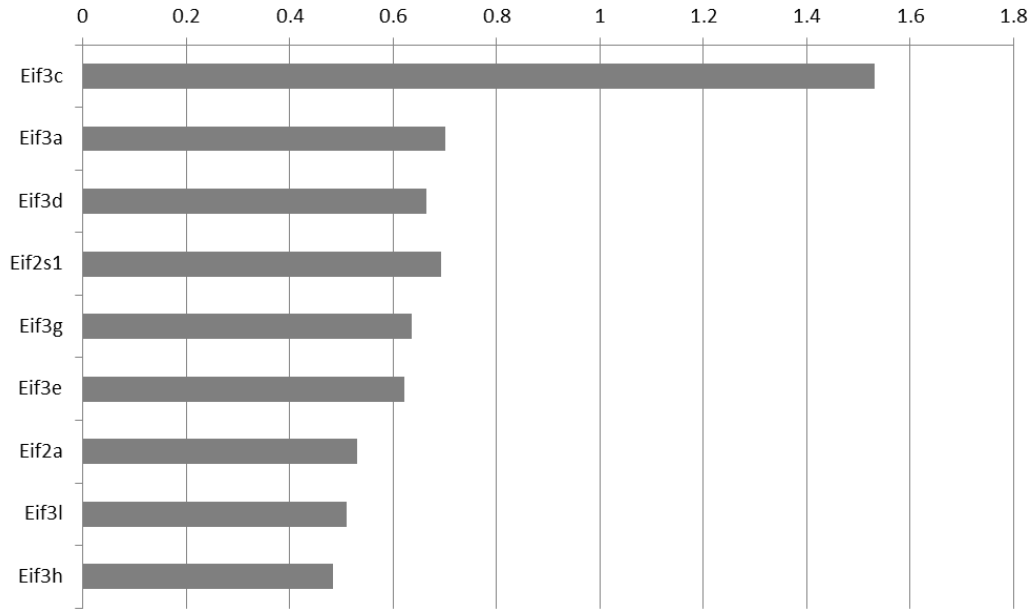

Figure 3.37: The eukaryotic translation initiation complex proteins are upregulated in Taz KO hearts compared to the wildtype. Data is expressed as Log2 of the Fold change, the 0 represents level of expression in the wildtype. Data is organized in order of significance.

Phospho-eIF2s1 activates transcription of ATF4 by initiating the transcription from a short open reading frame in the 5' UTR of the gene. ATF4 accumulates in the cells and acts as a transcription factor inducing the expression of CHOP (Ddit3), GADD34 (PPP1r15a) and genes for the control of amino acid metabolism and modulation of the oxidative stress response.

We proceeded to verify the expression of ATF4 and its target genes (Figure 3.38). ATF4 expression is enhanced by about 4 fold showing ATF4 transcription activation by eIF2s1. Consequently, expression of major ATF4 targets is upregulated as well. As previously stated CHOP (Ddit3) is more than 3 times upregulated, moreover the expression of GADD34 (Ppp1r15a) is doubled and expression of Trib3 is 25 times upregulated in Taz KO hearts compared to the wildtype. The metabolomics data and the gene expression profile also indicate amino acid processing is enhanced in Taz KO hearts compared to the wildtype with upregulation of synthesis, trafficking and processing of the amino acids.

Taken together, the data points strongly towards a confirmation of our initial hypothesis of an activation of the unfolded protein response in the heart tissue triggered by a knockout of Taz.

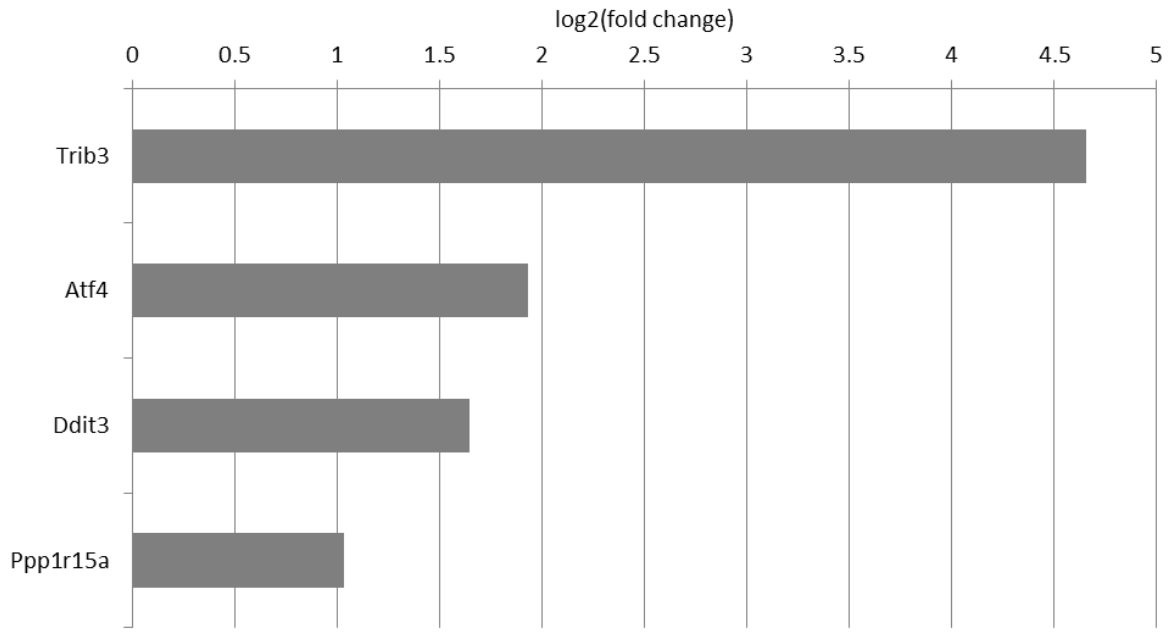

Figure 3.38: Upregulation of ATF4 and its key target genes in Taz KO hearts caused by an activation of the PERK/eIF2s1 axis of ER stress response. Data is expressed as Log2 of the Fold change, the 0 represents level of expression in the wildtype. Data is organized in order of significance.

3.3.2.3 Activation of the mitochondrial UPR in Taz KO hearts

Phosphorylation of eIF2s1 by PERK triggers the initiation of translation of a number of genes through the use of a short open reading frame in their 5' UTR. Among these we find ATF5, mammalian homologous of ATFS-1 and master regulator of the mitochondrial UPR (UPR^{MT}). Activation of the translation of ATF5 and its accumulation in the cell triggers a complex genetic programme for the restore of proteostasis in the mitochondria. ATF5 is almost 10 times upregulated in our system (p=6E-129), suggesting activation of the pathway by eIF2s1. Consistently the downstream targets of ATF5 activation are upregulated in Taz KO hearts compared to the wildtype. In particular LonP1, a peptidase resident of the mitochondria is about 5 times upregulated in our system; this data is of particular interest because LonP1 acts on mitochondrial RNA (mtRNA) translation by cleaving the endonuclease responsible for the editing of the pre-mtRNA and de-facto preventing the formation of mature mtRNA.

ATF5 also enhances the transcription of mitochondrial chaperones DNAJA3, HSPA9 and HSPD1, with the aim of improving mitochondria protein folding and restore of mitochondria proteostasis (Figure 3.39).

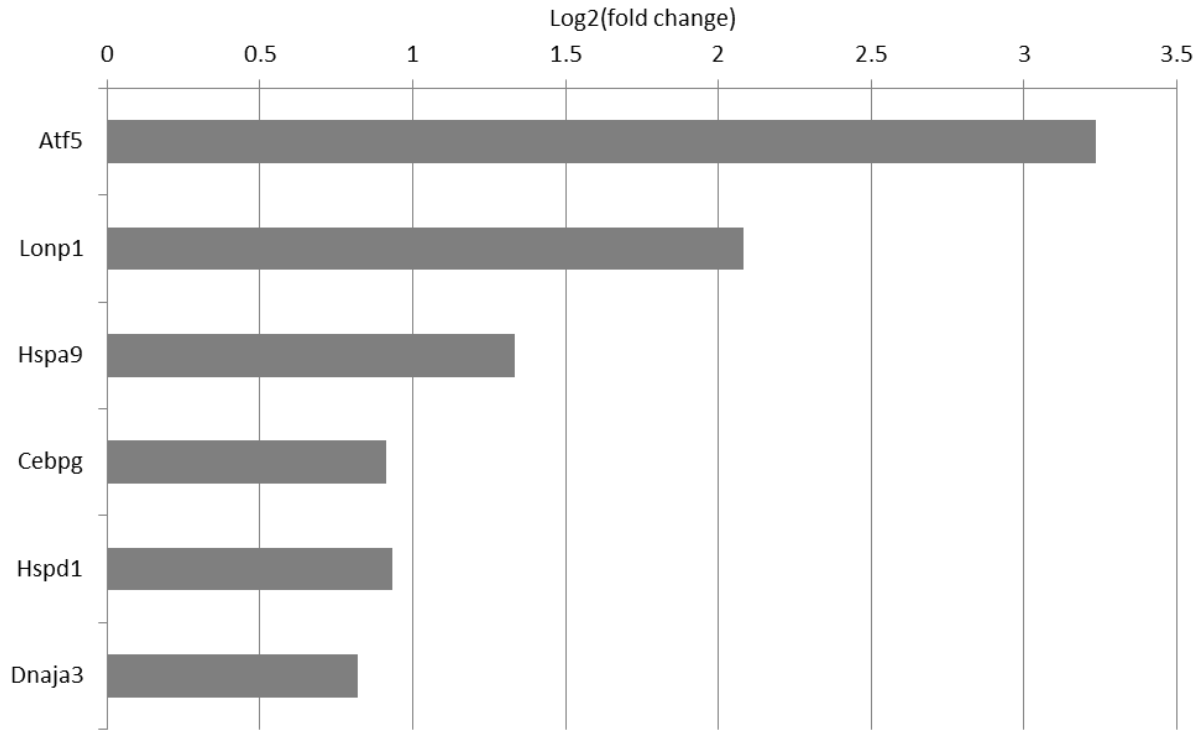

Figure 3.39: Taz KO causes the upregulation of the expression key components of the UPR^{MT} pathway. Data is expressed as Log2 of the Fold change, the 0 represents level of expression in the wildtype. Data is organized in order of significance.

3.3.2.4 UPRER and UPRMT cooperate to initiate damage repair in Taz KO Hearts

As was shown in the previous paragraph the UPR^{MT} machinery appears to be working to improve protein quality check in the mitochondria, with blockage of translation aimed to prevent further accumulation of unfolded proteins and the induction of mitochondrial chaperones to improve folding capability.

The stress response triggered by an unfolded protein stimulus sensed by the ER, leads to a range of reactions aimed to ensure the survival of the cell.

The ATF6 branch of the UPR^{ER} is responsible for the induction of several molecular chaperones whose function is to facilitate a correct protein folding to end the unfolded protein stimulus. In addition to the ones shown before (Figure 3.36), we identified a number of chaperones which are upregulated in our system including six out of 8 subunits of the cytosolic CCT complex (Figure 3.40), a key chaperonin complex for the correct folding of denaturated proteins.

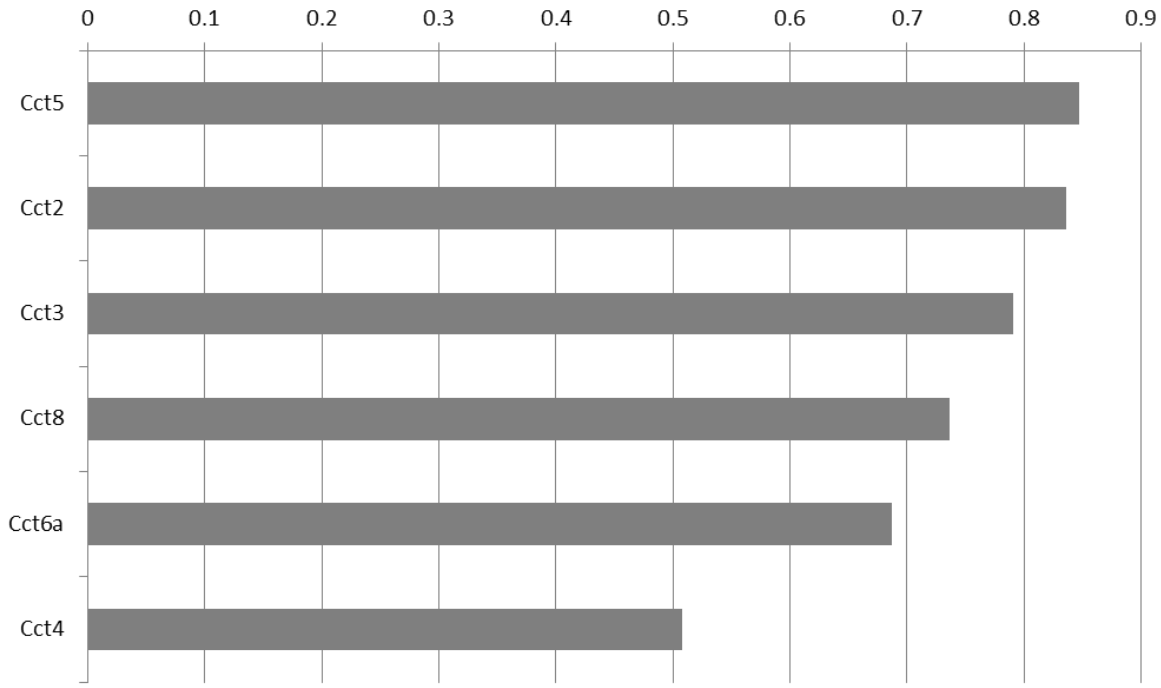

Figure 3.40: Taz KO causes the upregulation of the expression of components of the CCT chaperonin complex. Data is expressed as Log2 of the Fold change, the 0 represents level of expression in the wildtype. Data is organized in order of significance.

PERK mediated phosphorylation of eIF2s1 acts as a stimulus to block mRNA translation in cells undergoing ER stress. This interruption in translation is necessary to avoid the accumulation of more unfolded proteins, so that the cell can repair the damage and resume its physiologic function. As we discussed before, eIF2s1 activates transcription of ATF4 which in turn activates transcription of GADD34 (Ppp1r15a). This protein acts as a counter to PERK kinase activity by dephosphorylating eIF2s1 and starting back the translation of proteins (Baird and Wek, 2012). RNAseq data shows enrichment in translation initiation and elongation complex components (Figure 3.41), accompanied by consistent upregulation of a number of ribosomal proteins (Figure 3.42 A, B).

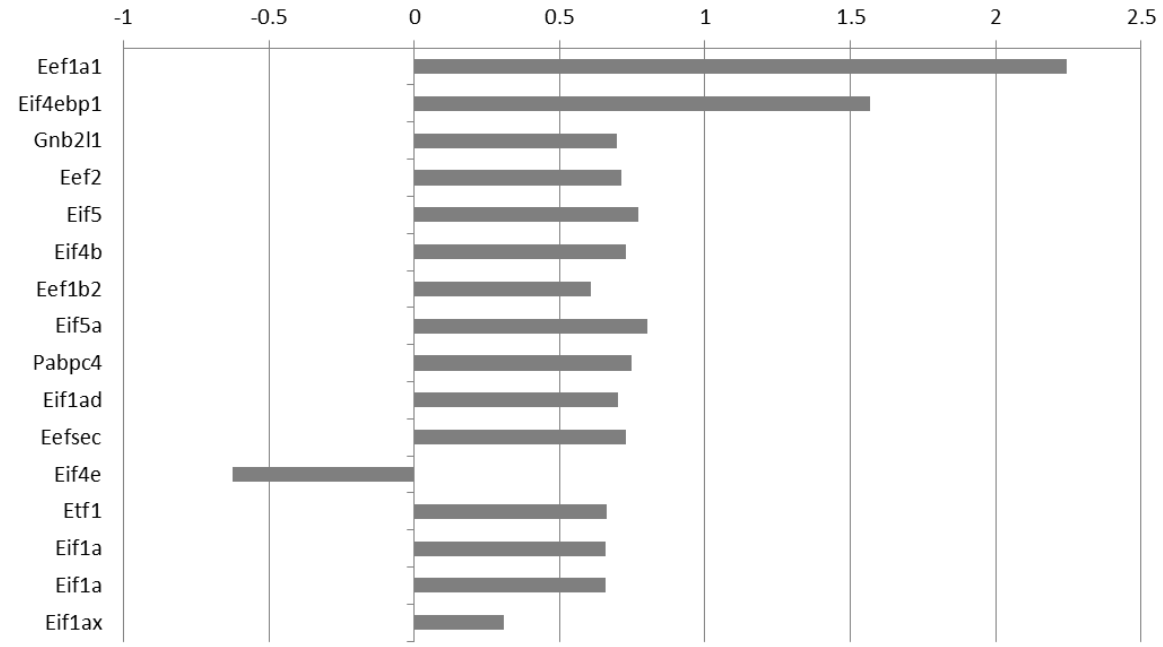

Figure 3.41: Taz KO causes the upregulation of components of the translation initiation and elongation machinery. Data is expressed as Log2 of the Fold change, the 0 represents level of expression in the wildtype. Data is organized in order of significance.

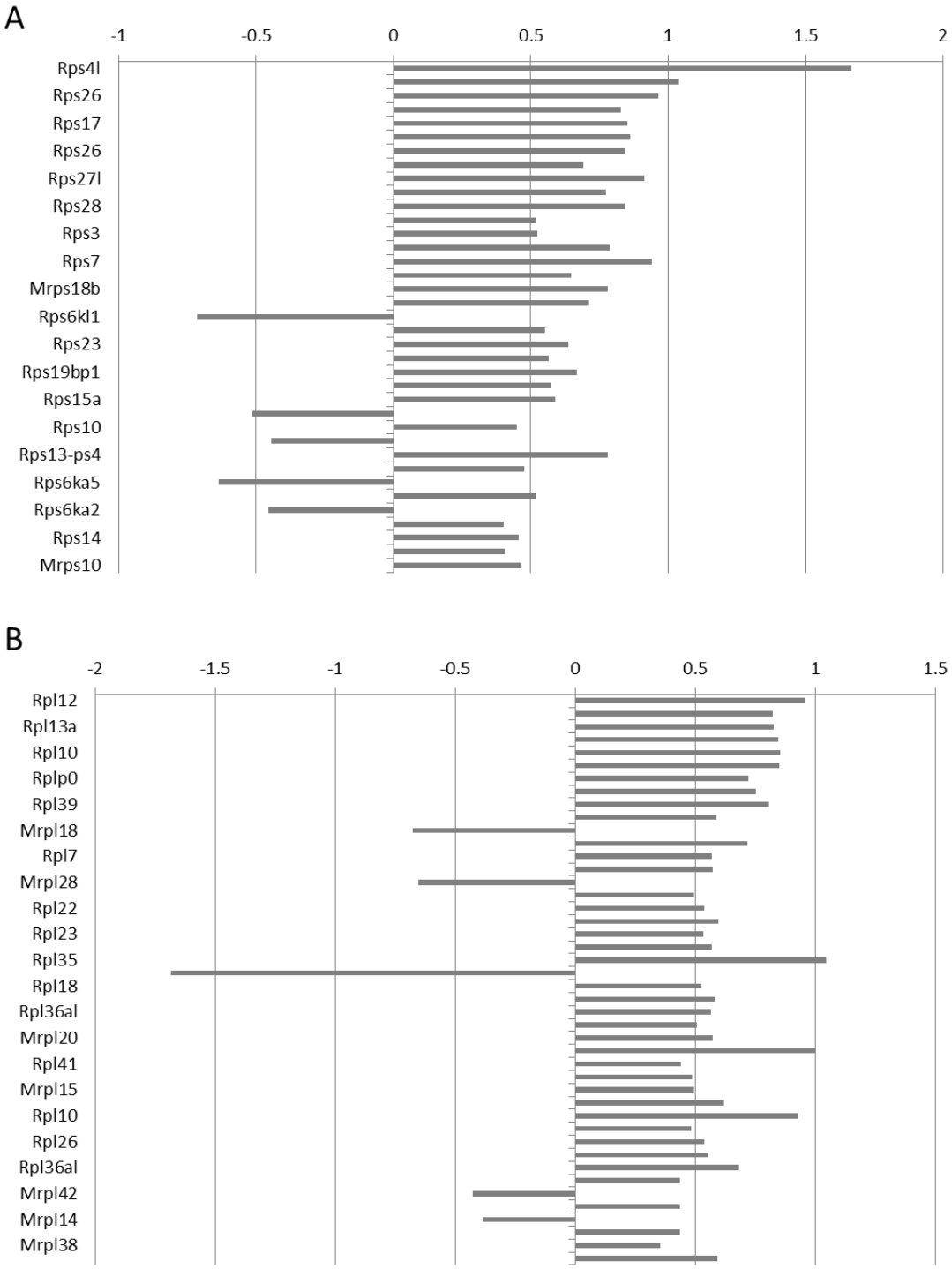

Figure 3.42: Taz KO causes the upregulation of numerous ribosomal proteins. A, expression levels of small ribosomal proteins; B, expression levels of large ribosomal proteins. Data is expressed as Log2 of the Fold change, the 0 represents level of expression in the wildtype. Data is organized in order of significance.

The enhancement of protein folding via enrichment of the expression of chaperones, together with the recovery of the translation via upregulation of the translation pathways in the cytosol, added to the induction of the mitochondrial protein quality check machinery indicates the activation in Taz KO hearts of mechanisms for the recovery of correct proteostasis.

Consistently CHOP induced apoptosis is impaired in our samples by the upregulation of anti-apoptotic Bcl2. However other members of the Bcl2 family of proteins appear to be upregulated in Taz KO hearts (Figure 3.43). All of these proteins, except for Bcl2, are pro apoptotic factors, which activate the mitochondrial outer membrane permeabilization followed by apoptosis.

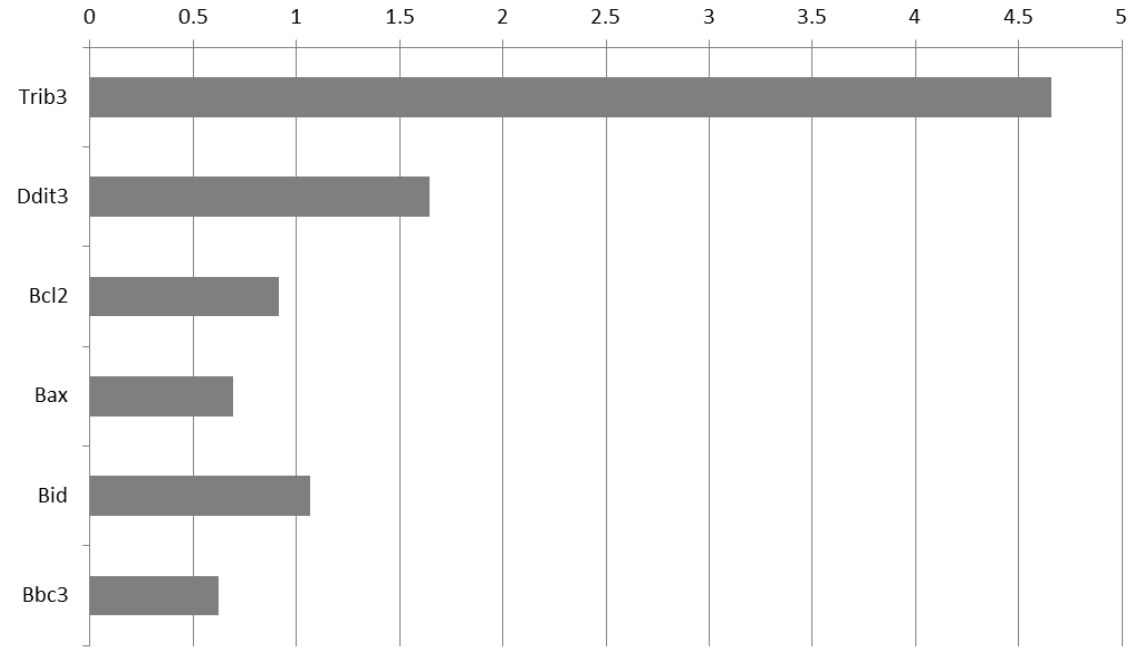

Figure 3.43: Taz KO causes the upregulation pro and anti-apoptotic factors in the heart. Data is expressed as Log2 of the Fold change, the 0 represents level of expression in the wildtype. Data is organized in order of significance.

3.3.3 Discussion

The data presented in this chapter paint a picture of a very complex phenotype produced by Taz knockout in the heart. The overall genetic expression pathway in Taz KO hearts is widely different from the wildtype counterpart, with close to 3000 highly significant differentially expressed genes.

Genes controlling cardiac function are widely deregulated with significant downregulation of several structural proteins controlling the correct assembling and function of the sarcomere. The downregulation pattern can also be found in the expression of proteins controlling calcium homeostasis and ionic balance of the cell, and in the expression of contraction regulatory elements. However, the data shown in this chapter are only partly reflected in the phenotype. As we have shown in chapter 3 the muscle fibres do not seem to be affected by the knockout of Taz, so the downregulation of the cytoskeletal proteins must be compensated in a way that allows for a correct sarcomere organization. Functionally, the defects of the calcium homeostasis machinery and the knockdown of the ion channel proteins seem to be coherent with the cardiac phenotype detected in Taz KO mice, with increased QT intervals and reduced fractional shortening.

This data suggests a general impairment of the correct production of the action potential caused by downregulation of major ion channel suggesting impairment in membrane polarization.

The other prominent phenotype suggested by our RNAseq data is an activation of the unfolded protein response machinery. Our data clearly identifies a general upregulation of the initiating molecules of the UPR^{ER} pathway followed by an activation of the ATF6 and PERK branches of the response machinery. The activation of these mechanisms can be clearly detected from the significant upregulation of the expression levels of the downstream targets of ATF6 (chaperones) and ATF4 (amino acid metabolism, CHOP, GADD34).

The upregulation of ATF4 targets is of particular interest because it triggers a series of downstream mechanisms designed to cope with an unfolded protein stress: through the upregulation of the amino acid metabolism pathway the cells aims to accumulate building blocks for protein synthesis, which in turn is re-

activated by the action of GADD34 on eIF2s1. This pro-survival mechanism is aided by a block in CHOP induced apoptosis caused by the upregulation of anti-apoptotic Bcl-2.

We can also clearly identify an activation of the UPR^{MT} with upregulation of ATF5 and its target genes, aimed to restore the proteostasis in the mitochondrion. The activation of these two cellular pathways indicates an attempt by the cells to remove the UPR stimulus and restore correct proteostasis.

This can also be inferred by the blockade of apoptosis operated by Bcl-2, previous work in the lab in fact has shown no evidence of anomalous induction of the apoptosis in the heart tissue, with no caspase 3 staining detected in histology slides (data not shown).

4. Conclusions, Discussion and Future work

4.1 Conclusion and Discussion

In the past thirty years, researchers and clinicians have contributed to the formation of a sizeable body of knowledge about Barth syndrome (BTHS), its aetiology, its symptoms and its diagnosis. Yet, the molecular mechanisms underlying Barth syndrome have not been fully elucidated.

Taz is a highly conserved gene across multiple species, this has allowed for the successful use of model organisms such as yeast, Drosophila and *C. elegans*, for the study of the biological role of Taz and its cellular interactions. However, the lack of a fully satisfactory mammalian model has been an obstacle for the understanding of the systemic consequences of the loss of *Taz* in a living organism.

In the past years, our lab has been working to address the lack of an appropriate murine model, capable of replicating the phenotypes identified in human patients with BTHS. A previous attempt to produce a working model of BTHS had been frustrated by the difficulties encountered in having a stable germline transmission of the allele caused by the unforeseen effect of Taz KO on the fertility of the mice (Cadalbert et al., 2015). By changing the strategic approach to the problem, we believe we have overcome the issue by utilizing a conditional model to circumvent the sterility phenotype we detected in our previous $Taz^{-/y}$ mouse.

We believe the production of the conditional knockout (KO) model of Taz is a promising first step on the road of fully understanding the molecular events leading from a mitochondrial defect to cardiomyopathy. The successful characterization of the model will be central in obtaining an effective pre-clinical model for the development of treatments for BTHS and other pathologies involving defects in the mitochondrial membrane as the aetiological trigger.

We used the new *Taz* KO model to characterize the mitochondrial phenotype of the heart. To check the efficiency of our model, we performed mass spectrometry analysis for cardiolipin (CL) utilizing heart, liver and skeletal muscle tissue harvested from Taz KO and wildtype mice. As predicted in studies from model organisms and human patients, analysis of all the examined tissues revealed that the lipid make-up of the membrane was altered in Taz KO conditions. Taz is vital

for the production of tetralinoleoylcardiolipin (4L-CL), the mature poly-unsaturated form of CL. Our data show clearly the reduction in 4L-CL accompanied by the accumulation of the immature precursor MLCL and of phosphatidylcholine and phosphatidylethanolamine, which are side chain donors in the reaction. Lack of CL and accumulation of MLCL can be clearly detected in all examined tissues; however other alterations in lipid composition are only identifiable in the heart, while liver and skeletal muscle display a relatively normal lipid composition.

Mitochondria ultrastructure is also altered, with Taz KO cardiac mitochondria displaying swollen morphology and defects in cristae formation. The formation of the cristae is not completely impaired: we can in fact clearly detect them in the mitochondria; however, Taz KO cardiac mitochondria display larger matrix space and less organisation in the cristae superstructure compared to the wildtype. Interestingly this difference in phenotype is only present in adult mice, with Taz KO cardiac mitochondria in newborn mice displaying no ultrastructure differences from the wildtypes. Our results also point to a reduction in the number of mitochondria in the heart tissue. This reduction could be due to an increase in mitophagy or to a reduction in biogenesis of the organelles. Increase of mitophagy is somehow unlikely in our system: previous studies reveal a role for CL in the sensing of oxidative stress and in the initiation of the mitophagy; moreover, even though we did not specifically test for mitophagy in our system, electron microscopy does not seem to show any trace of enlarged autophagosomes or other hints to augmented mitochondria recycling. So, a possible explanation for the reduction of mitochondria numbers could be an impairment of the biogenesis of the mitochondria possibly due to defects in the mitochondria fission mechanism.

Cardiac muscle fibre ultrastructure does not seem to be altered in Taz KO mice. This observation is in contrast with the data reported in BTHS patients, who displayed altered sarcomere organization (Barth et al., 1983, Wang et al., 2014). The apparent lack of defects in the organization of the muscle fibres could be explained with the presence in the mouse of a compensating mechanism that repairs the sarcomere damage caused by loss of Taz in the human cells.

Data obtained in model organisms revealed a dramatic effect of the loss of Taz on the metabolic phenotype of the cell (section 1.4). The presence of defects in the metabolism and energy production could be a key factor in the aetiology of BTHS,

contributing to the severity of the symptoms and to the outcome of the pathology. We performed mass spectrometry analysis on heart, liver and skeletal muscle tissue to identify changes in the metabolism and detected a striking heart specific phenotype.

We detected an overall decrease in the concentration of glycolytic intermediates in our samples, which however do not affect the overall amount of pyruvate being produced by the pathway for use in the tricarboxylic acid (TCA) cycle. As previously hypothesised this observation can be justified by an increase in conversion of lactate to pyruvate via lactate dehydrogenase. Consistently, the concentration of lactate decreases across all our sample tissues.

This observation is somehow in contrast with the data coming from BTHS patients. A percentage of BTHS patients have been displaying a dramatic increase in the activity of the Cori cycle that powers the muscles through conversion of glucose to lactate through glycolysis in the muscle, followed by export of the lactate to the liver through the bloodstream. In the liver lactate is converted back to glucose via gluconeogenesis. The activation of the pathway serves the purpose of providing glucose to produce ATP via glycolysis in the muscle to compensate for blockage of the TCA cycle (section 1.1.3). Enhanced activation of the Cori cycle in the patients can be identified by detection of lactic acidosis in the plasma.

Activation of the Cori cycle in our system would result in increased liver concentration of lactate; however, we detected a decrease in the metabolite across all examined tissue, leading us to infer a generalized whole-body upregulation of the lactate to pyruvate conversion machinery. Lack of increase of lactate could be linked to the fact that animals are normally sampled during the day, which is the inactive part of their circadian cycle and in resting conditions. The situation may vary if we measured the metabolite content in heightened physical activity conditions.

We showed a heart-specific dysregulation of the activity of the TCA cycle with increased concentration of citrate and α-ketoglutarate and decreased concentration of succinate and malate. The metabolomic analysis of the pathway seems to indicate a blockade of the cycle at the α-ketoglutarate to succinate conversion stage, with accumulation of the metabolites prior to this stage and

decrease of the following ones. This observation is consistent with the body of knowledge gathered from model organisms, showing an inhibition of the TCA cycle caused by accumulation of NADH and FADH caused by disruption of the electron transport chain (ETC) (Kiebish et al., 2013). Consistently the NAD^+/NADH ratio in our samples is altered, with prevalence of the reduced NADH over NAD^+. This data supports the presence of product inhibition of the α-ketoglutarate dehydrogenase operated by NADH. However, isocitrate dehydrogenase is also sensitive to inhibition by high concentration of NADH, but the reaction does not seem to be impaired in our system. It has been reported in literature that α-ketoglutarate dehydrogenase is sensitive to reactive oxygen species (ROS) concentration in the mitochondria. At the moment, we have not yet performed ROS testing on our samples, but the presence of elevated ROS could explain why the inhibition of enzymatic activity seems to be specific to the α-ketoglutarate dehydrogenase. Gaining a better understanding of the mechanism behind the inhibition of the α-ketoglutarate dehydrogenase could offer useful insights to the enzymes function in our system. Plans are in place to identify and characterise this mechanism through enzymatic activity assays and metabolic flux analysis using labelled metabolites. These tests will allow us to identify the critical metabolic point for the inhibition of the TCA cycle.

Despite the apparent decrease in the activity of the glycolytic pathway and of the TCA cycle we did not identify a decrease in the energy charge in the examined tissues, with no alteration in the ATP/ADP/AMP ratios. This surprising observation is in sharp contrast with what is known about CL in the literature. It has been shown that CL plays a key role in IMM organization: it associates with and modifies the function of several membrane proteins. Notably CL associates with multiple components of the ETC including cytochrome C and the ATP synthase (Houtkooper and Vaz, 2008) and it has been proposed that it plays an active role in proton transport across the ion channels (Arnarez et al., 2013). With these premises it was reasonable to expect an effect in the energetic balance of the cells. Our experiments however, did not identify any perturbation in global ATP output; this could indicate that the cells are somehow compensating for the impairments in the energy production described above, by enhancing other metabolic pathways. Further investigation is needed to address this point.

Aiming to dissect the mitochondrial respiration ability of the heart, we optimized the rat neonatal cardiomyocytes model to our system, adapting the protocols to work with murine tissue and used the resulting cardiomyocytes for Seahorse analysis. The analysis however detected no differences in the respiration rates of Taz KO cardiomyocytes compared to the wildtype. The observation clashes with the data collected from model organisms, detecting a disruption of the ETC and reduced production of ATP through respiration. Our negative result on mitochondrial respiration could depend on different factors. Wang et al., in their work on patient derived induced pluripotent stem cells (iPSCs), detected a difference in respiration only when their iPSCs-derived cardiomyocytes were cultured in a medium containing galactose instead of glucose as a source of carbon which reduced glycolytic ability of the cells, forcing the cell metabolism towards mitochondrial respiration (Wang et al., 2014). Another possible reason for our failure to identify changes in the respiration rate of our cells could be that the neonatal cardiomyocyte system is less than ideal as a model to identify changes in adult tissue. As previously discussed, new-born heart tissue does not seem to bear the same mitochondria ultrastructure alterations as the adult. The problems with the seahorse experiment prompted us to perform a metabolic analysis on P1 mice using the same conditions we used in the adults. The alterations of the metabolome are much more evident in the adults than they are in the newborn. Mass spec analysis of samples of heart and liver for P1 mice showed fewer alteration overall in all the metabolites examined.

The different metabolomic makeover and the difference in the ultrastructure detected in the P1 mice compared to the adult lead us to postulate that our phenotype is linked to post-natal maturation of the cells. It has been reported that after birth the foetal mitochondrial complement of the cells is recycled and replaced with mature mitochondria (Gong et al., 2015). This mechanism could be a contributing reason to the differences observed in P1 vs adult mice.

Our efforts to obtain adult cardiomyocytes to use in Seahorse testing have been frustrated by intrinsic technical difficulties in deriving healthy cardiomyocytes from the adult heart. The techniques available for cardiomyocyte extraction from the adult heart offer poor efficiency and produce cells in poor health condition that tend to die after about 24h in culture. It is our opinion that cells in these

conditions are probably not the most accurate system to use in our studies. We believe it would be challenging to tell if changes detected in these cardiomyocytes due to the presence of an actual phenotype or to the distress condition of the cells.

Data from the mass spec. experiments also revealed a significant alteration in the metabolic content of a number of amino acids. Starting with this information we hypothesised the altered concentration could be linked to ATF4 activation caused by unfolded protein stimulus. To explore this hypothesis, we analysed the gene expression profile of the heart of adult mice looking for alterations.

The RNAseq data revealed a complex phenotype in Taz KO mice, with more than 3000 significantly altered genes. We detected significant alterations in the muscle organization and function gene networks, with dysregulation of structural proteins, calcium homeostasis machinery components and ion channels. The gene expression profile however is not fully mirrored in the phenotype. The changes in the expression of various structural proteins responsible for the correct formation of the sarcomeres, is somehow compensated in our system, resulting in normal muscle phenotype with no effect on the organization of the fibres. On the other hand, the downregulation of numerous ion channels and regulators of the cardiac contractility like the troponin complex is coherent with the data collected from ultrasound imaging of the heart (section 1.2). Our data on the contractility showed lower fractional shortening and increased QT interval. This observation is coherent with reduced expression of the ion channels and de-regulation of the genes responsible for the regulation of the contractility.

Our examination of the RNAseq also supported our hypothesis of an activation of the unfolded protein response (UPR) caused by loss of Taz function. Our data reveals that both the endoplasmic reticulum (ER) and the mitochondria are involved in the UPR, with activation of all the main signalling pathways involved in this stress response mechanism. In recent years, there has been a surge of evidence of a crosstalk between the ER UPR (UPR^{ER}) and the mitochondrial UPR (UPR^{MT}) aimed to stress resistance and cell survival.

In Taz KO hearts both the UPR^{ER} and the UPR^{MT} appear to be activated, with increased transcription of ATF4, ATF5 and ATF6, which activate a repair

programme aimed to the removal of the UP stimulus via enhancement of the protein folding machinery. Autophagy and apoptosis do not seem to be activated in our system. It has been reported that UPR^{ER} and UPR^{MT} cooperate to activate a complex response mechanism known as the integrated stress response (ISR) (Salminen et al., 2017). The ISR acts as a response mechanism to a number of stimuli including amino acid starvation, presence of double strand RNA in the cytosol, metal stress and ER and mitochondria stress. The activation of these initiating stimuli leads to phosphorylation of eIF2α and the inhibition of protein translation (Pakos-Zebrucka et al., 2016, Baird and Wek, 2012). Phosphorylation of eIF2α leads to the transcription of stress-response transcripts like ATF4 and ATF5 and to the activation of a genetic programme aimed to the reduction of the stress stimulus and the recovery of the homeostasis. Besides its cellular roles ATF4 plays a key role in the ISR as a regulator of the response machinery by inducing the transcription of *Fgf21* (Schaap et al., 2013, De Sousa-Coelho et al., 2012). FGF21 is an endocrine molecule of the FGF family with a role in systemic metabolism, development and survival. The activation of the transcription, translation and secretion of the molecule results in a whole-body enhancement of the stress resistance mechanisms. *Fgf21* has both paracrine and autocrine signalling functions and performs different roles in different tissues (Salminen et al., 2017). Analysis of our samples indicate a massive increase in *Fgf21* levels in the heart of Taz KO mice (+98 fold enrichment p=3.7E-89) it has been reported that *Fgf21* has a cardioprotective function in myocardial ischemia and in ER/mitochondria induced stress, in our system *Fgf21* could be contributing to the survival of the cardiac cells in a non-cell-autonomous way, in cooperation with the cell-autonomous pro-survival mechanisms activated by the UPR^{ER} and UPR^{MT}.

Our current data suggest a possible explanation of the phenotypes observed in this thesis: IMM instability caused by lack of mature CL causes the disruption of the ETC and a perturbation of the membrane potential. Alterations of the membrane potential cause the production of ROS which influence the correct protein folding in the mitochondrial matrix and in the cytosol. The resulting unfolded proteins trigger the activation of the UPR and of the ISR in an attempt to restore homeostasis (Figure 4.1). Further investigation is needed to verify the mechanism.

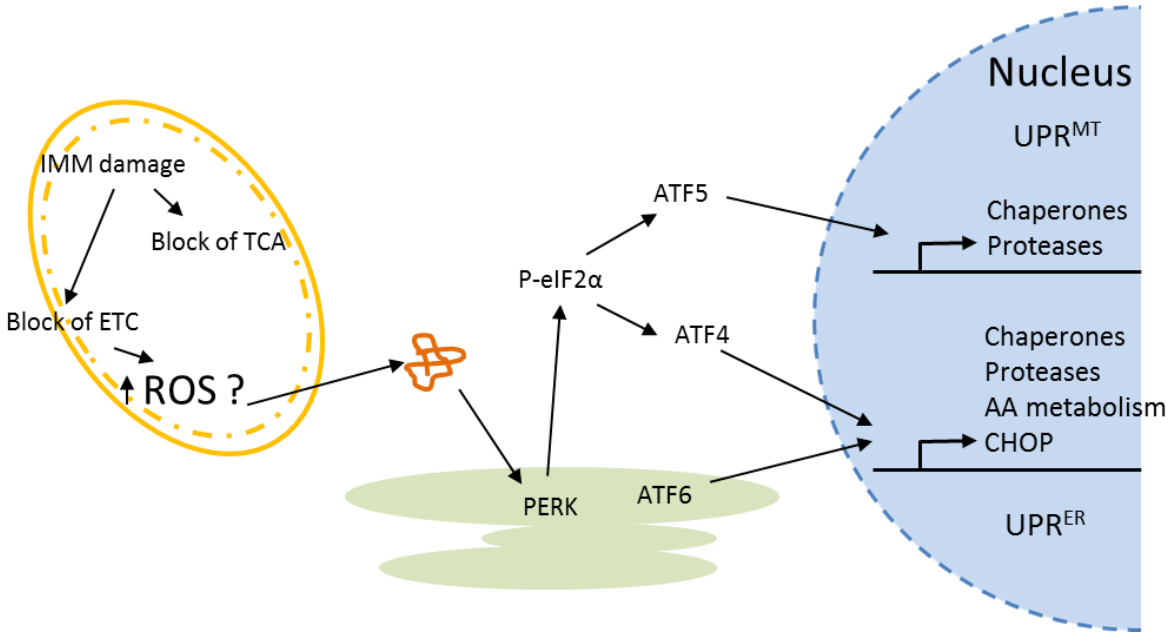

Figure 4.1: Proposed mechanism of action of Taz KO on the mitochondrial metabolism and on the activation of the UPR

4.2 Future directions

In this study we showed an extensive effect of Taz KO on mitochondria structure and function, metabolic content and gene expression.

The characterization of the mitochondrial changes in our model of BTHS is still not complete, with many questions left unanswered. At this point we do not have a verified mechanism for the reduction of the number of mitochondria we detected in both heart tissue and skin fibroblasts. In the discussion we proposed the reduction in the number of mitochondria could be related to defects in the mitochondrial dynamics. To verify this hypothesis mitotracker, a live mitochondria dye, could be used to follow the cells dynamically using the IncuCyte live cell analysis system. This system would allow us to image mitochondria in skin fibroblasts in real time, following the changes of fission, fusion and remodelling of the organelles.

Another interesting aspect of the mitochondria biology we would like to explore is the level of reactive oxygen species generated in the mitochondrial matrix. Because of the membrane defects we identified in our model, we anticipate a

perturbation of ROS levels in the matrix. A change in ROS could hold a big biological significance since it could contribute to paint a more complex picture of the mitochondrial environment. Moreover, high ROS levels could contribute to metabolic changes and could affect the protein folding machinery, contributing to the UPR.

The metabolic changes of the mice also need further investigation. Our analysis offered us a snapshot of the metabolic situation of the heart, liver and skeletal muscle. However more in-depth analysis could offer us invaluable information about the active metabolic pathways in a mammalian model of BTHS. The vast majority of the information we possess about the metabolic pathways activated by loss of Taz derive from model organism, so a systemic approach, with information about whole-organ and whole-body metabolic effects could prove useful to gain new insights in BTHS biology and for drug development.

We proposed an involvement of the unfolded protein response in the preservation of cell homeostasis in Taz KO hearts. We offered preliminary evidence of the activation of both the UPR^{ER} and UPR^{MT} in the heart and proposed a cooperation of the two in an integrated stress response mechanism aimed to protect the heart from stress and damage. The hypothesis needs further verification to be confirmed. First step to obtain this verification would be an RTqPCR analysis on RNA extracted from the heart and possibly other tissue, to obtain an independent measure of the gene expression and to verify if the UPRs are active in other tissues. Next step would be to test the specific branches of the UPR pathways to try and identify the key elements necessary for the response in our system. Finally, it would be interesting to explore the autocrine and paracrine role of *Fgf21* on BTHS mice.

In this study we showed that our model displays many of the features of BTHS, however the model is not a 100% match to the human phenotype, in fact our mice are not exhibiting signs of muscular defects nor of neutropenia. Neutrophil presence in the blood was investigated using an IDEXX ProCyte blood analyser and FACS analysis, both methods gave no sensible difference in neutrophil count between the wildtype and the KO animals. We also performed FACS analysis on bone marrow samples, but again no difference was detected between the 2 genotypes (data not shown). Neutropenia is a highly volatile phenotype in BTHS

patients, so further studies might be necessary to verify the presence of the phenotype. Unfortunately, the size of the animals and consequently the amount of blood that can be harvested prevent us from performing serial bleedings or time course experiments. As we previously discussed, Taz is highly evolutionarily conserved; however, in the primates, Taz displays an extra exon compared to other mammals. This could be a reason why murine Taz does not seem to have the exact same functions of the human one. To test this idea, the lab is working on humanizing the Taz locus by deleting the murine sequence in ESCs and exchanging it with the human homologue. A murine model created using the humanized locus could be an important step forward to the obtainment of a BTHS model that fully recapitulates the human phenotype.

5. References

ACEHAN, D., KHUCHUA, Z., HOUTKOOPER, R. H., MALHOTRA, A., KAUFMAN, J., VAZ, F. M., REN, M., ROCKMAN, H. A., STOKES, D. L. & SCHLAME, M. 2009. Distinct effects of tafazzin deletion in differentiated and undifferentiated mitochondria. *Mitochondrion,* 9**,** 86-95.

ACEHAN, D., VAZ, F., HOUTKOOPER, R. H., JAMES, J., MOORE, V., TOKUNAGA, C., KULIK, W., WANSAPURA, J., TOTH, M. J., STRAUSS, A. & KHUCHUA, Z. 2011. Cardiac and skeletal muscle defects in a mouse model of human Barth syndrome. *J Biol Chem,* 286**,** 899-908.

ACEHAN, D., XU, Y., STOKES, D. L. & SCHLAME, M. 2007. Comparison of lymphoblast mitochondria from normal subjects and patients with Barth syndrome using electron microscopic tomography. *Lab Invest,* 87**,** 40-8.

ADES, L. C., GEDEON, A. K., WILSON, M. J., LATHAM, M., PARTINGTON, M. W., MULLEY, J. C., NELSON, J., LUI, K. & SILLENCE, D. O. 1993. Barth syndrome: clinical features and confirmation of gene localisation to distal Xq28. *Am J Med Genet,* 45**,** 327-34.

ANCES, B. M., SULLIVAN, J., WEIGELE, J. B., HWANG, V., MESSE, S. R., KASNER, S. E. & LIEBESKIND, D. S. 2006. Stroke associated with Barth syndrome. *J Child Neurol,* 21**,** 805-7.

ARIYASU, D., YOSHIDA, H. & HASEGAWA, Y. 2017. Endoplasmic Reticulum (ER) Stress and Endocrine Disorders. *Int J Mol Sci,* 18.

ARNAREZ, C., MARRINK, S. J. & PERIOLE, X. 2013. Identification of cardiolipin binding sites on cytochrome c oxidase at the entrance of proton channels. *Sci Rep,* 3**,** 1263.

BAIRD, T. D. & WEK, R. C. 2012. Eukaryotic initiation factor 2 phosphorylation and translational control in metabolism. *Adv Nutr,* 3**,** 307-21.

BARTH, P. G., SCHOLTE, H. R., BERDEN, J. A., VAN DER KLEI-VAN MOORSEL, J. M., LUYT-HOUWEN, I. E., VAN 'T VEER-KORTHOF, E. T., VAN DER HARTEN, J. J. & SOBOTKA-PLOJHAR, M. A. 1983. An X-linked mitochondrial disease affecting cardiac muscle, skeletal muscle and neutrophil leucocytes. *J Neurol Sci,* 62**,** 327-55.

BARTH, P. G., WANDERS, R. J. & VREKEN, P. 1999. X-linked cardioskeletal myopathy and neutropenia (Barth syndrome)-MIM 302060. *J Pediatr,* 135**,** 273-6.

BARTH SYNDROME FOUNDATION. 2006. *Barth Syndrome FAQs* [Online]. https://www.barthsyndrome.org/home. Available: https://www.barthsyndrome.org/CMFiles/BarthSyndrome/BarthSyndromeFAQs_FINAL_May200637UHJ-5282006-2468.pdf [Accessed march 2017].

BARTH SYNDROME FOUNDATION. 2018. *Human tafazzin mutation database* [Online]. Available: https://www.barthsyndrome.org/research/tazdatabase.html [Accessed 03/05/2018 2018].

BASHIR, A., BOHNERT, K. L., REEDS, D. N., PETERSON, L. R., BITTEL, A. J., DE LAS FUENTES, L., PACAK, C. A., BYRNE, B. J. & CADE, W. T. 2017. Impaired cardiac and skeletal muscle bioenergetics in children, adolescents, and young adults with Barth syndrome. *Physiol Rep,* 5.

BERTOLOTTI, A., ZHANG, Y., HENDERSHOT, L. M., HARDING, H. P. & RON, D. 2000. Dynamic interaction of BiP and ER stress transducers in the unfolded-protein response. *Nat Cell Biol,* 2**,** 326-32.

BISSLER, J. J., TSORAS, M., GORING, H. H., HUG, P., CHUCK, G., TOMBRAGEL, E., MCGRAW, C., SCHLOTMAN, J., RALSTON, M. A. & HUG, G. 2002. Infantile dilated X-linked cardiomyopathy, G4.5 mutations, altered lipids, and ultrastructural malformations of mitochondria in heart, liver, and skeletal muscle. *Lab Invest,* 82**,** 335-44.

BOLHUIS, P. A., HENSELS, G. W., HULSEBOS, T. J., BAAS, F. & BARTH, P. G. 1991. Mapping of the locus for X-linked cardioskeletal myopathy with neutropenia and abnormal mitochondria (Barth syndrome) to Xq28. *Am J Hum Genet,* 48**,** 481-5.

BOLYARD, A. A., MARRERO, T. M., BONILLA, M. A., PHAN, L. & STEWARD, C. 2013. Barth Syndrome and Neutropenia. *Blood,* 122**,** 3465-3465.

BOWRON, A., HONEYCHURCH, J., WILLIAMS, M., TSAI-GOODMAN, B., CLAYTON, N., JONES, L., SHORTLAND, G. J., QURESHI, S. A., HEALES, S. J. & STEWARD, C. G. 2015. Barth syndrome without tetralinoleoyl cardiolipin deficiency: a possible ameliorated phenotype. *J Inherit Metab Dis,* 38**,** 279-86.

CADALBERT, L. C., GHAFFAR, F. N., STEVENSON, D., BRYSON, S., VAZ, F. M., GOTTLIEB, E. & STRATHDEE, D. 2015. Mouse Tafazzin Is Required for Male Germ Cell Meiosis and Spermatogenesis. *PLoS One,* 10**,** e0131066.

CADE, W. T., REEDS, D. N., PETERSON, L. R., BOHNERT, K. L., TINIUS, R. A., BENNI, P. B., BYRNE, B. J. & TAYLOR, C. L. 2017. Endurance Exercise Training in Young Adults with Barth Syndrome: A Pilot Study. *JIMD Rep,* 32**,** 15-24.

CAO, J., LIU, Y., LOCKWOOD, J., BURN, P. & SHI, Y. 2004. A novel cardiolipin-remodeling pathway revealed by a gene encoding an endoplasmic reticulum-associated acyl-CoA:lysocardiolipin acyltransferase (ALCAT1) in mouse. *J Biol Chem,* 279**,** 31727-34.

CHU, C. T., BAYIR, H. & KAGAN, V. E. 2014. LC3 binds externalized cardiolipin on injured mitochondria to signal mitophagy in neurons: implications for Parkinson disease. *Autophagy,* 10**,** 376-8.

CHU, C. T., JI, J., DAGDA, R. K., JIANG, J. F., TYURINA, Y. Y., KAPRALOV, A. A., TYURIN, V. A., YANAMALA, N., SHRIVASTAVA, I. H., MOHAMMADYANI, D., WANG, K. Z. Q., ZHU, J., KLEIN-SEETHARAMAN, J., BALASUBRAMANIAN, K., AMOSCATO, A. A., BORISENKO, G., HUANG, Z., GUSDON, A. M., CHEIKHI, A., STEER, E. K., WANG, R., BATY, C., WATKINS, S., BAHAR, I., BAYIR, H. & KAGAN, V. E. 2013. Cardiolipin externalization to the outer mitochondrial membrane acts as an elimination signal for mitophagy in neuronal cells. *Nat Cell Biol,* 15**,** 1197-1205.

CLARKE, S. L., BOWRON, A., GONZALEZ, I. L., GROVES, S. J., NEWBURY-ECOB, R., CLAYTON, N., MARTIN, R. P., TSAI-GOODMAN, B., GARRATT, V., ASHWORTH, M., BOWEN, V. M., MCCURDY, K. R., DAMIN, M. K., SPENCER, C. T., TOTH, M. J., KELLEY, R. I. & STEWARD, C. G. 2013. Barth syndrome. *Orphanet J Rare Dis,* 8**,** 23.

COSSON, L., TOUTAIN, A., SIMARD, G., KULIK, W., MATYAS, G., GUICHET, A., BLASCO, H., MAAKAROUN-VERMESSE, Z., VAILLANT, M. C., LE CAIGNEC, C., CHANTEPIE, A. & LABARTHE, F. 2012. Barth syndrome in a female patient. *Mol Genet Metab,* 106**,** 115-20.

DE SOUSA-COELHO, A. L., MARRERO, P. F. & HARO, D. 2012. Activating transcription factor 4-dependent induction of FGF21 during amino acid deprivation. *Biochem J,* 443**,** 165-71.

DUDEK, J., CHENG, I. F., CHOWDHURY, A., WOZNY, K., BALLEININGER, M., REINHOLD, R., GRUNAU, S., CALLEGARI, S., TOISCHER, K., WANDERS, R. J., HASENFUSS, G., BRUGGER, B., GUAN, K. & REHLING, P. 2016. Cardiac-specific succinate dehydrogenase deficiency in Barth syndrome. *EMBO Mol Med,* 8**,** 139-54.

FIORESE, C. J., SCHULZ, A. M., LIN, Y. F., ROSIN, N., PELLEGRINO, M. W. & HAYNES, C. M. 2016. The Transcription Factor ATF5 Mediates a Mammalian Mitochondrial UPR. *Curr Biol,* 26**,** 2037-2043.

FISHER, S., BARRY, A., ABREU, J., MINIE, B., NOLAN, J., DELOREY, T. M., YOUNG, G., FENNELL, T. J., ALLEN, A., AMBROGIO, L., BERLIN, A. M., BLUMENSTIEL, B., CIBULSKIS, K., FRIEDRICH, D., JOHNSON, R., JUHN, F., REILLY, B., SHAMMAS, R., STALKER, J., SYKES, S. M., THOMPSON, J., WALSH, J., ZIMMER, A., ZWIRKO, Z., GABRIEL, S., NICOL, R. & NUSBAUM, C. 2011. A scalable, fully automated process for construction of sequence-ready human exome targeted capture libraries. *Genome Biol,* 12**,** R1.

FRY, M. & GREEN, D. E. 1981. Cardiolipin requirement for electron transfer in complex I and III of the mitochondrial respiratory chain. *J Biol Chem,* 256**,** 1874-80.

GABRIEL, J. L. & PLAUT, G. W. 1984. Inhibition of bovine heart NAD-specific isocitrate dehydrogenase by reduced pyridine nucleotides: modulation of inhibition by ADP, NAD+, Ca2+, citrate, and isocitrate. *Biochemistry,* 23**,** 2773-8.

GALBRAITH, L. C. A. 2014. The role of cardiolipin in mitophagy.

GONG, G., SONG, M., CSORDAS, G., KELLY, D. P., MATKOVICH, S. J. & DORN, G. W., 2ND 2015. Parkin-mediated mitophagy directs perinatal cardiac metabolic maturation in mice. *Science,* 350**,** aad2459.

GONZALVEZ, F., D'AURELIO, M., BOUTANT, M., MOUSTAPHA, A., PUECH, J. P., LANDES, T., ARNAUNE-PELLOQUIN, L., VIAL, G., TALEUX, N., SLOMIANNY, C., WANDERS, R. J., HOUTKOOPER, R. H., BELLENGUER, P., MOLLER, I. M., GOTTLIEB, E., VAZ, F. M., MANFREDI,

G. & PETIT, P. X. 2013. Barth syndrome: cellular compensation of mitochondrial dysfunction and apoptosis inhibition due to changes in cardiolipin remodeling linked to tafazzin (TAZ) gene mutation. *Biochim Biophys Acta,* 1832**,** 1194-206.

HARDING, H. P., ZHANG, Y., BERTOLOTTI, A., ZENG, H. & RON, D. 2000. Perk is essential for translational regulation and cell survival during the unfolded protein response. *Mol Cell,* 5**,** 897-904.

HARDING, H. P., ZHANG, Y., ZENG, H., NOVOA, I., LU, P. D., CALFON, M., SADRI, N., YUN, C., POPKO, B., PAULES, R., STOJDL, D. F., BELL, J. C., HETTMANN, T., LEIDEN, J. M. & RON, D. 2003. An integrated stress response regulates amino acid metabolism and resistance to oxidative stress. *Mol Cell,* 11**,** 619-33.

HAYNES, C. M., PETROVA, K., BENEDETTI, C., YANG, Y. & RON, D. 2007. ClpP mediates activation of a mitochondrial unfolded protein response in C. elegans. *Dev Cell,* 13**,** 467-80.

HAYNES, C. M., YANG, Y., BLAIS, S. P., NEUBERT, T. A. & RON, D. 2010. The matrix peptide exporter HAF-1 signals a mitochondrial UPR by activating the transcription factor ZC376.7 in C. elegans. *Mol Cell,* 37**,** 529-40.

HOFFMANN, B., STOCKL, A., SCHLAME, M., BEYER, K. & KLINGENBERG, M. 1994. The reconstituted ADP/ATP carrier activity has an absolute requirement for cardiolipin as shown in cysteine mutants. *J Biol Chem,* 269**,** 1940-4.

HORIBE, T. & HOOGENRAAD, N. J. 2007. The chop gene contains an element for the positive regulation of the mitochondrial unfolded protein response. *PLoS One,* 2**,** e835.

HOUTKOOPER, R. H., MOUCHIROUD, L., RYU, D., MOULLAN, N., KATSYUBA, E., KNOTT, G., WILLIAMS, R. W. & AUWERX, J. 2013. Mitonuclear protein imbalance as a conserved longevity mechanism. *Nature,* 497**,** 451-7.

HOUTKOOPER, R. H. & VAZ, F. M. 2008. Cardiolipin, the heart of mitochondrial metabolism. *Cell Mol Life Sci,* 65**,** 2493-506.

HUANG, Y., POWERS, C., MOORE, V., SCHAFER, C., REN, M., PHOON, C. K., JAMES, J. F., GLUKHOV, A. V., JAVADOV, S., VAZ, F. M., JEFFERIES, J. L., STRAUSS, A. W. & KHUCHUA, Z. 2017. The PPAR pan-agonist bezafibrate ameliorates cardiomyopathy in a mouse model of Barth syndrome. *Orphanet J Rare Dis,* 12**,** 49.

IKON, N. & RYAN, R. O. 2016. On the origin of 3-methylglutaconic acid in disorders of mitochondrial energy metabolism. *J Inherit Metab Dis,* 39**,** 749-56.

IKON, N. & RYAN, R. O. 2017. Barth Syndrome: Connecting Cardiolipin to Cardiomyopathy. *Lipids,* 52**,** 99-108.

KELLEY, R. I., CHEATHAM, J. P., CLARK, B. J., NIGRO, M. A., POWELL, B. R., SHERWOOD, G. W., SLADKY, J. T. & SWISHER, W. P. 1991. X-linked dilated cardiomyopathy with neutropenia, growth retardation, and 3-methylglutaconic aciduria. *J Pediatr,* 119**,** 738-47.

KIEBISH, M. A., YANG, K., LIU, X., MANCUSO, D. J., GUAN, S., ZHAO, Z., SIMS, H. F., CERQUA, R., CADE, W. T., HAN, X. & GROSS, R. W. 2013. Dysfunctional cardiac mitochondrial bioenergetic, lipidomic, and signaling in a murine model of Barth syndrome. *J Lipid Res,* 54**,** 1312-25.

KOSHKIN, V. & GREENBERG, M. L. 2002. Cardiolipin prevents rate-dependent uncoupling and provides osmotic stability in yeast mitochondria. *Biochem J,* 364**,** 317-22.

KUIJPERS, T. W., MAIANSKI, N. A., TOOL, A. T., BECKER, K., PLECKO, B., VALIANPOUR, F., WANDERS, R. J., PEREIRA, R., VAN HOVE, J., VERHOEVEN, A. J., ROOS, D., BAAS, F. & BARTH, P. G. 2004. Neutrophils in Barth syndrome (BTHS) avidly bind annexin-V in the absence of apoptosis. *Blood,* 103**,** 3915-23.

LI, X. X., TSOI, B., LI, Y. F., KURIHARA, H. & HE, R. R. 2015. Cardiolipin and its different properties in mitophagy and apoptosis. *J Histochem Cytochem,* 63**,** 301-11.

LOUCH, W. E., SHEEHAN, K. A. & WOLSKA, B. M. 2011. Methods in cardiomyocyte isolation, culture, and gene transfer. *J Mol Cell Cardiol,* 51**,** 288-98.

MAKARYAN, V., KULIK, W., VAZ, F. M., ALLEN, C., DROR, Y., DALE, D. C. & APRIKYAN, A. A. 2012. The cellular and molecular mechanisms for neutropenia in Barth syndrome. *Eur J Haematol,* 88**,** 195-209.

MALHOTRA, A., EDELMAN-NOVEMSKY, I., XU, Y., PLESKEN, H., MA, J., SCHLAME, M. & REN, M. 2009. Role of calcium-independent phospholipase A2 in the pathogenesis of Barth syndrome. *Proc Natl Acad Sci U S A,* 106**,** 2337-41.

MARTINUS, R. D., GARTH, G. P., WEBSTER, T. L., CARTWRIGHT, P., NAYLOR, D. J., HOJ, P. B. & HOOGENRAAD, N. J. 1996. Selective induction of mitochondrial chaperones in response to loss of the mitochondrial genome. *Eur J Biochem,* 240**,** 98-103.

MCCULLOUGH, K. D., MARTINDALE, J. L., KLOTZ, L. O., AW, T. Y. & HOLBROOK, N. J. 2001. Gadd153 sensitizes cells to endoplasmic reticulum stress by down-regulating Bcl2 and perturbing the cellular redox state. *Mol Cell Biol,* 21**,** 1249-59.

MCLAIN, A. L., CORMIER, P. J., KINTER, M. & SZWEDA, L. I. 2013. Glutathionylation of alpha-ketoglutarate dehydrogenase: the chemical nature and relative susceptibility of the cofactor lipoic acid to modification. *Free Radic Biol Med,* 61**,** 161-9.

MOULLAN, N., MOUCHIROUD, L., WANG, X., RYU, D., WILLIAMS, E. G., MOTTIS, A., JOVAISAITE, V., FROCHAUX, M. V., QUIROS, P. M., DEPLANCKE, B., HOUTKOOPER, R. H. & AUWERX, J. 2015. Tetracyclines Disturb Mitochondrial Function across Eukaryotic Models: A Call for Caution in Biomedical Research. *Cell Rep*.

MUNCH, C. & HARPER, J. W. 2016. Mitochondrial unfolded protein response controls matrix pre-RNA processing and translation. *Nature,* 534**,** 710-3.

NARGUND, A. M., FIORESE, C. J., PELLEGRINO, M. W., DENG, P. & HAYNES, C. M. 2015. Mitochondrial and nuclear accumulation of the transcription factor ATFS-1 promotes OXPHOS recovery during the UPR(mt). *Mol Cell,* 58**,** 123-33.

NARGUND, A. M., PELLEGRINO, M. W., FIORESE, C. J., BAKER, B. M. & HAYNES, C. M. 2012. Mitochondrial import efficiency of ATFS-1 regulates mitochondrial UPR activation. *Science,* 337**,** 587-90.

NOVOA, I., ZHANG, Y., ZENG, H., JUNGREIS, R., HARDING, H. P. & RON, D. 2003. Stress-induced gene expression requires programmed recovery from translational repression. *EMBO J,* 22**,** 1180-7.

ORSTAVIK, K. H., ORSTAVIK, R. E., NAUMOVA, A. K., D'ADAMO, P., GEDEON, A., BOLHUIS, P. A., BARTH, P. G. & TONIOLO, D. 1998. X chromosome inactivation in carriers of Barth syndrome. *Am J Hum Genet,* 63**,** 1457-63.

PAKOS-ZEBRUCKA, K., KORYGA, I., MNICH, K., LJUJIC, M., SAMALI, A. & GORMAN, A. M. 2016. The integrated stress response. *EMBO Rep,* 17**,** 1374-1395.

PAPA, L. & GERMAIN, D. 2014. SirT3 regulates the mitochondrial unfolded protein response. *Mol Cell Biol,* 34**,** 699-710.

PELLEGRINO, M. W., NARGUND, A. M., KIRIENKO, N. V., GILLIS, R., FIORESE, C. J. & HAYNES, C. M. 2014. Mitochondrial UPR-regulated innate immunity provides resistance to pathogen infection. *Nature,* 516**,** 414-7.

PHOON, C. K., ACEHAN, D., SCHLAME, M., STOKES, D. L., EDELMAN-NOVEMSKY, I., YU, D., XU, Y., VISWANATHAN, N. & REN, M. 2012. Tafazzin knockdown in mice leads to a developmental cardiomyopathy with early diastolic dysfunction preceding myocardial noncompaction. *J Am Heart Assoc,* 1.

PIGNATELLI, R. H., MCMAHON, C. J., DREYER, W. J., DENFIELD, S. W., PRICE, J., BELMONT, J. W., CRAIGEN, W. J., WU, J., EL SAID, H., BEZOLD, L. I., CLUNIE, S., FERNBACH, S., BOWLES, N. E. & TOWBIN, J. A. 2003. Clinical characterization of left ventricular noncompaction in children: a relatively common form of cardiomyopathy. *Circulation,* 108**,** 2672-8.

RAVEN, J. F., BALTZIS, D., WANG, S., MOUNIR, Z., PAPADAKIS, A. I., GAO, H. Q. & KOROMILAS, A. E. 2008. PKR and PKR-like endoplasmic reticulum kinase induce the proteasome-dependent degradation of cyclin D1 via a mechanism requiring eukaryotic initiation factor 2alpha phosphorylation. *J Biol Chem,* 283**,** 3097-108.

RENNER, L. D. & WEIBEL, D. B. 2011. Cardiolipin microdomains localize to negatively curved regions of Escherichia coli membranes. *Proc Natl Acad Sci U S A,* 108**,** 6264-9.

RIGAUD, C., LEBRE, A. S., TOURAINE, R., BEAUPAIN, B., OTTOLENGHI, C., CHABLI, A., ANSQUER, H., OZSAHIN, H., DI FILIPPO, S., DE LONLAY, P., BORM, B., RIVIER, F., VAILLANT, M. C.,

MATHIEU-DRAMARD, M., GOLDENBERG, A., VIOT, G., CHARRON, P., RIO, M., BONNET, D. & DONADIEU, J. 2013. Natural history of Barth syndrome: a national cohort study of 22 patients. *Orphanet J Rare Dis,* 8**,** 70.

ROBERTS, A. E., NIXON, C., STEWARD, C. G., GAUVREAU, K., MAISENBACHER, M., FLETCHER, M., GEVA, J., BYRNE, B. J. & SPENCER, C. T. 2012. The Barth Syndrome Registry: distinguishing disease characteristics and growth data from a longitudinal study. *Am J Med Genet A,* 158A**,** 2726-32.

RONVELIA, D., GREENWOOD, J., PLATT, J., HAKIM, S. & ZARAGOZA, M. V. 2012. Intrafamilial variability for novel TAZ gene mutation: Barth syndrome with dilated cardiomyopathy and heart failure in an infant and left ventricular noncompaction in his great-uncle. *Mol Genet Metab,* 107**,** 428-32.

SALMINEN, A., KAARNIRANTA, K. & KAUPPINEN, A. 2017. Integrated stress response stimulates FGF21 expression: Systemic enhancer of longevity. *Cell Signal,* 40**,** 10-21.

SCHAAP, F. G., KREMER, A. E., LAMERS, W. H., JANSEN, P. L. & GAEMERS, I. C. 2013. Fibroblast growth factor 21 is induced by endoplasmic reticulum stress. *Biochimie,* 95**,** 692-9.

SCHRODER, M. & KAUFMAN, R. J. 2005. The mammalian unfolded protein response. *Annu Rev Biochem,* 74**,** 739-89.

SHEN, J., CHEN, X., HENDERSHOT, L. & PRYWES, R. 2002. ER stress regulation of ATF6 localization by dissociation of BiP/GRP78 binding and unmasking of Golgi localization signals. *Dev Cell,* 3**,** 99-111.

SMITH, C. M., BRYLA, J. & WILLIAMSON, J. R. 1974. Regulation of mitochondrial alpha-ketoglutarate metabolism by product inhibition at alpha-ketoglutarate dehydrogenase. *J Biol Chem,* 249**,** 1497-505.

SOEHNLEIN, O., STEFFENS, S., HIDALGO, A. & WEBER, C. 2017. Neutrophils as protagonists and targets in chronic inflammation. *Nat Rev Immunol,* 17**,** 248-261.

SOUSTEK, M. S., FALK, D. J., MAH, C. S., TOTH, M. J., SCHLAME, M., LEWIN, A. S. & BYRNE, B. J. 2011. Characterization of a transgenic short hairpin RNA-induced murine model of Tafazzin deficiency. *Hum Gene Ther,* 22**,** 865-71.

SPENCER, C. T., BRYANT, R. M., DAY, J., GONZALEZ, I. L., COLAN, S. D., THOMPSON, W. R., BERTHY, J., REDFEARN, S. P. & BYRNE, B. J. 2006. Cardiac and clinical phenotype in Barth syndrome. *Pediatrics,* 118**,** e337-46.

SPENCER, C. T., BYRNE, B. J., BRYANT, R. M., MARGOSSIAN, R., MAISENBACHER, M., BREITENGER, P., BENNI, P. B., REDFEARN, S., MARCUS, E. & CADE, W. T. 2011. Impaired cardiac reserve and severely diminished skeletal muscle O(2) utilization mediate exercise intolerance in Barth syndrome. *Am J Physiol Heart Circ Physiol,* 301**,** H2122-9.

SPENCER, C. T., BYRNE, B. J., GEWITZ, M. H., WECHSLER, S. B., KAO, A. C., GERSTENFELD, E. P., MERLISS, A. D., CARBONI, M. P. & BRYANT, R. M. 2005. Ventricular arrhythmia in the X-linked cardiomyopathy Barth syndrome. *Pediatr Cardiol,* 26**,** 632-7.

SU, B. & RYAN, R. O. 2014. Metabolic biology of 3-methylglutaconic acid-uria: a new perspective. *J Inherit Metab Dis,* 37**,** 359-68.

TAYLOR, W. A. & HATCH, G. M. 2009. Identification of the human mitochondrial linoleoyl-coenzyme A monolysocardiolipin acyltransferase (MLCL AT-1). *J Biol Chem,* 284**,** 30360-71.

TRETTER, L. & ADAM-VIZI, V. 2005. Alpha-ketoglutarate dehydrogenase: a target and generator of oxidative stress. *Philos Trans R Soc Lond B Biol Sci,* 360**,** 2335-45.

URANO, F., WANG, X., BERTOLOTTI, A., ZHANG, Y., CHUNG, P., HARDING, H. P. & RON, D. 2000. Coupling of stress in the ER to activation of JNK protein kinases by transmembrane protein kinase IRE1. *Science,* 287**,** 664-6.

VABULAS, R. M., RAYCHAUDHURI, S., HAYER-HARTL, M. & HARTL, F. U. 2010. Protein folding in the cytoplasm and the heat shock response. *Cold Spring Harb Perspect Biol,* 2**,** a004390.

VAN RAAM, B. J. & KUIJPERS, T. W. 2009. Mitochondrial defects lie at the basis of neutropenia in Barth syndrome. *Curr Opin Hematol,* 16**,** 14-9.

VAZ, F. M., HOUTKOOPER, R. H., VALIANPOUR, F., BARTH, P. G. & WANDERS, R. J. 2003. Only one splice variant of the human TAZ gene encodes a functional protein with a role in cardiolipin metabolism. *J Biol Chem,* 278**,** 43089-94.

VINET, L., ROUET-BENZINEB, P., MARNIQUET, X., PELLEGRIN, N., MANGIN, L., LOUEDEC, L., SAMUEL, J. L. & MERCADIER, J. J. 2008. Chronic doxycycline exposure accelerates left ventricular hypertrophy and progression to heart failure in mice after thoracic aorta constriction. *Am J Physiol Heart Circ Physiol,* 295**,** H352-60.

WALTER, P. & RON, D. 2011. The unfolded protein response: from stress pathway to homeostatic regulation. *Science,* 334**,** 1081-6.

WANG, G., MCCAIN, M. L., YANG, L., HE, A., PASQUALINI, F. S., AGARWAL, A., YUAN, H., JIANG, D., ZHANG, D., ZANGI, L., GEVA, J., ROBERTS, A. E., MA, Q., DING, J., CHEN, J., WANG, D. Z., LI, K., WANG, J., WANDERS, R. J., KULIK, W., VAZ, F. M., LAFLAMME, M. A., MURRY, C. E., CHIEN, K. R., KELLEY, R. I., CHURCH, G. M., PARKER, K. K. & PU, W. T. 2014. Modeling the mitochondrial cardiomyopathy of Barth syndrome with induced pluripotent stem cell and heart-on-chip technologies. *Nat Med,* 20**,** 616-23.

WU, J., RUTKOWSKI, D. T., DUBOIS, M., SWATHIRAJAN, J., SAUNDERS, T., WANG, J., SONG, B., YAU, G. D. & KAUFMAN, R. J. 2007. ATF6alpha optimizes long-term endoplasmic reticulum function to protect cells from chronic stress. *Dev Cell,* 13**,** 351-64.

XU, Y., CONDELL, M., PLESKEN, H., EDELMAN-NOVEMSKY, I., MA, J., REN, M. & SCHLAME, M. 2006. A Drosophila model of Barth syndrome. *Proc Natl Acad Sci U S A,* 103**,** 11584-8.

XU, Y., PHOON, C. K., BERNO, B., D'SOUZA, K., HOEDT, E., ZHANG, G., NEUBERT, T. A., EPAND, R. M., REN, M. & SCHLAME, M. 2016. Loss of protein association causes cardiolipin degradation in Barth syndrome. *Nat Chem Biol,* 12**,** 641-7.

XU, Y., SUTACHAN, J. J., PLESKEN, H., KELLEY, R. I. & SCHLAME, M. 2005. Characterization of lymphoblast mitochondria from patients with Barth syndrome. *Lab Invest,* 85**,** 823-30.

YE, J., RAWSON, R. B., KOMURO, R., CHEN, X., DAVE, U. P., PRYWES, R., BROWN, M. S. & GOLDSTEIN, J. L. 2000. ER stress induces cleavage of membrane-bound ATF6 by the same proteases that process SREBPs. *Mol Cell,* 6**,** 1355-64.

YOSHIDA, H., MATSUI, T., HOSOKAWA, N., KAUFMAN, R. J., NAGATA, K. & MORI, K. 2003. A time-dependent phase shift in the mammalian unfolded protein response. *Dev Cell,* 4**,** 265-71.

YOSHIDA, H., MATSUI, T., YAMAMOTO, A., OKADA, T. & MORI, K. 2001. XBP1 mRNA is induced by ATF6 and spliced by IRE1 in response to ER stress to produce a highly active transcription factor. *Cell,* 107**,** 881-91.

ZHAO, Q., WANG, J., LEVICHKIN, I. V., STASINOPOULOS, S., RYAN, M. T. & HOOGENRAAD, N. J. 2002. A mitochondrial specific stress response in mammalian cells. *EMBO J,* 21**,** 4411-9.

ZHOU, D., PALAM, L. R., JIANG, L., NARASIMHAN, J., STASCHKE, K. A. & WEK, R. C. 2008. Phosphorylation of eIF2 directs ATF5 translational control in response to diverse stress conditions. *J Biol Chem,* 283**,** 7064-73.

ZINSZNER, H., KURODA, M., WANG, X., BATCHVAROVA, N., LIGHTFOOT, R. T., REMOTTI, H., STEVENS, J. L. & RON, D. 1998. CHOP is implicated in programmed cell death in response to impaired function of the endoplasmic reticulum. *Genes Dev,* 12**,** 982-95.